Diss. ETH No. 9713

Potentiometric Detection of Cations in Capillary Zone Electrophoresis

A dissertation submitted to the

SWISS FEDERAL INSTITUTE OF TECHNOLOGY
ZURICH

for the degree of Doctor of Natural Sciences

presented by

Carsten Haber

Ingénieur E.H.I.C.S.

European Higher Institute of Chemistry, Strasbourg (France)

born on August 27, 1961

accepted on the recommendation of

Prof. Dr. W. Simon, examiner

Prof. Dr. W. Schneider, co-examiner
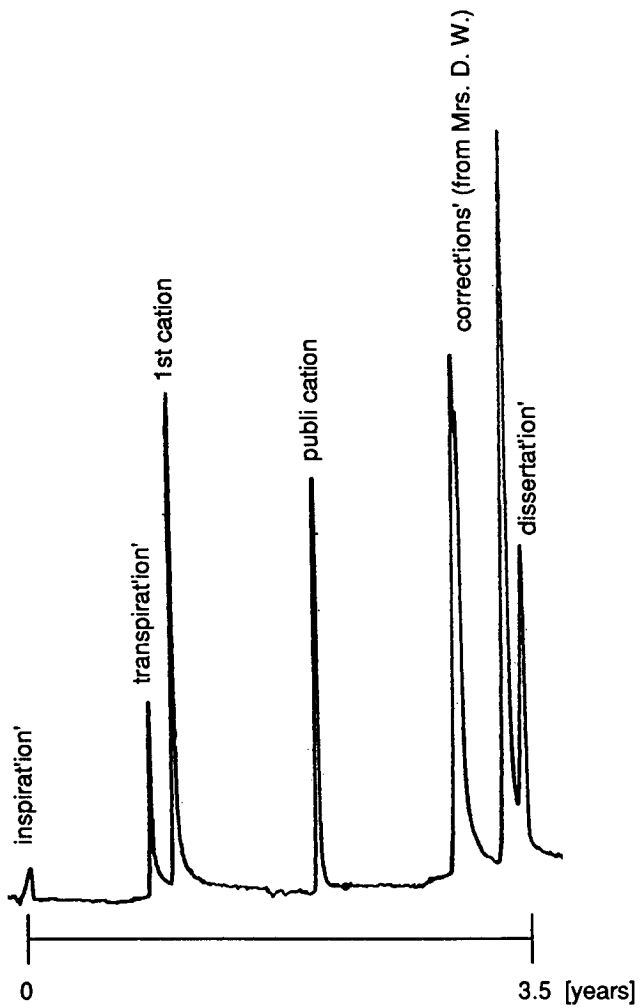
Dr. W. E. Morf, co-examiner

Zurich 1992

Leer - Vide - Empty

To Eva

Leer - Vide - Empty

'Ion'ic highlights in the scientific life of a CE researcher:

Leer - Vide - Empty

Acknowledgements

Leer - Vide - Empty

Table of Contents

1. Introduction and Summary

1.1. Introduction

Electrophoresis is the migration of charged particles or ions in solution due to an applied electric field. The basic experimental principle of this technique is still the same as in 1808 when von Reuss performed the first experiments [1]. He placed two vertical glass tubings into a lump of moist clay, filled them with water and inserted an electrode in each of them. After applying a potential to the electrodes he observed that the liquid rose in one tubing and sank in the other. This first observation of electrically induced particle migration was followed by the pioneering work of Hittorf [2,3], Nernst [4], Kohlrausch [5] and Tiselius [6,7] who described the fundamentals of the electrophoretic process. This basic knowledge led to the development of different methods having the same principle.

In 1950, the moving boundary electrophoresis was replaced by zone electrophoresis (ZE) which is performed in electrolyte solutions adsorbed on various supporting media, such as paper, cellulose powder and gels of polyacrylamide or agarose [8 -11].

In the early 1960s, new methods, e. g. disc electrophoresis [12], isoelectric focusing [13] and isotachophoresis (displacement electrophoresis) [14] made it possible to highly increase the efficiency of electrophoretic separations. Especially isotachophoresis turned out to be an important separation technique, and continuous efforts were made to improve the theoretical knowledge in this field [15]. The first commercially available instrument based on the isotachophoretic principle was presented by Everaerts and Verheggen in 1968. Further advances were achieved by the development of suitable detectors based on UV absorption [16] and conductivity [17].

At the beginning of the 1980s, the availability of narrow-bore fused-silica capillaries and the improvements of the detection systems in terms of response and sensitivity added the 'high performance' dimension to electrophoresis [18 - 20] New developments in instrumentation and methodology, e. g. (free solution) capillary electrophoresis (CE) [19, 21], capillary gel electrophoresis (CGE) [22] capillary micellar electrokinetic chromatography (MEKC) [23] and capillary electroosmotic chromatography [24], now severely compete with existing separation techniques, such as liquid chromatography (LC) and conventional slab-gel electrophoresis. The fact that open-tubular liquid chromatography (OTLC) so far has not yet reached a

commercial stage seems to indicate a turning point away from the pressure-driven towards the electrically driven separation techniques [25].

Future prospects lie in the further miniaturization of these separation systems for performing high speed electrophoretic analyses [26]. This could be achieved by combining the concept of highly integrated electrophoretic separation systems, based on planar technology [27], with powerful laser-induced fluorescence or electrochemical detection. Reproducible separations with an analysis time corresponding to the response time of a microsensor could be an interesting prospect and help to overcome the problems of selective measurements.

1.1.1. Principles of Electrophoretic Techniques

Electrophoretic methods nowadays are among the most widely used high resolution techniques for analytical and preparative separations. Although increasingly diversified, they still have in common the same principle of separation based on different migration velocities of the ionic constituents in the presence of an electric field gradient. In a simple classification three main types of electrophoresis (Fig. 1.1) [28] are distinguished:

- *Moving boundary electrophoresis* (**a**) as the analogon of chromatographic front analysis,

- *Zone electrophoresis* (**b**), which can be compared with the elution principle in chromatography,

- *Isotachophoresis* (**c**), applying the electrophoretic displacement principle.

Combinations of these principles also lead to interesting applications. Disc electrophoresis [12], for example, is a combination of isotachophoresis and zone electrophoresis. Electrophoretic techniques can also be amplified by using additional force fields and multiple dimensions.
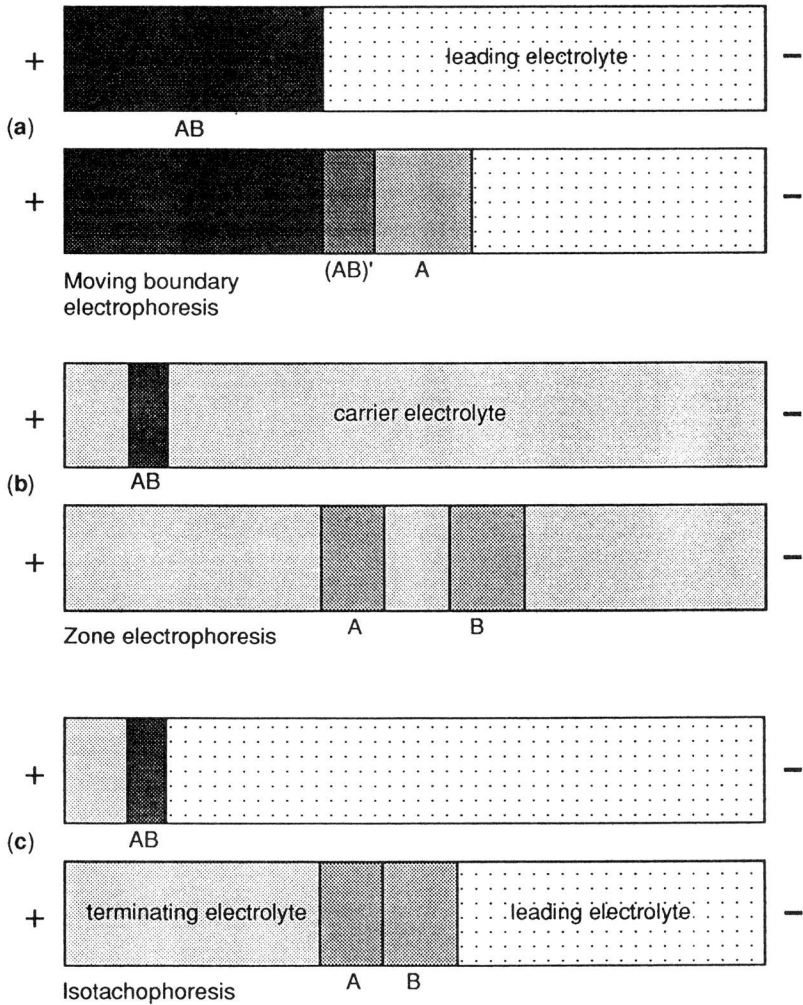
Figure 1.1 - *Electrophoretic methods.*

1.1.1.1. Moving Boundary Electrophoresis (Figure 1.1 - a)

A sample solution (AB) containing a mixture of two or more different ions is placed in a reservoir at the anodic end of the separation compartment, while the cathodic end is filled with a leading electrolyte having a higher mobility than the sample ions. By applying a voltage across the system, the cations tend to migrate towards the cathode. The ion with the highest mobility forms a pure zone (A) behind a stable moving boundary, followed by the other sample ions migrating in mixed zones (AB)'. As an analytical method, the moving boundary electrophoresis has only limited value, but the principle itself is present in almost every electrophoretic separation process during its initial state [29].

1.1.1.2. Zone Electrophoresis (Figure 1.1 - b)

In zone electrophoresis, a single electrolyte, the so-called carrier or background electrolyte, connects the anode with the cathode. The sample mixture is introduced as a discrete zone (AB) usually having a lower concentration than the background electrolyte. By applying a voltage across the separation compartment, the sample components migrate according to their individual electrophoretic mobilities. At an early stage, the system develops a moving boundary which is followed by the formation of individual zones depending on the local conditions (pH, conductance, driving current). After a certain time, the separated pure zones (A and B) are superimposed by carrier electrolyte. The migrating profiles never reach a steady state as in the case of isotachophoresis (see below). The principle of zone electrophoresis can be compared with elution chromatography [30, 31].

1.1.1.3. Isotachophoresis (Figure 1.1 - c)

Isotachophoresis (iso = equal, tachos = rapid) can be understood as a moving boundary electrophoresis with a discrete amount of sample [32]. The sample zone (AB) is placed between a leading and a terminating electrolyte. The former must contain the ion with the highest mobility and the latter that with the lowest mobility among the different electrolytes present in the system. The electric field is applied in such a way that the sample ions are directed

towards the leading electrolyte. At the beginning of the electrophoretic process, the system develops a moving boundary and, after sufficient time of migration, the sample components are completely separated into chemically pure zones (A and B). Due to the constant current density across the whole system, the zones will move with the same velocity as the leading electrolyte and will be arranged according to their electrophoretic mobilities. Owing to the Kohlrausch regulating function and the moving boundary phenomenon (see Chapter 2), the concentration within each zone is strictly regulated and the different zone boundaries have self-sharpening properties, thus preventing convective disturbances [33]. The length of the individual zones provides quantitative information on the analyzed sample.

In this work, capillary zone electrophoresis (CZE), now called high performance capillary electrophoresis (HPCE) in analogy to HPLC, was employed as the method of choice. A major part covers the practical aspects concerning the combination of capillary electrophoresis (CE) with a microelectrode as potentiometric detector, which, so far, has not yet been described in the literature. The basic theory of the electrophoretic process, which is necessary for understanding the experimental results, will be given in Chapter 2.

1.2. Summary

For the first time, the application of ion-selective microelectrodes for the potentiometric detection of inorganic and organic cations separated by capillary zone electrophoresis is described in the present work. Electrophoretic working conditions require field gradients ranging from 15 - 25 kV m^{-1}; on the other hand, the precise measurement of potentiometric signals between 0.1 and 100 mV, corresponding to changes in ion activities, requires zero current conditions. For this purpose, capillaries of 50 μm i.d. (internal diameter) were electrically segmented by cutting them at a short distance from the detection end and coupling the two parts with a section of porous glass tubing (porous glass joint). The electric field applied at the injection end of the capillary, was then grounded at this joint, so that the potentiometric measurement at the detection end occurred under the required zero current conditions. Initial electrophoretic experiments with potentiometric detection of ions were successful, but the resolution was not satisfactory due to broadening of the profiles in the detection segment. It was also found that considerable field effects still prevail even after the insulating joint, and that the sensor additionally responds to changes in the electric field gradient. Better resolution was achieved with unsegmented capillaries of 50 μm i.d. However, the signal of the potentiometric detector suffered from considerable noise so that insertion of the microelectrode tip into the end of the capillary (on-column detection) was not possible. Furthermore, the geometrical arrangement of the potentiometric detector, cathode, reference and common electrodes at the detection end of the capillary is critical in terms of noise and drift levels. Relatively low interferences were obtained by placing the sensor tip close to the cathode beside the lumen of the capillary at a distance which approximately corresponded to its i.d. Still better results were achieved when the cathode was deposited as a metal layer (Pt or Au) on the front part of the microelectrode. In the course of the experiments it was found that considerable potential drifts were caused by the saturated calomel reference electrode (SCE). Under the conditions used in capillary electrophoresis (CE), the common electrode (Pt wire) gave a more stable potential than the SCE. A better signal / noise ratio was obtained by decreasing the capillary i.d. to 25 μm. The higher internal resistance of the capillary significantly reduced interferences from the electric current, which also allowed the sensor tip to be inserted into the capillary end. However, the best compromise between noise and drift behaviour of the baseline on the one hand and extra-column band

broadening of the profiles on the other was achieved when the distance between the potentiometric detector and the capillary end corresponded to the i.d. of the capillary (post-column detection). The liquid membrane of the microelectrode was optimized so that its response to analytically relevant cations was more or less the same. The best results were obtained with a membrane cocktail consisting of the neutral ionophore 2,2'-[1,2-phenylenebis(oxy-2,1-ethanediyloxy)]bis(N,N-diphenylacetamide) with 68.5 mol % (relative to the ionophore) of potassium tetrakis-(4-chlorophenyl)borate in 2-(nitrophenyl) octyl ether. Mg^{2+}, being the most discriminated ion in the selectivity pattern, was used as background ion of the electrophoretic system. According to the Nicolsky-Eisenman equation, the electromotive force (and hence the detector signal) is determined by the activity ratios of the different cations against the ionic background and the corresponding selectivity coefficients. The direct potentiometric measurement thus provides a sensitive detection method for many cations.

With the system described, alkali and alkaline-earth metal ions as well as some organic cations could be successfully detected at concentrations of approximately 10^{-8} mol l^{-1}. Due to their small detection volume, high internal resistance and low detection limit, liquid membrane microelectrodes in CE represent a powerful alternative to other detection methods currently in use.

1.3. Zusammenfassung

Im Rahmen der vorliegenden Arbeit wurde erstmals die ionenselektive Mikroelektrode als potentiometrischer Detektor zum Nachweis von anorganischen und organischen Kationen in der Kapillarelektrophorese eingesetzt. Üblicherweise werden bei der Elektrophorese Feldstärken von 15 - 25 kV m^{-1} verwendet; die potentiometrische Erfassung von Aktivitätsänderungen (entsprechend Signalen zwischen 0.1 und 100 mV) am Detektionsende der Kapillare erfordert hingegen stromlose Bedingungen. Deshalb wurden zunächst Kapillaren von 50 µm Innendurchmesser durch eine künstlich erzeugte und speziell präparierte Bruchstelle (einen sog. Joint aus porösem Glas) kurz vor dem Detektionsende elektrisch unterbrochen (segmentiert). Dabei wird die am Injektionsende der Kapillare angelegte Hochspannung an dieser Bruchstelle auf Erde geführt, so dass die eigentliche Detektion im feldfreien Ende der Teilkapillare stattfindet. Die ersten Trennungen zur potentiometrischen Erfassung von Ionen unter Verwendung dieser segmentierten Kapillaren verliefen erfolgreich, die Qualität der Auflösung war jedoch wegen der Konzentrationprofil-Verbreiterung im Detektionssegment der Kapillaren nicht zufriedenstellend. Ausserdem zeigte sich, dass auch mit dem Joint aus porösem Glas noch Feldeffekte am Detektionsende vorhanden sind und die Mikroelektrode zusätzlich auf Änderungen des elektrischen Feldgradienten anspricht. Bessere Ergebnisse hinsichtlich der Auflösung erhielt man mit unsegmentierten Kapillaren von 50 µm Innendurchmesser. Wegen der Interferenzen durch den elektrophoretischen Stromtransport über die Kapillare wies das Detektorsignal jedoch einen beträchtlichen Anteil an Rauschen auf, der eine Einführung der Mikroelektrodenspitze in die Kapillare (sog. on-column detection) zunächst verunmöglichte. Zudem wurde festgestellt, dass die geometrische Anordnung des potentiometrischen Detektors, der Kathode sowie der Referenz- und Common-Elektrode am Detektionsende der Kapillare bezüglich Potentialdrift und Rauschen kritisch ist. Ein relativ störungsfreies Signal erhielt man beim Plazieren der Sensorspitze in geringem Abstand von der Kathode (ungefähr dem Innendurchmesser der Kapillare entsprechend) am Rand der Kapillaröffnung. Eine verbesserte Sensorvariante bestand aus einer Glaspipette, auf deren vorderem Teil die Kathode in Form einer dünnen Metallbeschichtung aufgedampft wurde. Weitere Untersuchungen ergaben, dass während der elektrophoretischen Trennungen ein beträchtlicher Driftanteil auf die Kalomel-Referenzelektrode zurückzuführen war. Es wurde

festgestellt, dass ein Platindraht als Common-Elektrode bei der Kapillarelektrophorese ein stabileres Basispotential liefert als die Kalomel-Referenzelektrode. Die Verringerung des Kapillarinnendurchmessers auf 25 µm brachte entscheidende Verbesserungen im Signal / Rauschverhältnis. Die Interferenzen durch den elektrischen Strom erwiesen sich wegen des erhöhten Kapillarinnenwiderstands als sehr gering, so dass der Detektor auch in die Kapillaröffnung eingeführt werden konnte. Die beste Lösung, um Potentialdrift und Rauschen der Basislinie einerseits und die Bandenverbreiterung der Signale andererseits gering zu halten, ergab sich jedoch, wenn zwischen dem potentiometrischen Detektor und der Trennsäule ein Abstand von einem Kapillarinnendurchmesser bestand (sog. post-column detection). Die Flüssigmembran der Mikroelektrode wurde dahingehend optimiert, dass ein für den Nachweis möglichst unselektives Verhalten bezüglich der meisten analytisch relevanten Kationen gewährleistet ist. Die besten Ergebnisse erzielte man mit einem Membrancocktail bestehend aus dem neutralen Ionophor 2,2'-[1,2-Phenylenbis(oxy-2,1-ethandiyloxy)]bis(N,N-diphenylacetamid) mit einem Anteil von 68.5 mol-% (bezogen auf den Liganden) Kalium tetrakis-(4-chlorphenyl)borat in 2-(Nitrophenyl)-octylether. Das auf der Selektivitätsskala am meisten diskriminierte Magnesiumion wurde im elektrophoretischen Trennsystem als Hintergrundion verwendet. Gemäss der Gleichung von Nicolsky-Eisenman wird die elektromotorische Kraft (und damit das Messsignal) durch die Aktivitätsverhältnisse des Hintergrundions zu den einzelnen Kationen des Messguts sowie durch die entsprechenden Selektivitätskoeffizienten bestimmt. Die direktpotentiometrische Erfassung der Messionen bedingt somit eine hohe Empfindlichkeit der Detektion.

Mit dem hier entwickelten System wurden Alkali- und Erdalkalimetallionen sowie einige weitere organische Kationen in Konzentrationen bis zu 10^{-8} mol l^{-1} erfasst.

In ihrer Applikation erweisen sich Flüssigmembran-Mikroelektroden wegen ihres geringen Detektionsvolumens, hohen Innenwiderstandes und ihrer tiefen Nachweisgrenze als nahezu perfekt für die elektrochemische Detektion von Ionen in der Kapillarelektrophorese.

2. The Electrophoretic Process

2.1. Electrophoresis as a Strongly Regulated Process

In 1897, Kohlrausch [34] concluded that the change of local electrolyte concentrations cannot be an arbitrary process, but must be strongly regulated. This he formulated in his concept of the regulating function and its mathematical expression of 'die beharrliche Funktion'. The function expresses mathematically that the sum of the concentrations of components divided by their mobilities has the same value on either side of the gradient. Kohlrausch derived his regulating function not with respect to a specific electrophoretic principle but as a general concept. Together with the moving boundary theory introduced by Tiselius [6], it is obvious that the different electrophoretic techniques are clearly governed by four basic principles:

- Ohm's law
- electroneutrality
- chemical equilibrium
- balance of mass [35]

2.2. The Concept of Mobility

The ionic mobility is defined as the speed of an ion in a field of unit strength (e. g. 1 V m^{-1}) [36]. Typical mobilities lie in the range of $(4 - 9) \cdot 10^{-8}$ m^2 s^{-1} V^{-1}. It should be noted that the ionic mobility is a signed quantity, positive for cations and negative for anions.

2.3. The Effective Mobility

An ionizable substance A in solution may represent a whole ensemble of neutral molecules and ionic species, A_0, A_1, A_2 .... A_k , involved in fast dynamic chemical equilibria, which, from the macroscopic point of view, behave as one entity [37]. For example, phosphate dissolved in water forms the species H_3PO_4, $H_2PO_4^-$, HPO_4^{2-} and PO_4^{3-}. From the electrophoretic point of view, in an electric field the whole ensemble of particles A_0, A_1, A_2 .... A_k, with ionic mobilities μ_0, μ_1, μ_2 .... μ_k and concentrations c_0, c_1, c_2 .... c_k, migrates as one

Cations	μ	Anions	$|\mu|$
H^+	36.23	OH^-	20.64
Li^+	4.01	F^-	5.70
Na^+	5.19	Cl^-	7.91
K^+	7.62	Br^-	8.09
Rb^+	7.92	I^-	7.96
Cs^+	8.01	NO_3^-	7.40
NH_4^+	7.63	HCO_3^-	4.60
Mg^{2+}	5.49	CO_3^{2-}	7.46
Ca^{2+}	5.56	SO_4^{2-}	8.29
Sr^{2+}	6.16	CH_3COO^-	4.24
Ba^{2+}	6.59	$HC_2O_4^-$	4.16

Table 2.1 - *Ionic mobilities in aqueous solution at* $25\,^{\circ}C$, μ [$10^{-8}\ m^2\ s^{-1}\ V^{-1}$][36].

uniform compound with the effective mobility $\bar{\mu}_A$ given by [7].

$$\bar{\mu}_A = \frac{1}{\bar{c}_A} \sum_{i=1}^{k} c_i\,\mu_i \qquad (2.1)$$

where $\bar{c}_A$ is the total (analytical) concentration of substance A.

The effective mobilities are influenced by several parameters, such as temperature, solvation, dissociation and complex formation. A change in pH of the background electrolyte results in a shift of the equilibrium reactions between the different subspecies, leading to a different value of the effective mobility of the apparent migrating compound.

2.4. Electric Current and Mass Transfer

In electrophoresis, the migration velocity, v, of a constituent i is given by the product of the ionic mobility μ (or effective mobility $\bar{\mu}$), and the local electric field strength, E:

$$v_i = \mu_i\, E \tag{2.2}$$

The electrophoretic separation is to be understood as a simultaneous transfer of both the electric charge and mass provided by the migration of ions in solution. Thus, the passage of the electric current through electrolyte solutions (ion movement) differs from the electric current in metals (electron movement) [38]. The relation between mass transfer in electrolytes and the corresponding electric current is expressed by means of the electric current density, and the migration distance by means of the amount of electricity passed [39]. When considering a tube filled with a homogeneous solution of ionized species dissolved in a liquid medium under a given voltage, Ohm's law (the first basic equation of electrophoresis) applies in the following form:

$$J = \frac{I}{S} = E\,\kappa \tag{2.3}$$

The electric voltage across the solution in the tube will result in an electric field of the intensity E which determines the magnitude of the electric current with a density $J = I/S$ (S being the area of a perpendicular plane at a given point). The electric conductivity κ characterizes the ability of a solution to conduct the electric current and is given by the sum of the contributions of all ionic species, *i. e.*

$$\kappa = F \sum_{i=1}^{s} c_i \,|z_i|\, \mu_i \tag{2.4}$$

where c_i is the concentration of the particular ionic species, s is the number of the different ionic species present in the solution, z_i the charge number, and F the Faraday constant. The electric conductivity, κ, links the modified Ohm's law (2.3) with the ionic mobilities, μ_i, of the different species and thus gives the electric field strength, E (an important electrophoretic parameter), a more chemical meaning.

From the macroscopic point of view, the whole solution remains electrically neutral, *i. e.*

$$\sum_{i=1}^{s} c_i \, z_i = 0 \qquad\qquad (2.5)$$

The condition of electroneutrality is the second basic equation of electrophoresis.

2.5. The Regulating Function

The Kohlrausch function can be derived in a simple way [40] by considering the following experiment (Figure 2.1). A solution of LiCl (zone 1) is layered behind a solution of KCl (zone 3), the latter having a higher mobility ($\mu_K > \mu_{Li}$). When an electric potential is applied as indicated, the cations start migrating towards the cathode. A moving boundary develops which is shifted from position x = 0 to x = l. At the rear side of the moving boundary a new zone 2 of LiCl is formed.

Three basic physical principles can be applied to this system with three monovalent ions:

(1) Conservation of electricity: $I_2 = I_3$

(2) Electroneutrality: $c_{Li.2} = c_{Cl.2}$ (zone 2) and $c_{K.3} = c_{Cl.3}$ (zone 3)

(3) Equal velocity of the pure migrating zones: $\mu_{Li} \, E_2 = \mu_K \, E_3$

From Condition (1) and with equation 2.3:

$$\frac{\kappa_3}{\kappa_2} = \frac{E_2}{E_3} \qquad\qquad (2.6)$$
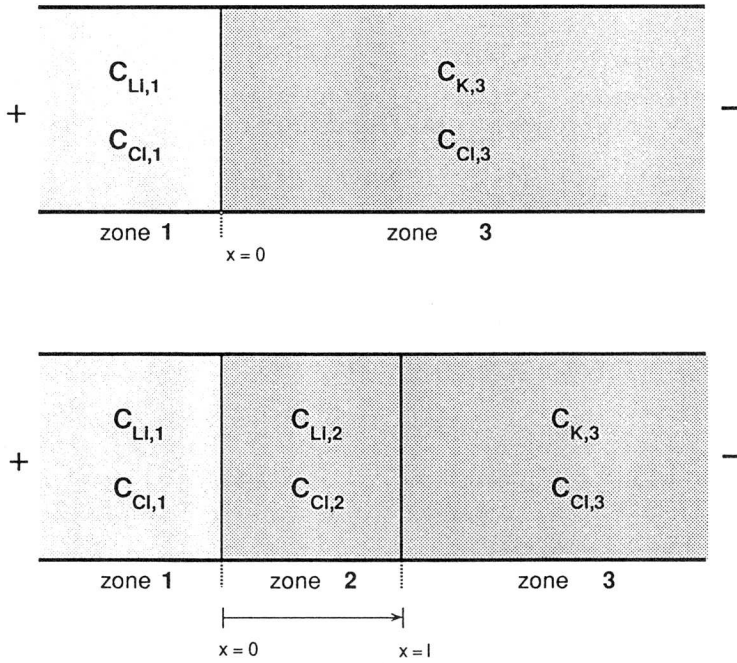
Fig. 2.1 - *Zone formation and regulating effect in the presence of an electric field.*

The specific conductivity κ in zones 2 and 3 is

$$\kappa_3 = c_{K,3}\,\mu_K + c_{Cl,3}\,|\mu_{Cl}| \quad \text{and} \quad \kappa_2 = c_{Li,2}\,\mu_{Li} + c_{Cl,2}\,|\mu_{Cl}| \tag{2.7}$$

Combining Equations (2.7) and (2.6) and taking into account Conditions (2) and (3) gives

$$\frac{c_{K,3}\,\mu_K + c_{Cl,3}\,|\mu_{Cl}|}{c_{Li,2}\,\mu_{Li} + c_{Cl,2}\,|\mu_{Cl}|} = \frac{E_2}{E_3} = \frac{\mu_K}{\mu_{Li}} \tag{2.8}$$

and after rearrangement and multiplication with $\dfrac{1}{|\mu_{Cl}|}$

$$\frac{c_{Cl,3}}{|\mu_{Cl}|} + \frac{c_{K,3}}{\mu_K} = \frac{c_{Cl,2}}{|\mu_{Cl}|} + \frac{c_{Li,2}}{\mu_{Li}} \qquad (2.9)$$

Expressed in a more general way, the relationship has the form [41]

$$\omega(x) = \sum_{i=1}^{s} \frac{c_i\, z_i}{\mu_i} \neq f(t) \qquad (2.10)$$

indicating that, in every electrophoretic zone, the sum of the concentrations of each ionic species divided by its mobility is equal over the whole length of the separation compartment.

For a given x, the regulating function $\omega(x)$ has a constant value, independent of time t, given by the composition of the homogeneous leading electrolyte prior to the passage of the electric current. The migrating zones of the sample then adjust to this constant value.

The concentration of LiCl in the newly formed zone 2 is

$$c_{Li,2} = \frac{\mu_{Li}}{\mu_{Li} + |\mu_{Cl}|} \cdot \frac{\mu_K + |\mu_{Cl}|}{\mu_K} \cdot c_{K,3} = 0.69\ c_{K,3} \qquad (2.11)$$

The expression indicates that the concentration of LiCl in zone 2 does not depend on its initial value in zone 1, but adjusts itself reaching a fixed level dictated by the concentration of KCl in zone 3.

The general mechanism indicates that any of the migrating zones follows the concentration profile which had been formed along the column before the electromigration started. This mechanism can be advantageously exploited for sharpening the injection pulse. In practice, this means that in order to maximize the concentrating capabilities, the sample should not be

equilibrated with the carrier electrolyte [18].

The regulating function also describes the discontinuities formed by the sample injection. The concentrations of ionic sample species are, after their passage across the stationary concentration boundary, adjusted to the value of the regulating function in the background electrolyte. A regulating imprint or 'gap', which can also be understood as a liquid memory [42], persists even after the sample ions have migrated away and this place is occupied by the background electrolyte. Two stationary concentration boundaries are formed at the point of injection and the concentration of the background electrolyte ions is adjusted to the value of the regulating function of the sample zone before the experiment started (system peak).

2.6. The Moving Boundary Equation

In order to study the electrophoretic process in further detail, it is necessary to establish a general relationship describing the electromigration properties of two neighbouring (consecutive) zones. Depending on the different conditions, the boundaries separating these zones can be stationary, moving or dispersive. The quantitative relationship involving the mass balance for the different constituents is called the moving boundary equation. It is the first integral of the transport equation and has the form [41]

$$\bar{c}_{i,1}\, \bar{\mu}_{i,1}\, E_1 \; - \; \bar{c}_{i,2}\, \bar{\mu}_{i,2}\, E_2 \; = \; v_{2 \rightarrow 1}\, (\bar{c}_{i,1} - \bar{c}_{i,2}) \qquad (2.12)$$

where the subscripts 1 and 2 denote the effective mobilities, analytical concentrations and electric field strength of the two neighbouring zones 1 and 2, respectively. $v_{2 \rightarrow 1}$ represents the migration velocity of the boundary between these two zones at unit current density.

2.7. Electrophoretic Boundaries

In all electrophoretic separation techniques, changes in electrolyte constituent concentrations will occur owing to the action of the external electric field.

These concentration gradients, which can be established and/or maintained by electric current inside a separation compartment, are usually divided by electrophoretic boundaries. These boundaries are distinguished in terms of their concentration distribution as a function of time (steady-state and unsteady-state boundaries) and in terms of their location as a function of time (stationary or moving boundaries). An electrophoretic boundary is typically marked by a change in a number of physical properties, such as conductivity, temperature, pH, refractive index and absorbance [42].

2.7.1. The Steady-State Boundary

A steady-state boundary is formed in a system of two electrolytes in which the ion with higher mobility migrates in front of that with lower mobility.
Figure 2.2 shows a typical concentration profile for this case. An injection plug of LiCl is introduced in a KCl background electrolyte ($\mu_{Li} < \mu_K$), with the concentration of the sample solution being lower than that of the KCl background. When current is passed through the system, the boundary initially located at $x = 0$ (a) is shifted to the position $x = I$ (b). A new zone 2, having a higher Li^+ concentration than the initial one, forms between zones 3 and 1 due to the regulating effect (constant value of the ω function). During the electrophoretic process, the entire concentration profile of the Li^+ sample will adjust to this concentration value. The rear boundary $2\rightarrow1$ of the K^+ zone migrating at a certain velocity v_K, forms the front boundary of the Li^+ zone, *i. e.* $v_{Li} = v_K$. The migration velocity of the moving boundary corresponds to

$$\bar{\mu}_{Li} E_2 = \bar{\mu}_K E_1 = v_{2\rightarrow1} = v_{Li} = v_K \tag{2.13}$$

and the Li^+ concentration is given according to Equation (2.11).
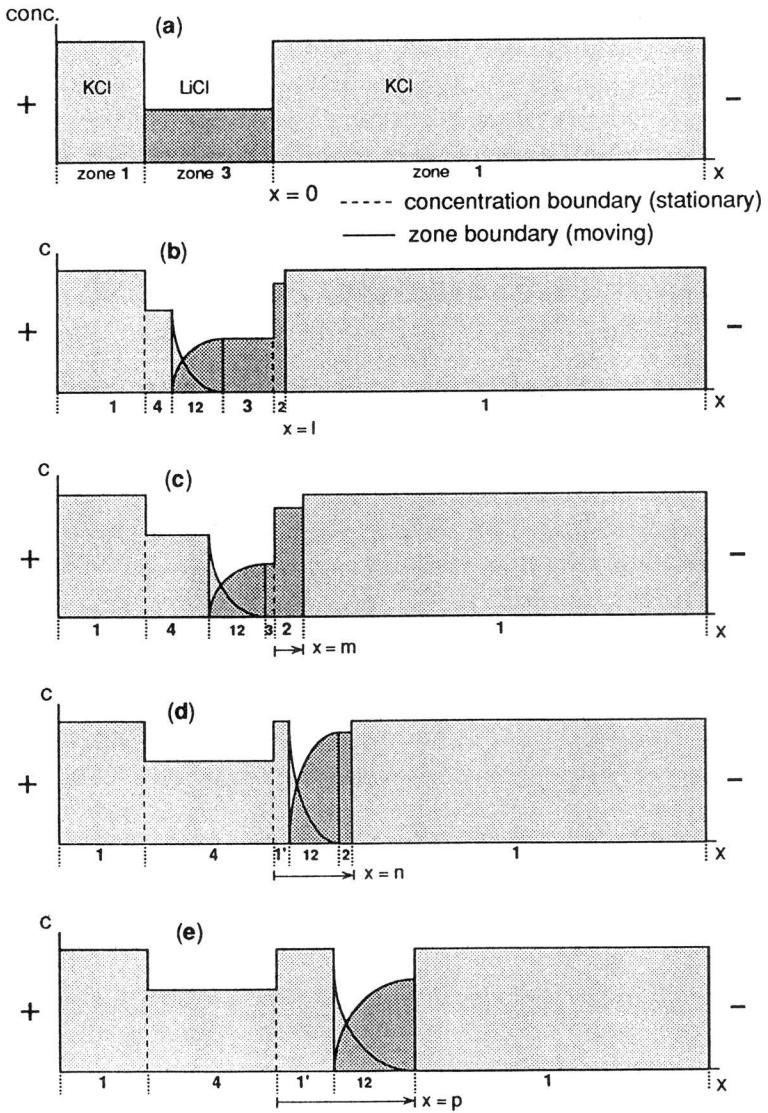
Fig. 2.2 - *Zone profile of LiCl migrating in a KCl background electrolyte.*

The moving boundary 2→1 is self-sharpening. The stable moving boundary only forms when one ion is followed by another ionic constituent, the latter having a lower ionic mobility. Because both zones move at the same speed according to Equation (2.13), the field strength in zone 2 must be higher than in zone 1. If Li^+ penetrates into zone 1, its speed diminishes due to the lower electric field strength $(E_2 > E_1)$ and it is quickly returned to zone 2. On the other hand, if K^+ penetrates into zone 2 possessing a higher field strength, it will be further accelerated until it again reaches zone 1. In this way, the self-sharpening effect balances the processes of dispersion [15].

On the rear side of the injected Li^+, this stability criterion cannot be met. K^+ penetrates into the Li^+ zone 3, possessing a higher field strength, and is further accelerated. This effect leads to the formation of a mixed zone 12 (b). Due to the higher mobility of K^+, the front boundary of this mixed zone 12 will move faster than the stable moving boundary 2→1. After a certain time, zone 2 completely vanishes and the front of the mixed zone 12 reaches the stable moving boundary 2→1 (e). At this point, Li^+ continues to migrate in a mixed zone together with K^+. The front remains sharp, while the rear side of the sample / background electrolyte zone 12 continually elongates with time due to the absence of a steady state (electromigration dispersion).

2.7.2. The Stationary Boundary (Concentration Boundary)

At the initial position of the boundary 1:3 (a), a certain discontinuity persists even during the passage of current. At this point, the background electrolyte solution is adjusted to a lower concentration level (zone 4, (b) to (e)) given by the value of the regulating function $\omega(x)$ of zone 3 before the electrophoretic process started. This process can be understood as an electrophoretically regulated dilution phenomenon. The remaining boundaries 1:4 and 4:1' in (d) and (e) are stationary and do not move during the electrophoretic experiment. In this case, the moving boundary equation can be written in the form [38]

$$\frac{c_{K.4}}{c_{K.1}} = \frac{E_1}{E_4} \qquad (2.14)$$

Qualitatively, zones 1 and 4 have the same composition, differing in their concentrations only. The ions passing across the stationary boundary 1:4 are accelerated due to the higher field strength and slowed down again when they reach zone 1'. This phenomenon is related to the fact that the different values of the Kohlrausch function in zones 1 and 3 (a) are locally invariant with time and persist during the passage of current through the separation compartment (system peak) [43].

2.7.3. The Unsteady-State Migration (Electromigration Dispersion)

Unsteady-state migration occurs, whenever an ionic constituent with a higher mobility migrates behind another having a lower mobility. This phenomenon can also be understood as a process of electrophoretic mixing. Initially pure zones form mixed zones which are continuously broadened by the dispersion resulting from the unsteady-state migration. The dispersive process depends in magnitude upon the differences between the ionic mobilities of the individual ionic constituents and leads to the typical assymetric profiles in electrophoresis.

The situation is illustrated in Figure 2.3. K^+, having the higher mobility, is now behind Li^+ (a). After switching on the electric current, K^+ forms an adjusted zone 2 according to the regulating function. However, in this case no stationary boundary develops. K^+ penetrates the rear boundary of zone 1 containing Li^+ and is further accelerated. Thus in front of the adjusted zone of pure KCl (zone 2) a time-variable mixed zone 12 containing Li^+ and K^+ is formed.

The regulating functions of zone 1, zone 2 and the mixed zone are [37]:

$$\omega_1 = \frac{\mu_{Li} + |\mu_{Cl}|}{\mu_{Li}} \cdot c_{Li1} = const; \quad t = 0, \ x > 0 \tag{2.15}$$

$$\omega_{12} = \frac{\mu_K + |\mu_{Cl}|}{\mu_K} \cdot c_{K.12} + \frac{\mu_{Li} + |\mu_{Cl}|}{\mu_{Li}} \cdot c_{Li2}; \quad t > 0, \ x > 0 \tag{2.16}$$

$$\omega_2 = \frac{\mu_K + |\mu_{Cl}|}{\mu_K} \cdot c_{K2}; \quad t > 0, x > 0 \tag{2.17}$$

33
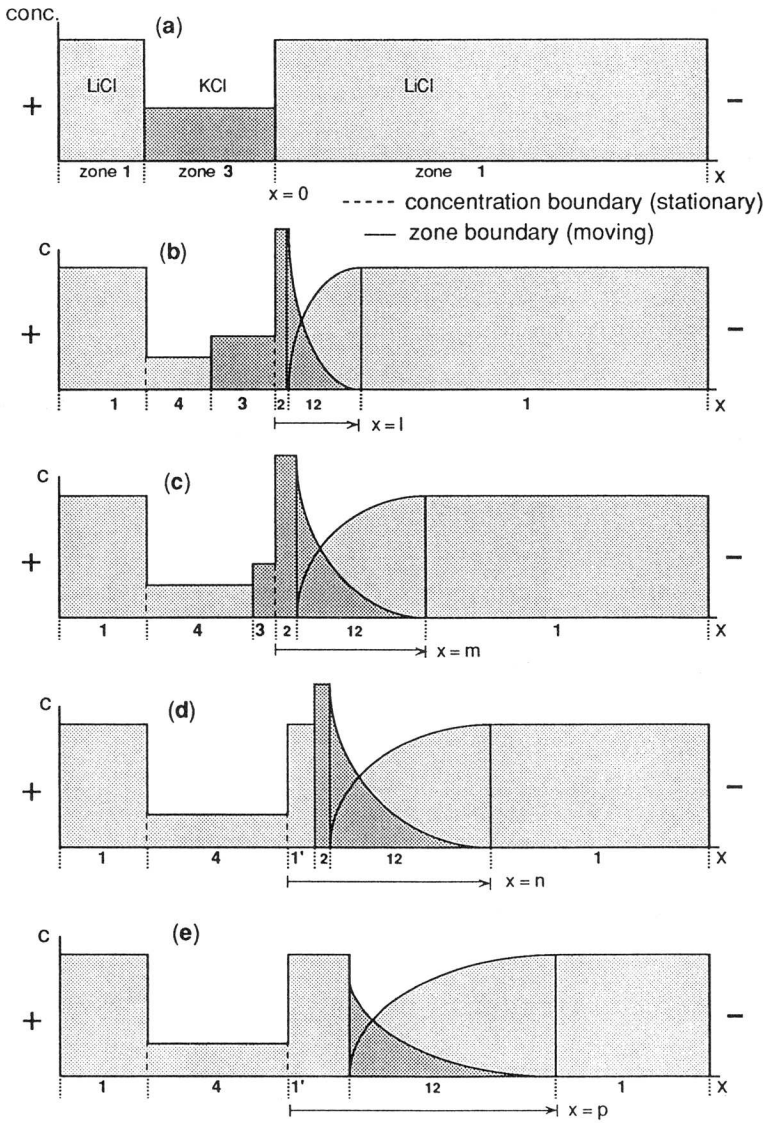
Fig. 2.3 - *Zone profile of KCl migrating in a LiCl background.*

Since the regulating function is time-independent,

$$\omega_1 = \omega_{12} = \omega_2 \qquad (2.18)$$

the composition of zone 2 can be determined from (2.15), (2.17) and (2.18):

$$c_{K2} = \frac{\mu_K}{\mu_K + |\mu_{Cl}|} \cdot \frac{\mu_{Li} + |\mu_{Cl}|}{\mu_{Li}} \cdot c_{Li1} = 1.45 \ c_{Li1} \qquad (2.19)$$

The migration velocity of Li⁺ the rear moving boundary of Li⁺, v_{Li}, is equal to its speed at the 2→12 boundary, so that in combination with (2.19) follows:

$$v_{Li} = \mu_{Li} \, E_2 = \frac{\mu_{Li}^2 \, I}{SF \ \mu_K \ (\mu_{Li} + |\mu_{Cl}|) \ c_{Li.1}} \qquad (2.20)$$

In analogy, the migration velocity of K⁺ is

$$v_K = \mu_K \, E_2 = \frac{\mu_{Li} \, I}{SF \ (\mu_K + |\mu_{Cl}|) \ c_{Li.1}} \qquad (2.21)$$

By combining equations (1.20) and (1.21),

$$v_K = \frac{\mu_{Li}^2}{\mu_K^2} \, v_{Li} \qquad (2.22)$$

it can be seen that the two boundaries move with different velocities, which means that the resulting mixed zone tends to elongate with time. The

concentration of the mixed zone therefore varies with time and coordinate. To establish the respective equations for the concentration of Li^+ and K^+ in the mixed zone, the non-linear variation of the concentration profile of the regulating function $\omega(x)$ with the corresponding current flow $I(t)$ has to be considered. A solution can be found by defining a factor Z having the form [37]

$$Z(x,t) = \sqrt{\frac{a(x)}{b(t)}} \qquad (2.23)$$

with

$$a(x) = 1 / F \, \mu_{Li} \, \mu_K \int_0^x \omega(x) \, dx \qquad (2.24)$$

and

$$b(t) = \frac{1}{S} \int_0^t I \, dt \qquad (2.25)$$

The concentration in the mixed zones are then given as [37]:

$$c_{K.12}(x,t) = c_{Li.1} \frac{\mu_K}{\mu_K - \mu_{Li}} \cdot \frac{\mu_{Li} + |\mu_{Cl}|}{\mu_K + |\mu_{Cl}|} \cdot \left(\frac{1}{F \, \mu_{Li} \, Z(x,t)} - 1 \right) \qquad (2.26)$$

$$c_{Li.12}(x,t) = c_{Li.1} \frac{1}{\mu_K - \mu_{Li}} \cdot \left(\mu_K - \frac{1}{F \, Z(x,t)} \right) \qquad (2.27)$$

In capillary zone electrophoresis, either the front or the rear boundary can represent a steady-state concentration distribution, but the entire shape of the sample zone actually never reaches a steady state. This entails an unsymmetrical broadening of the moving zones which, to some extent, is always present when the mobilities of sample and carrier components are not the same.

2.7.4. The Moving Reaction Boundary

A very important aspect in electrophoresis is the degree of interaction between sample and buffer, which influences the migration behaviour. During an electrophoretic separation in systems containing weak electrolytes, both mechanical movement of ions and chemical reactions are observed. This interaction is reflected in the magnitude of the conductivity (or electric field) change across the migrating sample zone. For weak electrolytes, such an interaction may also result in a pH value differing from that of the carrier buffer [44, 45].

The effect is illustrated in Figure 2.4. A solution of NaCl in hydrochloric acid is layered behind a potassium acetate buffer (**a**). After switching on the electric voltage, the hydrogen ions at the sample-buffer interface react with the acetate of the buffer solution to form undissociated acetic acid (zone 2 in (**b**)). Depending on the buffer capacity and the pH in the sample plug, this situation might produce a major change in pH and conductivity across the moving boundary 2→3.

The migration velocity of the hydrogen ions is a function of their effective mobility and depends on the electrolyte system. The mass balance for the H^+ in zone 2 can be expressed as follows [45]:

$$v_{2 \to 3} \, \tilde{c}_{H2} = c_{H2} \, \mu_H \, E_2 + v_{2 \to 3} \, c_{HAc2} \qquad (2.28)$$

where $v_{2 \to 3}$ is the speed of the migrating reaction boundary, μ_H the ionic mobility of H^+ and E_2 the electric field strength in zone 2. The total concentration of H^+ in zone 2 can be written as

$$\tilde{c}_{H.2} = c_{H.2} + c_{HAc\,2} \qquad (2.29)$$

The effective mobility of the hydrogen ions in zone 2 is then given by

$$\bar{\mu}_{H.2} = \frac{v_{2 \to 3}}{E_2} \qquad (2.30)$$

which, after combination with (2.28), can be written in the form

$$\bar{\mu}_{H.2} = \mu_H \cdot \frac{c_{H.2}}{\bar{c}_{H.2} - c_{HAc\,3}}$$

(2.31)

Undissociated acetic acid contributes to the mass transfer of H^+ and therefore influences its effective mobility.

In zone electrophoresis, due to the absence of a steady state a situation as described in Figure 4 is only temporary.
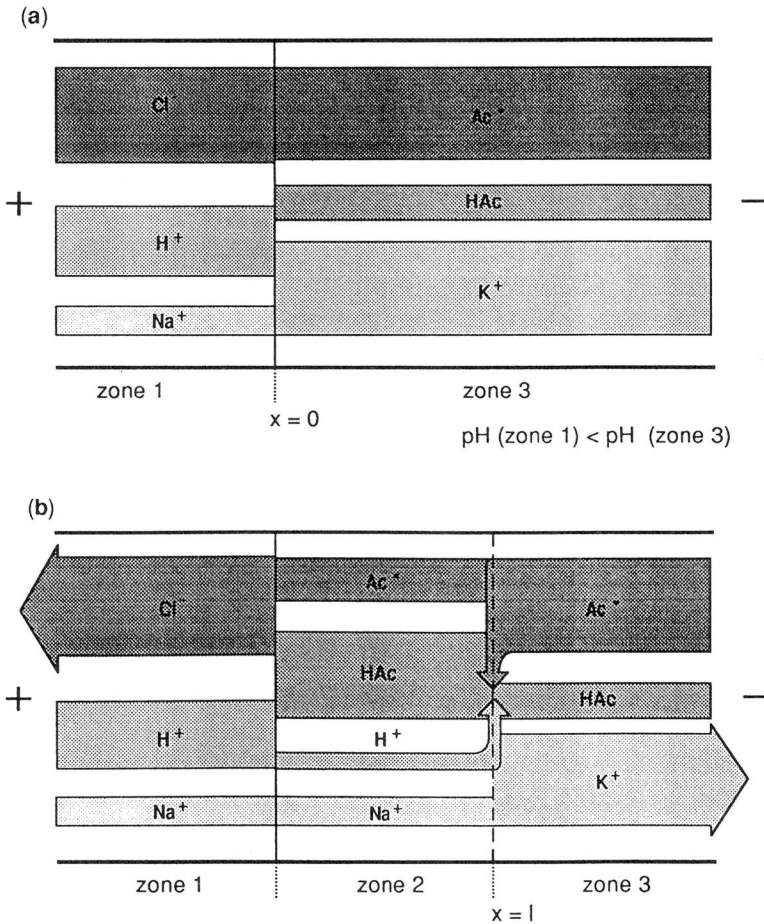
Fig. 2.4 - *Moving reaction boundary.*

3. Band Broadening in Capillary Zone Electrophoresis

3.1. Concentration Distributions

In zone electrophoresis, like in any other separation method, the effluent concentration as a function of time can be represented by a distribution which may be symmetrical or non-symmetrical. The initial profile of rectangular geometry undergoes various processes of dispersion and is continuously broadened during the passage through the separation compartment. Due to molecular diffusion the profiles tend to elongate symmetrically, while adsorption and electromigration processes lead to a non-symmetrical broadening of the zones.

In order to compare the adverse effects in terms of their relative magnitude of influence, it is useful to assume a Gaussian distribution for a given solute band and to consider all the dispersive forces as symmetrical. Every particular dispersion effect is then expressed as a standard deviation, σ_i, and increases the total width of the distribution curve. The individual variances, given by the square of the standard deviations, σ_i^2, can then be summed up to yield the total variance, σ^2, under the assumption of zero correlation between the variables [46].

The normal distribution plotted in Figure 3.1, describes a symmetrical distribution profile and is represented by the equation [46]

$$f(x) = \frac{1}{\sigma \sqrt{2\pi}} \exp\left[-0.5 \left(\frac{x - \mu}{\sigma} \right)^2 \right] \tag{3.1}$$

The standard deviation σ is half the width at the point of inflection, which, for a Gaussian curve, corresponds to measuring at 0.607 times its maximum height. The full width at half height (for Gaussian peak shape) is 1.177 times the width defined above [47, 48].

The peak variance σ^2 is related to the peak width at half height, $w_{0.5}$, as follows:

$$\sigma^2 = \frac{w_{0.5}^2}{5.54} \tag{3.2}$$
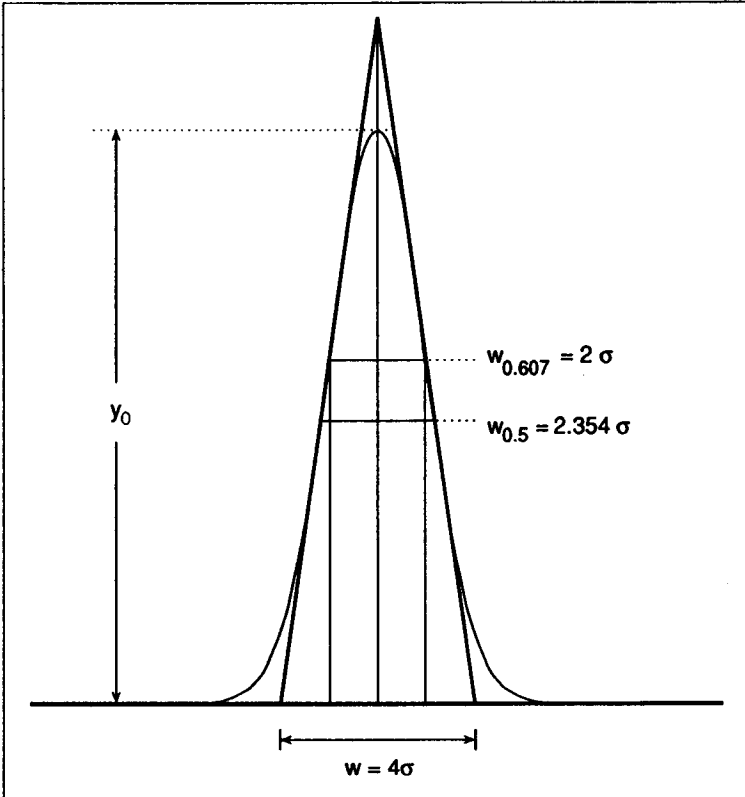
Figure 3.1 - *Normal distribution.*

For a quantitative description of the separation efficiency in zone electrophoresis, the concept of number of theoretical plates has been proposed [49]. The number of theoretical plates is given by the expression

$$N = \frac{L^2}{\sigma^2} \qquad (3.3)$$

where L is the length of the separation compartment.

Combining Equations (3.2) and (3.3) yields a relationship between the peak

width at half height and the number of theoretical plates:

$$N = 5.54 \; \frac{L^2}{w_{0.5}^2} \tag{3.4}$$

3.2. Dispersion Effects in Zone Electrophoresis

The magnitude of influence of the different dispersion effects on the concentration distribution during a zone electrophoretic experiment is measured by the total variance. This total variance is considered as the sum of the variances due to particular sources of dispersion, like injection, detection, diffusion, electromigration, temperature gradients (Joule heat) and adsorption [50].

$$\sigma^2 = \sigma_{inj}^2 + \sigma_{det}^2 + \sigma_{diff}^2 + \sigma_{mig}^2 + \sigma_{temp}^2 + \sigma_{ads}^2 \tag{3.5}$$

Except for σ_{inj}^2 and σ_{det}^2, the variance corresponding to a solute peak in an electrophoretic system is directly proportional to the analysis time and increases in proportion to the migrated distance. The time-dependent variance contributions are given by

$$\sigma_i^2 = 2 \, t \, D_i \tag{3.6}$$

where t is the migration time and D_i the respective dispersion coefficient.
The total variance of the sample distribution therefore corresponds to the sum of the time-independent contributions (injection and detection) plus the time-dependent contributions:

$$\sigma^2 = \sigma_{inj}^2 + \sigma_{det}^2 + 2 \, t \, \Sigma \, D_i \tag{3.7}$$

3.2.1. Band Broadening due to Injection

The injection variance σ_{inj}^2 can be expressed as [25]:

$$\sigma_{inj}^2 = \frac{l_{inj}^2}{12} \tag{3.8}$$

where l_{inj} is the length of the injection plug.
The length of the injected zone has considerable influence upon the total variance. For short injection plugs, the zone length is controlled by diffusion, while for longer ones it is predominantly determined by the variance of the injected zone [47].

3.2.2. Band Broadening due to Detection

The variance contribution for a finite detector path length is [51]:

$$\sigma_{det}^2 = \frac{l_{det}^2}{12} \tag{3.9}$$

where l_{det} is the path length of the detector cell. In the case of on-column detection (see Chapter 9), the detection process itself does not contribute to the variance except in terms of the capillary section which corresponds to the detector cell volume [52].

3.2.3. Band Broadening due to Diffusion

The variance contribution due to longitudinal diffusion is

$$\sigma_{diff}^2 = 2 D t \tag{3.10}$$

The diffusion coefficients can be calculated from the Einstein equation [53]:

$$D = \frac{\mu k_b T}{ez} \tag{3.11}$$

where μ denotes the ionic mobility, k_b the Boltzmann constant, T the absolute temperature, e the electric charge and z the charge number of the respective ion.

3.2.4. Band Broadening due to Conductivity Differences between Zones (Electromigration Dispersion)

The distribution profiles and shapes of the zones due to differences in the conductivity between sample and buffer ions has already been qualitatively explained in Chapter 2. The effect can be quantitatively described by expressions established by Mikkers et al. [54]. In the case, where the mobility of the sample ion is smaller than that of the buffer ion, i.e. $\mu_s < \mu_b$, the band broadening due to electromigration dispersion is given by

$$\delta_{mig} = x_{max} - x_{min} = c_s\, l_{inj}\, a_s + 2\,\sqrt{c_s\, l_{inj}\, a_s\, \mu_b\, r_s\, E\, t} \tag{3.12}$$

and for $\mu_s > \mu_b$:

$$\delta_{mig} = x_{max} - x_{min} = c_s\, l_{inj}\, a_s + 2\,\sqrt{c_s\, l_{inj}\, a_s\, (l_{inj} - \mu_s\, E\, t)} \tag{3.13}$$

with

$$a_s = \frac{1}{c_b}\left(\frac{r_s - r_c}{1 - r_c}\right)\left(\frac{1 - r_s}{r_s}\right) \tag{3.14}$$

In these equations l_{inj} is the initial width of the sample plug, c_s and c_b denote the concentration of the sample and buffer ion, respectively; r_s and r_c are the mobilities of the sample and counter ions relative to the buffer ion, E is the electric field strength in the separation compartment and t the time of migration. The term a_s is a factor which serves to correct the zone length due to the regulating function (concentration effect). The total width of the sample band, δ_{mig}, is given by the difference of the maximum distance, x_{max}, and the minimum distance, x_{min}, that the sample ion has migrated in a given time interval t.

When the sample ion has a lower mobility than the background electrolyte, as described previously, the leading front of the sample zone will always be sharp, whereas the rear is continually dispersed (Figure 1.2). This is due to the fact that, at the peak front the moving boundary is stable [55], but at the rear side this stability criterion cannot be met. The situation is reversed, when the sample ion has a higher mobility than the background electrolyte (Figure 2.3). In the former case, the process of electromigration dispersion occurs on the rear side of the peak, in the latter on the front side. Differences in the conductivity between sample and buffer therefore result in a non-symmetrical broadening of the zones. The effect is further enhanced, because a sharp moving boundary, created by two different potential gradients in the neighbouring zones, may counteract the longitudinal diffusion. Depending on the conditions, the diffusion at this boundary might even be completely compensated (zone sharpening). In this condition, some restriction has to be made regarding the summing up of the variances, because this is only fulfilled, when the asymmetry is small and the peak profile can be approximated by a symmetrical Gaussian distribution. If the asymmetry is too pronounced, it is better to operate with the total zone width [56].

The effect of electromigration dispersion tends to distort the peak shape non-symmetrically. However, for small sample concentrations, the distortion will be insignificant since the conductivity in the sample zone is mainly determined by the background electrolyte. In this case, a Gaussian distribution may be assumed and the total width of the sample band is then equivalent to:

$$\delta_{mig} = 4\,\sigma \tag{3.15}$$

With this approximation, the band broadening due to electromigration dispersion may be compared to the variance determined by longitudinal diffusion.

From the point of injection until detection, a zone profile which migrates in a background electrolyte, is mainly subject to three different processes:

- The concentration adaptation of the sample plug relative to the ionic background according to the regulating function, the magnitude depending on the relative mobilities and concentrations of sample and background electrolyte.

- The process of electromigration dispersion, determined by the conductivity differences between the migrating zones.

- The longitudinal diffusion, which continually elongates the zones during their electrophoretic passage through the separation compartment.

Figure 3.2 shows distributions of a LiCl zone after a migration period of 15 minutes in a KCl background. LiCl is injected in different concentrations as a sample profile of rectangular geometry and 0.5 mm width. If the sample zone is only subject to longitudinal diffusion during the separation period of 15 minutes, the final distribution corresponds to the Gaussian profile (a) and does not depend upon the initial concentrations. According to Equation 3.12, the variance due to electromigration dispersion is determined by the concentration and the relative mobilities of the ionic constituents in the separation compartment. Pure electromigration dispersion will therefore continually elongate the zones according to their conductivity differences. However, the fact that for identical migration periods the final peak profiles (b - d) are more or less strongly dispersed by the process of electromigration, is a consequence of the concentration adaptation (Table 3.2). In the separation compartment, a diluted sample adapts to a certain concentration level which is predetermined by the value of the regulating function of the buffer. The adaptation process is independent of the initial sample concentration. In an early state of the separation, the sample plug with a low concentration is therefore 'compressed' to a very narrow zone, until the processes of diffusion and electromigration dispersion again elongate the profile to reach its final shape. According to Figure 3.2, longitudinal diffusion and electromigration dispersion (including the concentration adaptation) tend to be of comparable

magnitude when the ratio of c_b /c_s ≈ 30 (the length of the injection plug being 0.5 mm). If this ratio is higher, the total variance is mainly determined by diffusion, and vice versa.

Conc. of KCl background electrolyte [mol l^{-1}]	Conc. of LiCl [mol l^{-1}]	σ^2_{mig}	σ^2_{diff}	Relative contri- bution of σ^2_{mig} to the total zone profile
$5 \cdot 10^{-3}$	10^{-5}	$1.25 \cdot 10^{-7}$	$1.85 \cdot 10^{-6}$	6 %
$5 \cdot 10^{-3}$	10^{-4}	$1.25 \cdot 10^{-6}$	$1.85 \cdot 10^{-6}$	40 %
$5 \cdot 10^{-3}$	$5 \cdot 10^{-4}$	$6.28 \cdot 10^{-6}$	$1.85 \cdot 10^{-6}$	77 %

Table 3.1 - *Relative contribution of electromigration dispersion to the total variance of a zone profile (given by the sum of the contributions of diffusion and electromigration dispersion), calculated as a function of the initial sample concentration of LiCl.*

Typical peak profiles of LiCl and NaCl migrating in a KCl background are shown in the figures 3.3 and 3.4, respectively. The final peak profiles (b) indicate that it is the longitudinal diffusion which mainly determines the bandwidth of a signal. The relative contribution of the electromigration dispersion to the total profile is as high as about 6 % for LiCl and 4 % for NaCl. This difference results from the individual concentration adaptation of the sample (factor ≈ 70 for LiCl and ≈ 80 for NaCl).

original concentration profile
(injection plug) at t = 0
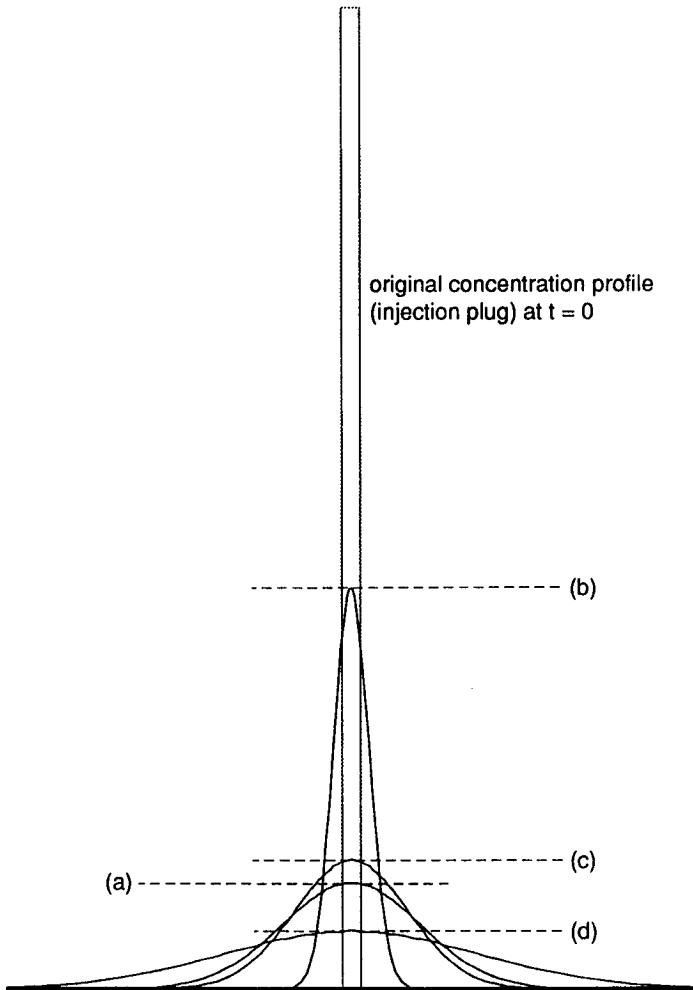
Fig. 3.2 - *Calculated concentration distributions of an initially rectangular LiCl zone after a migration period of 15 min in a KCl background. The zone profiles are obtained for diffusion only (a) and for electromigration dispersion (including concentration adaptation) at different ratios of background electrolyte/sample (b - d). Background electrolyte $5 \cdot 10^{-3}$ M KCl; sample LiCl 10^{-5} M (b), 10^{-4} M (c) and $5 \cdot 10^{-4}$ M (d); length of injection plug 0.5 mm; migration time of sample zone 15 min; field gradient 20 kV m^{-1}.*
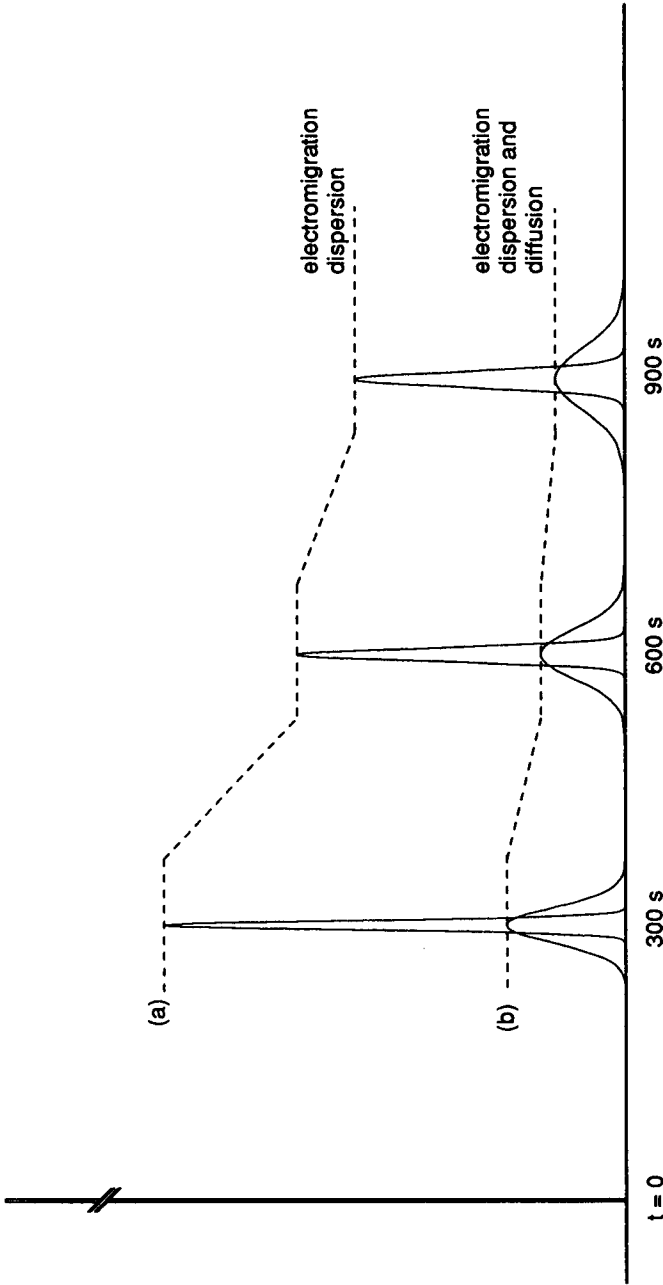
Fig. 3.3 - Calculated concentration profiles of a 10^{-4} M LiCl zone migrating in a 10^{-2} M KCl background. The initial sample plug (t = 0) has a rectangular profile. Profiles (a) show the band broadening due to electromigration dispersion only. The final peak profiles (b) are obtained by adding the contribution of the longitudinal diffusion to the zone profiles (a). Length of injection plug 0.1 mm; field gradient 20 kV m^{-1}.

48
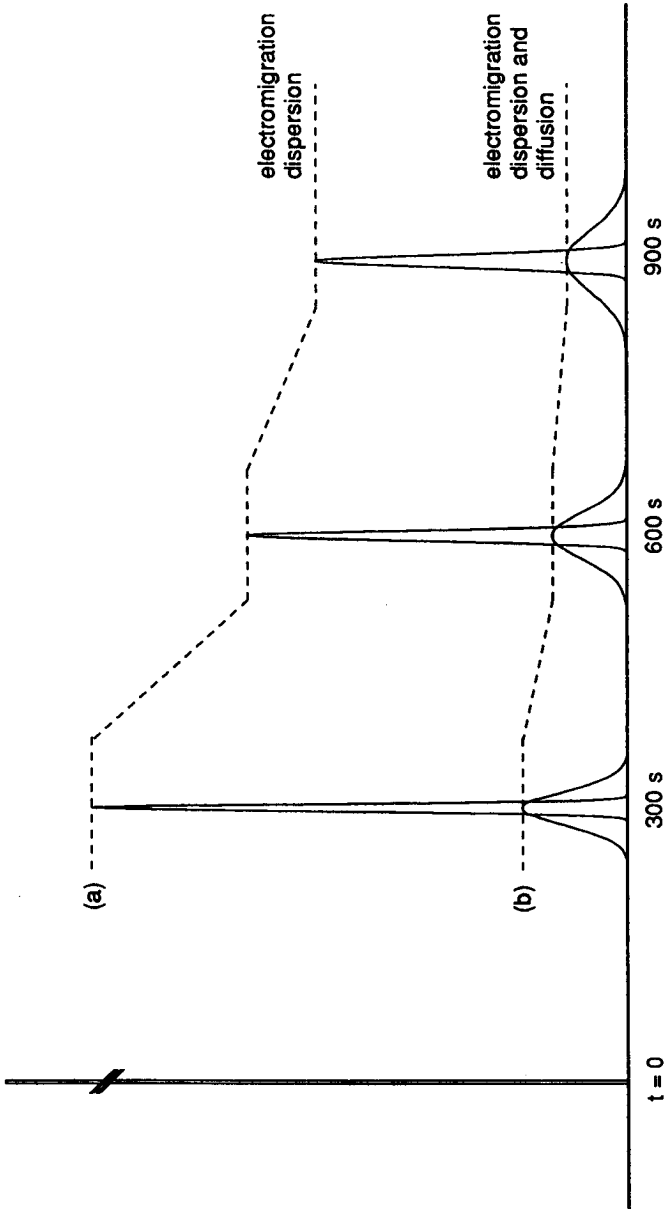
Fig. 3.4 - Calculated concentration profiles of a 10^{-4} M NaCl zone migrating in a 10^{-2} M KCl background. The profiles are obtained under the same conditions as for the example in Fig. 3.3.

3.2.5. Temperature Effects (Joule Heat)

During the passage of electric current, I, through a separation compartment of cross section S filled with an electrolyte of conductivity κ, the Joule heat per unit volume is given by [37]

$$P = \frac{E\,I}{S} = \frac{I^2}{\kappa\,S^2} \qquad (3.16)$$

where P is the dissipated electric power [W m^{-3}].

Heat generated along the entire volume of the electrolyte, is dissipated only through the wall of the separation compartment. This leads to a parabolic temperature distribution with the maximum temperature along the axis of the tube. As the mobility (in pure buffer) increases by about 2.0 % [40] and the viscosity drops by 2.7 % per °C [56], the liquid in the center of the migrating zones will move faster. These two effects will distort the flat flow profile into a radial geometry and can cause significant band broadening. The exact temperature profile in a tubular column is described by Bessel functions [57], but can be closely approximated by simple parabolic profiles [58, 59]. In this case, the time-dependent variance contribution has the form

$$\sigma^2_{temp} = 2\,t\,D_T \qquad (3.17)$$

with the dispersion coefficient due to Joule heat given by [60]

$$D_T = \frac{\kappa^2\,\delta_T^2\,\mu^2\,E^6\,r^6}{3072\,D\,\lambda_T^2} \qquad (3.18)$$

where κ is the electric conductivity and λ_T the thermal conductivity of the
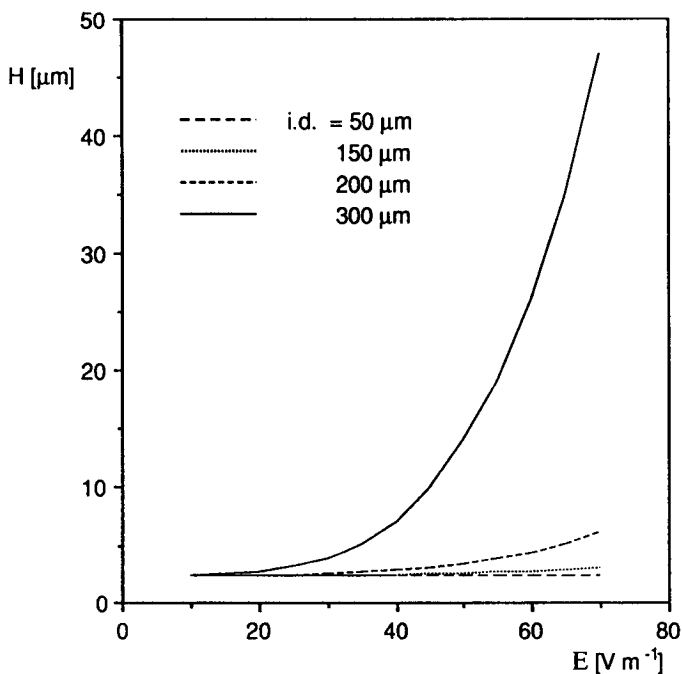
Fig. 3.5 - *Calculated contribution of Joule heat to plate height (H), in capillaries of different inner diameter (i.d.). Background electrolyte $2 \cdot 10^{-2}$ M MgAc$_2$; sample 10^{-5} M KCl; capillary length 1 m; zone velocity 0.1 m min^{-1} .*

background electrolyte, D the diffusion coefficient of the sample ion, δ_T the temperature coefficient of its mobility μ, and r the radius of the separation capillary.

The influence of thermal band broadening strongly depends upon the concentration (conductivity) of the buffer, the electric field strength and the volume of the separation compartment. The effect is illustrated in the Figures 3.5 and 3.6. Decreasing the column radius and increasing the column length will have a significant effect on reducing the thermal load which has to be dissipated by a given length of capillary. If a capillary has a small enough i.d. and/or is long enough, the heat will be dissipated quickly enough to prevent
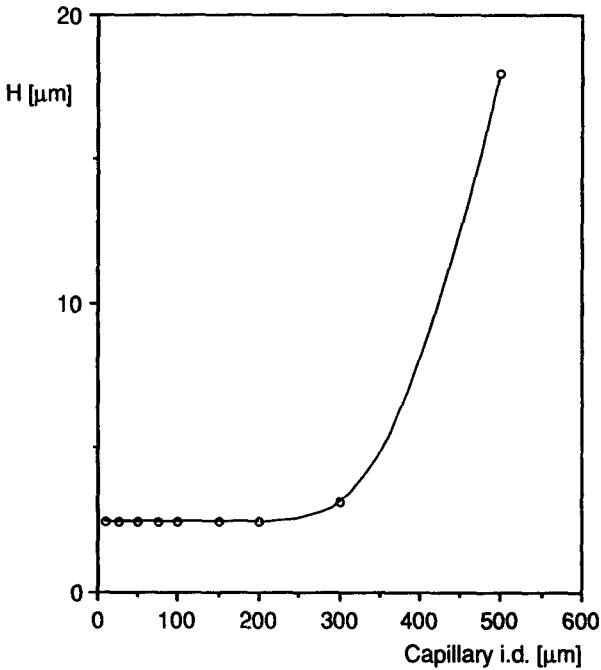
Fig. 3.6 - *Calculated contribution of Joule heat to plate height (H) as a function of the inner diameter (i.d.) of the capillary. Field gradient 25 kV m⁻¹; background electrolyte 2 · 10⁻² M MgAc₂; sample 10⁻⁵ M KCl; capillary length 1 m; zone velocity 0.1 m min⁻¹.*

thermally induced band broadening. In capillaries of 50 μm i.d. or less, operated with diluted buffer solutions, the degree of thermally induced band broadening is practically negligible.

In capillary electrophoresis, a total efficiency curve can be derived for a given inner diameter of the capillary and concentration of the buffer solution. In analogy to chromatography, the maximum efficiency here too is a compromise between the longitudinal diffusion at low field strengths (slow speed) and the deterioration in resolution at high field strengths (fast separations) due to thermally induced band broadening.
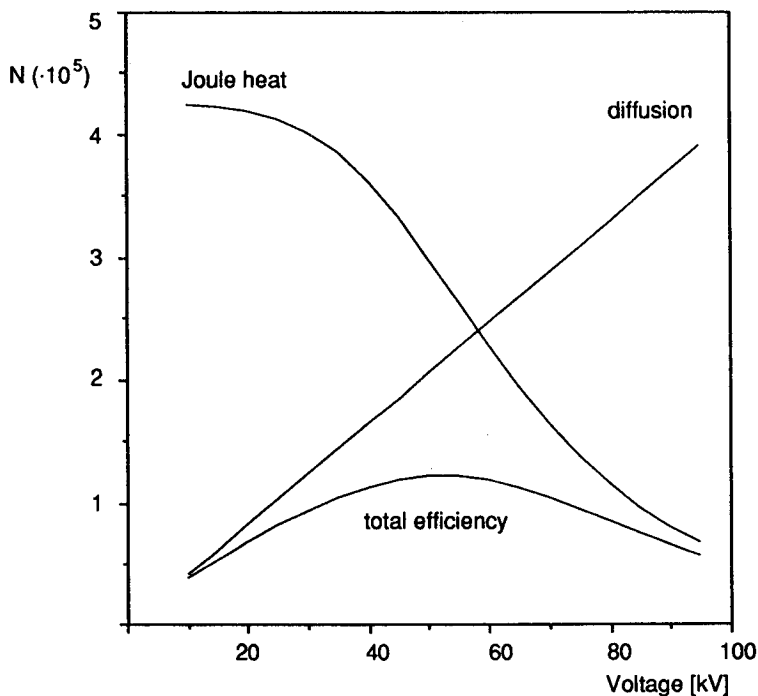
Fig. 3.7 - *Simulated total efficiency curve given by the number of theoretical plates (N) and the applied voltage (kV). Background electrolyte $2 \cdot 10^{-2}$ M $MgAc_2$; sample 10^{-5} M KCl; capillary i.d. 200 μm; capillary length 1 m; zone velocity 0.1 m min^{-1}.*

3.2.6. Adsorption

Adsorptive interaction of ions or molecules with the surface of the separation compartment can be described by defining an 'adsorptive state' with zero velocity [40]. Every adsorptive interaction makes the particle disappear from the mobile electrophoretic phase to appear again after some time. Strong interaction of the particle with the surface of the separation compartment can lead to significant tailing and affects the apparent electrophoretic migration time.

The fractional concentration of free particles, R_c, is given by the ratio of the zone velocity, v_m, divided by the total velocity, which is equal to the sum of the electrophoretic (v_{el}) and electroosmotic velocity (v_{osm})

$$R_c = \frac{v_m}{v_{el} + v_{osm}} \qquad (3.19)$$

The difference between these two velocities is equivalent to the mean lifetime of the adsorbed particle.
The variance of the spreading due to adsorptive interaction is then given by

$$\sigma^2_{ads} = \frac{2 R_c^2 (1 - R_c) (v_{el} + v_{osm})^2 E^2 t}{k_{ads}} \qquad (3.20)$$

where k_{ads} is the mean lifetime in the adsorbed state.
Determined by the surface / volume ratio, the possibility for a solute to be adsorbed increases, as the radius of the tube is decreased. Particularly macromolecules (e. g. proteins) tend to interact strongly with negative sites present on glass surfaces.

3.2.7. Other Sources of Band Broadening

Beneath the main dispersive forces, like diffusion, electromigration, adsorption and Joule heat, which under normal working conditions determine the zone profile, other dispersion forces of minor importance exist, which are only treated qualitatively in this work:

- The electroosmotic flow in open tubular capillaries is usually laminar and therefore considered as non-dispersive, i. e. $\sigma^2_{osm} = 0$ [37]. Additional peak broadening occurs in the case where local variations of the zeta potential along the separation path are caused, e. g. by the adsorption of macromolecules, thus generating local turbulences [61].

- Microheterogeneity is described as an additional reversible boundary spreading due to deviations in size, shape or charge of the migrating species[62, 63].

- Electrodiffusion is observed when an electric field is applied to species existing in different migration states which are rapidly interconvertible [64, 65]. In electrophoresis, the extent of electrodiffusion due to ionization processes is found to be negligible [66].

- Additional dispersion can be caused by gravitational effects, due to any density differences between the fluid and the sample [67].

3.3. Computer Simulations of an Electrophoretic Experiment

In recent years, important progress has been made by the use of digital computers which allow to solve transport equations containing both electromigrational and diffusional flux terms. Simulation of the time-dependent shape and evolution of zone profiles provides substantial insight into the fundamental electrophoretic phenomena. The first description of the transient behaviour of electrolyte systems was published by Thormann et al. [68 - 70]. The underlying theoretical model is one-dimensional and based upon the principles of electroneutrality and conservation of mass and charge. It comprises the dispersive influence of electromigration and longitudinal diffusion. A detailed explanation of the model is given elsewhere [71, 68].

Figures 3.8 - 3.11 represent simulated electrophoretic separations of Na^+, K^+ and Rb^+ (each 10^{-5} M, with Ac^- as counter-ion) migrating in a background electrolyte consisting of LiAc ($2 \cdot 10^{-2}$ M). The total migration time is 100 min at a constant current density of 25 A m^{-2}. The initial width of the injected sample zone at $t = 0$ corresponds to 2 % of the total length of the separation compartment. The evolution of the concentration profiles of the three cations is shown in snapshots taken at different migration times as indicated.

For Figures 3.8 and 3.10, the sample zone at $t = 0$ contains no background electrolyte, so that the sample profiles are adapted to higher concentration levels according to their individual concentration / mobility ratio (see profiles for $t = 4$ min). This effect is not observed when the sample is previously dissolved in background electrolyte (Figures 3.9 and 3.11). Due to the

dispersive influence of the longitudinal diffusion, the zone sharpening effect will be compensated, so that for higher migration times (t ≥ 48 min) the profiles are almost identical in both cases (Figures 3.10 and 3.11). A small difference is observed in the distance migrated by the ions, which is slightly higher when the sample initially contained no background electrolyte. Furthermore, the symmetry of the peaks obviously indicates that diffusional dispersion is primarily responsible for the shape of the zone profiles [68]. This is due to the fact that the concentration of the background electrolyte is more than three orders of magnitude higher than that of the sample and thus determines the conductivity within the column. Typical profiles which are asymmetrical as a consequence of electromigration dispersion will be observed when individual sample constituents significantly contribute to the conductivity of the zones, *i. e.* for higher sample concentrations.
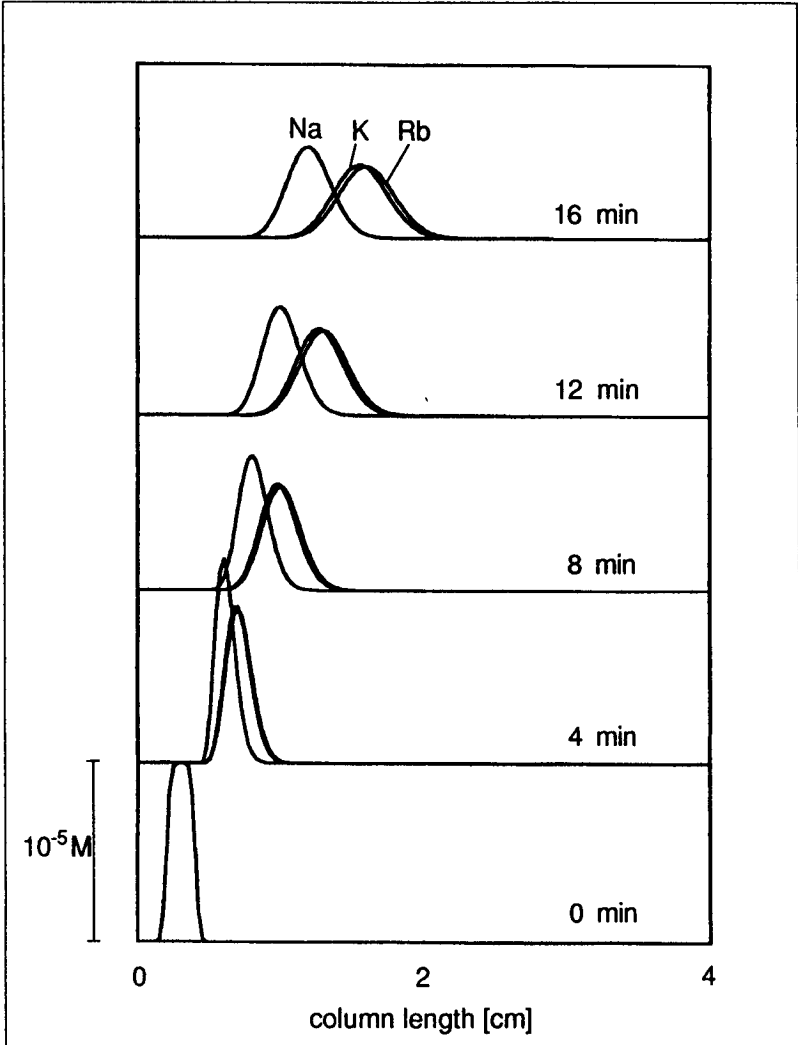
Fig. 3.8 - *Simulated electrophoretic separation of 10^{-5} M Na+, K+ and Rb+ (acetates) migrating in a background electrolyte of $2 \cdot 10^{-2}$ M LiAc. The initial width of the sample zone at t = 0 min corresponds to 2 % of the total length of the separation compartment; the sample contains no background electrolyte. Current density 25 A m^{-2}; separation period 0 - 16 min [72].*
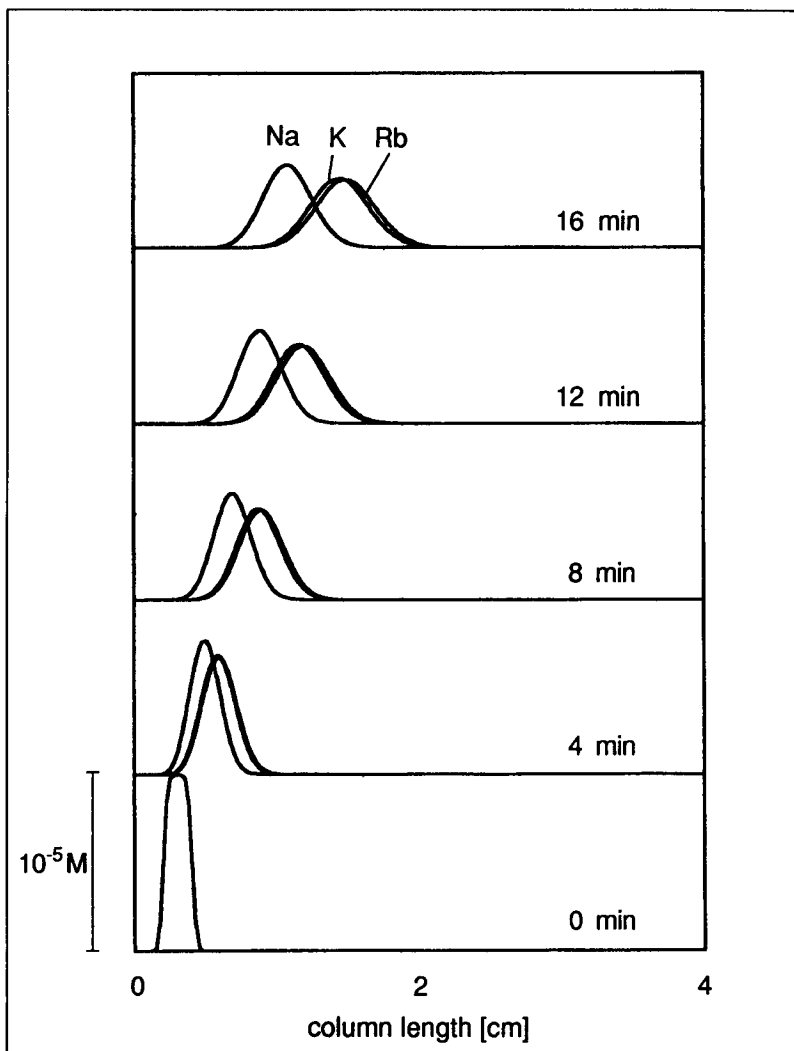
Fig. 3.9 - *Simulated electrophoretic separation of 10^{-5} M Na^+, K^+ and Rb^+ (acetates) migrating in a background electrolyte of $2 \cdot 10^{-2}$ M LiAc. The initial width of the sample zone at t = 0 min corresponds to 2 % of the total length of the separation compartment; the sample is previously dissolved in background electrolyte. Current density 25 A m^{-2}; separation period 0 - 16 min [72].*
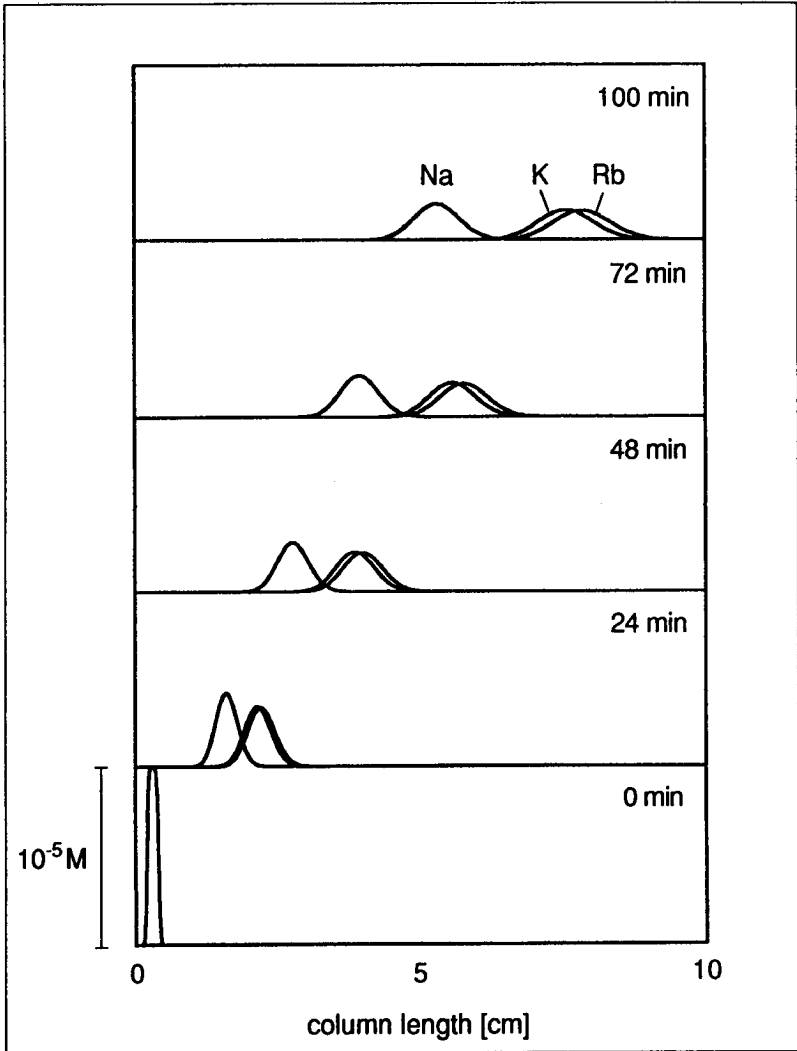
Fig. 3.10 - *Same conditions as for Figure 3.8; separation period 0 - 100 min [72].*
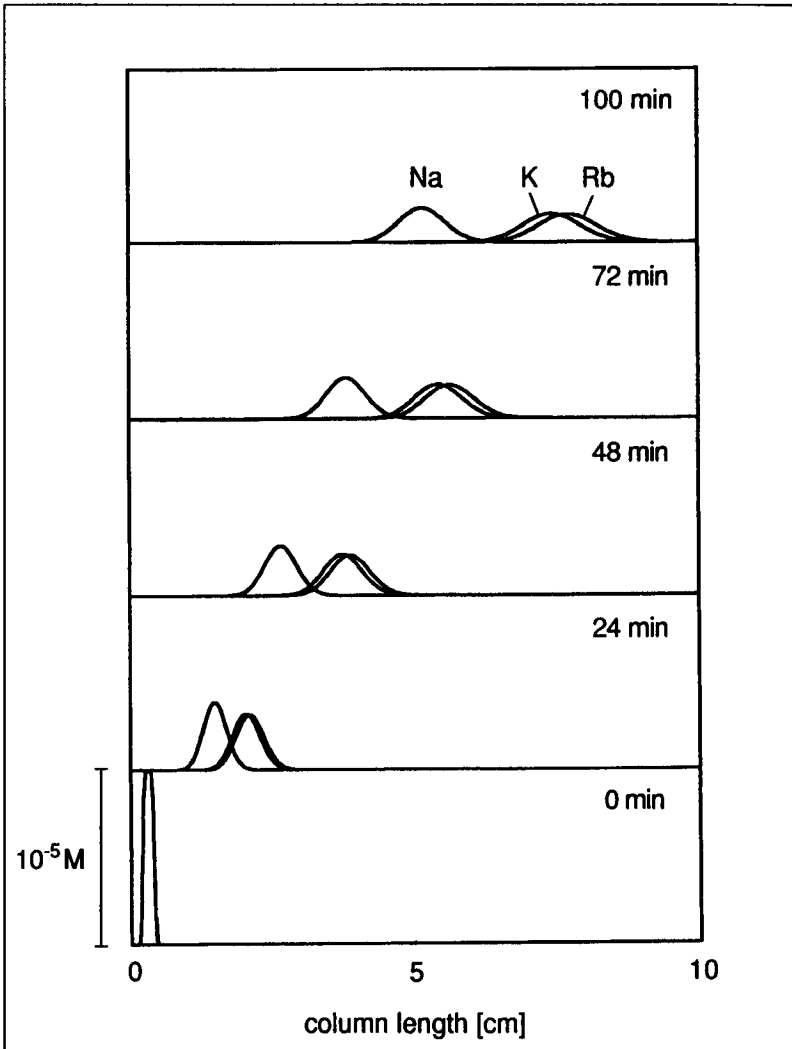
Fig. 3.11 - *Same conditions as for Figure 3.9; separation period 0 - 100 min* [72].

4. Physical and Chemical Aspects of Silica and Fused Silica

4.1. The Structure of Fused Silica

Fused silica is made from silicon dioxide, produced by hydrogen flame decomposition of high purity synthetic silicon tetrachloride, and usually contains as much as 0.1 % hydroxyl groups and less than one ppm of metal ion contamination [73].

The structure and physical properties of fused silica can be compared to those of quartz, which is formed in naturally occurring deposits and is characterized by a relatively high content of metal ions [73].

Fused silica and quartz are amorphous products like porous silica. In all their modifications, each silicon atom is surrounded by four oxygen atoms to give the tetrahedral unit $[SiO_4]^{4-}$. The polymorphism of silica is based on different degrees of linkage between the $[SiO_4]^{4-}$ units. Quartz, a supercooled liquid, possesses the structure of highest density of the three enantiotropic forms (Figure 4.1) [74].

liquified silica

1983 K

β - cristobalite 473 - 548 K α - cristobalite

1743 K

β - tridymite 393 - 433 K α - tridymite

1143 K

846 K

β - quartz α - quartz

supercooled liquid
(vitreous silica, quartz glass)
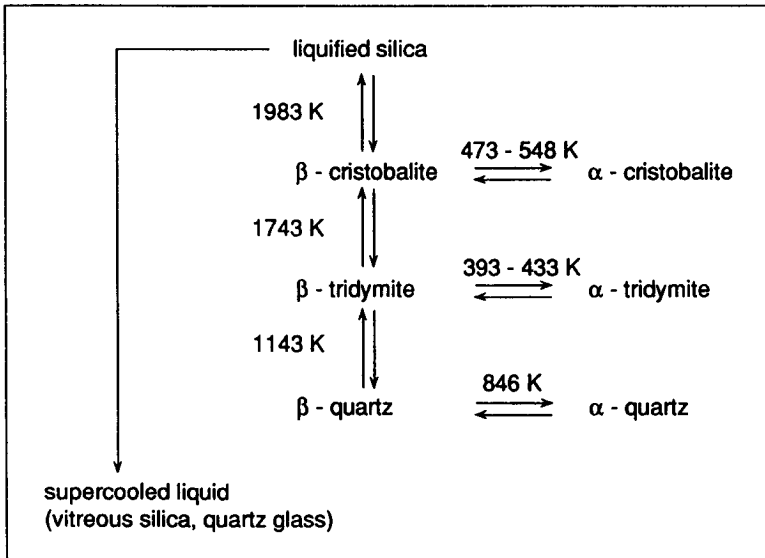
Fig. 4.1 - *Polymorphic forms of silica [74].*

Fused-silica capillaries are manufactured from fused silica at temperatures of ~ 2000 °C under clean-room conditions [75], using continuous infrared laser monitors coupled with a feedback control circuitry. Remarkably uniform capillaries are drawn at rates of approx. 1 - 2 m s^{-1}. Dandeneau and Zerenner first used fused-silica columns with a wall thickness of 25 μm [76]. The thin wall imparts a high degree of flexibility, but, on the other hand, is subject to rapid corrosion, which occurs on exposure to the atmosphere and makes the column extremely fragile. Therefore, a protective sheath of polyimide coating is applied to the outer side of the capillary as it emerges from the drawing oven [77].

4.2. The Surface of Silica and Fused Silica

The glass surface is covered with hydroxyl groups that are attached in various ways to the silicon atoms. Due to the amorphous structure, the silicon atoms carrying the hydroxyl groups (surface silanols) are not equidistant from each other [78]. Therefore, different types of surface silanols can be distinguished [79] (Figure 4.2):

- Isolated silanol groups are assumed to be separated by a distance between two adjacent hydroxyl groups which is considerably larger than 0.31 nm. They are acidic (pK_a = 6.8) and incapable of forming hydrogen bonds with other surface silanol groups.

- For vicinal silanol groups, the distance between adjacent hydroxyl groups is less than 0.31 nm, so that they can interact with other surface silanol groups via hydrogen bonding [80]. Over the range from 0.24 - 0.31 nm, the interaction of the hydrogen bonding is expected to vary in strength. The paired hydroxyl groups are considered to be more reactive than the isolated ones and to play a dominant role in adsorption and reaction processes of silica [81]. Bound silanol groups can undergo dehydration to yield siloxane bridges [77].

- Silanediols (with geminal hydroxyl groups) are most probably present on silica surfaces, but their existence has not yet been proved experimentally [82].

4.3. Chemical and Physical Behaviour of Silica Surfaces

The silanol groups at the surface are involved in a temperature-dependent dehydroxylation-hydroxylation reaction written as [74]

$$
\begin{array}{c}
\text{H} \quad\quad \text{H} \\
/ \quad\quad\quad / \\
\text{O} \quad\quad \text{O} \quad\quad\quad\quad \text{O} \\
| \quad\quad\quad | \quad\quad\quad\quad / \backslash \\
\text{Si} \;+\; \text{Si} \;\rightleftharpoons\; \text{Si} \quad \text{Si} \;+\; \text{H}_2\text{O} \\
/|\backslash \quad /|\backslash \quad\quad /|\backslash /|\backslash
\end{array}
$$
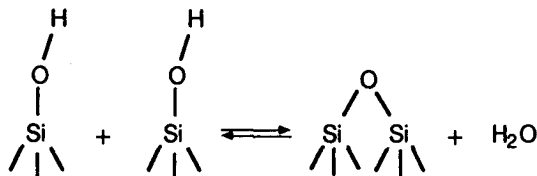
On a fully hydroxylated surface, the water molecules first cover all the SiOH groups by multiple hydrogen bonding [78]. This physically adsorbed water can be removed at 393 K.

Dehydroxylation starts at temperatures above 500 K, causing siloxane bridges to be formed as surface sites which are less polar than the hydroxyl groups. This condensation proceeds with increasing temperature until, at 1473 K, the concentration of hydroxyl groups is negligibly small [78].

The rehydration of strained siloxane bridges is reversible for every type of silica [83]. At higher temperatures however, the parent silicon atoms in the lattice may be shifted and provide strain relief, making rehydration more difficult [84, 85]. The more complete the dehydroxylation of the surface, the more time is necessary for rehydration [86]. In a first step, the rehydration involves the adsorption of water, so that the process probably occurs on siloxane sites next to silanol groups, because the siloxane surface in itself is essentially hydrophobic [87, 88]. The hydroxylated area then grows in patches as the hydration proceeds along the boundary between the rehydrated and the siloxane areas. The surface silanol groups therefore provide the 'nucleation sites' for rehydration. Due to the low concentration of surface silanol groups, this rehydration process proceeds very slowly on fused-silica surfaces.
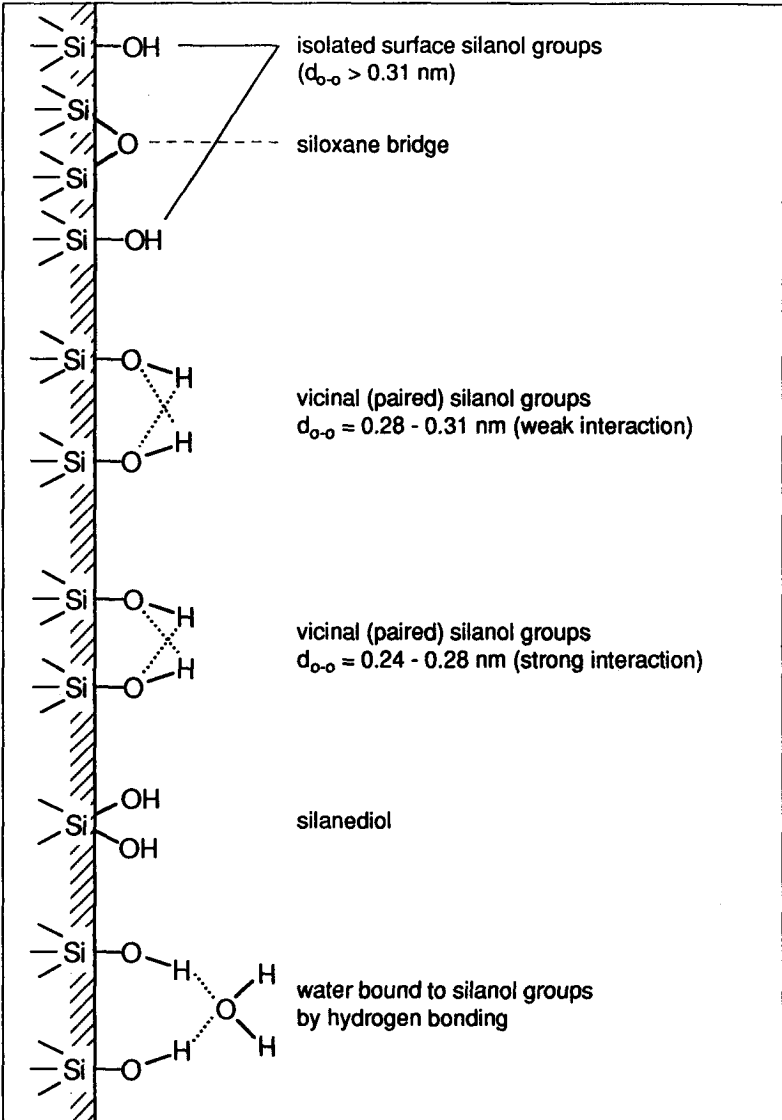
Fig. 4.2 - *Simplified scheme of a silica surface (d_{o-o}: distance between the oxygen atoms of two neighbouring silanol groups).*

4.4. Concentration of Surface Silanol Groups

The concentration of surface silanol groups on a fully hydroxylated, smooth and nonporous amorphous silica surface is, according to the most frequently cited values in review papers, 4 - 5 SiOH groups / nm^2, which remain even when the sample is dried at 120 - 150 °C [86, 89 - 93]. In fused silica capillaries, this value is considerably lower due to the high temperature of manufacture. A value of 0.21 SiOH groups / nm^2 (0.35 μmole SiOH / m^2) has been determined [94].

In principle, it is possible to rehydrate the fused-silica surface. It seems that this process of 'surface aging' proceeds slowly but constantly whenever the surface is in contact with water or moist air [95]. Leaching, e. g. with alkali [96], or hydrothermal treatment with water at 95 °C for a certain period of time [97, 98]. most probably accelerates the process of rehydration on the fused-silica surface. Etching with hydrofluoric acid [78] is not convenient as it dissolves the entire silica framework.

4.5. Ion Exchange Properties of Silica

The acidity of silicic acid increases upon polymerization. The highest pK_a value is reported to be 10.7 for $H_2Si_2O_7$ and decreases to 6.5 for highly polymerized silicic acid [99]. The ratio of undissociated / dissociated silanol groups on a silica surface strongly depends on the pH of the electrolyte. At a pH of about 2, the surface silanol groups of the silica are completely undissociated, i. e., the surface is electrically neutral. In highly basic solutions (pH > 9), the silanol groups become increasingly deprotonated and exhibit strong interaction with metal cations [74].

4.6. Electric Conductivity of the Silica Surface

In the presence of a potential gradient, a glass tube filled with electrolyte provides regions of different conductivity. Beside the ions in the bulk solution, mobile ions in the fixed [100] and in the diffuse [101] double layer (Figure 4.1) can also contribute to the conductivity. In the fixed double layer, the conductivity is due to the hydrogen ions of the silanol groups and depends on the temperature and the concentration of these groups on the silica surface, but was found to be negligibly small [102].
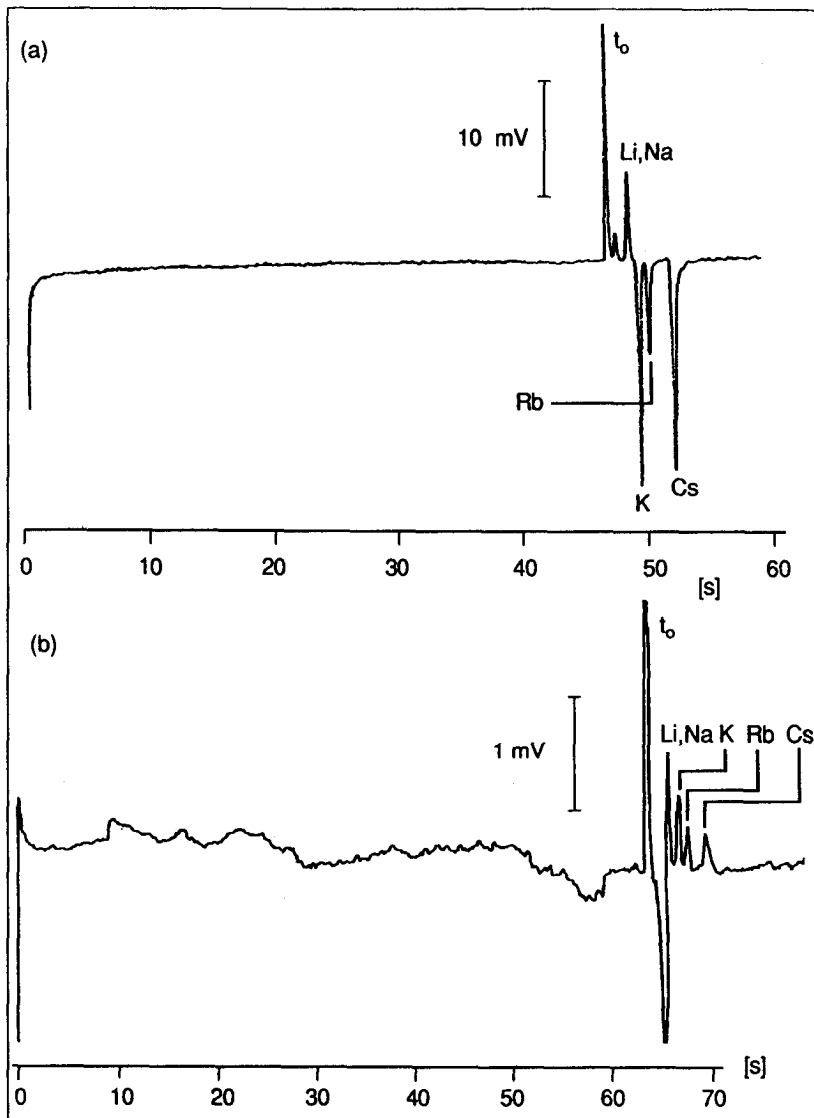
Fig. 4.3 - *Retention due to electrostatic interaction of alkali metal ions with surface silanol groups of untreated fused-silica capillaries of 3.3 μm (a) and 2.3 μm (b) i.d., detected with an ion-selective microelectrode (liquid membrane composition 1, see Table 9.1). Sample 10^{-4} - 10^{-3} M alkali chlorides; mobile phase NH_4Cl, NH_3, pH 9.5; pressure gradient 200 atm (a), 170 atm (b); capillary length 57 cm (a), 44 cm (b).*

The conductivity in the diffuse double layer of thickness δ, κ_δ, can be calculated according to the formula [103]

$$\kappa_\delta = \frac{(\varepsilon_0 \varepsilon_r)^2 \zeta^2}{\eta \, \delta} \qquad (4.1)$$

where ε_0 is the permittivity of vacuum, ε_r the relative dielectric constant of the solvent, η its viscosity and ζ the zeta potential.

The total resistance R per unit length of a capillary with radius r is given by

$$\frac{1}{R} = \pi \, r^2 \kappa \left(1 + \frac{2\kappa_\delta}{r \, \kappa} \right) \qquad (4.2)$$

where $\frac{2\kappa_\delta}{r \, \kappa}$ is the contribution of the surface conductivity in the diffuse double layer to the bulk conductivity κ.

Concentration of the bulk solution [mol l^{-1}]	Capillary i.d. [μm]	Ratio of surface conductivity / bulk conductivity
10^{-2}	25	0.17 %
$5 \cdot 10^{-3}$	25	0.24 %
10^{-5}	25	5.5 %
10^{-2}	10	0.44 %
$5 \cdot 10^{-3}$	10	0.62 %
10^{-5}	10	14 %

Table 4.1 - *Relative contribution of surface conductivity in the diffuse layer to the conductivity of the bulk solution in a fused-silica capillary.*

5. Zeta Potential and Electroosmosis

5.1. The Zeta Potential

When an aqueous electrolyte solution comes into contact with a solid surface, a fixed electric double layer in the form of a plate condenser establishes at the interface (Figure 4.1). The charge will be distributed in a way that the phase with higher dielectric constant is always positively charged [104], which is usually the case for aqueous solutions in contact with silica or teflon surfaces. Cations are adsorbed onto the surface, retaining their hydration shell [105]. Specifically adsorbed anions lose their hydration shell, so that they can approach the surface closer than the hydrated cations. According to Graham [106], the plane through the centers of the of the adsorbed anions (inner Helmholtz plane) encloses the inner Helmholtz layer (Stern layer). The outer Helmholtz plane is limited by the centers of the hydrated cations which, under the influence of electrostatic forces, have a minimum distance from each other. The hydrated cations thus form a rigid layer of fixed charges along the negatively charged surface which is called the outer Helmholtz layer (Figure 4.1). On the liquid-phase side of the interface, thermal motion continually disperses ions to a greater distance from the phase boundary. This so-called diffuse or Gouy layer of electric charges reaches into the bulk solution [107]. The charge accumulated by the specifically adsorbed cations on the outer Helmholtz plane is partly compensated by a change in the charge of the diffuse double layer [108].

The potential and the distribution of the ions in the diffuse double layer is given by the Gouy-Chapman theory [109, 110], which is based on the combination of the Poisson and Boltzmann equations. The surface charge per unit area, e_s, on the outer Helmholtz plane generates a Helmholtz potential, φ_0, given by the relation

$$e_s = \left(\frac{2n \, \varepsilon_0 \, \varepsilon_r \, k_b T}{\pi} \right)^{0.5} \sinh \frac{ze\varphi_0}{2k_bT} \qquad (5.1)$$

where ε_0 is the permittivity of vacuum, ε_r the relative dielectric constant of the solvent, k_b the Boltzmann constant, T the absolute temperature, z the charge number, e the electric charge, and n the number of ions in the diffuse double layer according to the Boltzmann distribution.

The operational equation for an aqueous solution at 25 °C is [107]:

$$e_s = 11.72 \, c^{0.5} \sinh (19.46 \, z \, \varphi_0) \tag{5.2}$$

where the units of e_s, c and φ_0 are $\mu C \, cm^{-2}$, mol l^{-1} and V, respectively.

In the rigid layer, *i. e.* the layer of closest approach of the cations to the surface [111], the surface potential decays linearly. With increasing distance x (x = 0 for the outer Helmholtz plane) the Helmholtz potential, φ_0, decreases exponentially into the bulk solution (Figure 4.1) [107]:

$$\varphi = \varphi_0 \exp \left(- \frac{x}{\delta} \right) \tag{5.3}$$

The zeta potential, ζ, is defined as the potential difference between the outer Helmholtz plane (x = 0) and the bulk solution (x = δ), where the Helmholtz potential, φ, reaches a level of 1 / e (e = 2.718) of its initial value, φ_0, and is given by [112]

$$\zeta = \frac{4 \pi \delta \, e_s}{\varepsilon_0 \, \varepsilon_r} \tag{5.4}$$

The term $\frac{\varepsilon_0 \, \varepsilon_r}{4 \pi \delta}$ is the capacity of a parallel plate condenser with the plate distance δ. The thickness of the diffuse double layer, δ, may be regarded as the distance at which the ionic charges accumulate. The zeta potential therefore is not a phase boundary, because it develops wholly within the liquid medium. Polar solvents, *e. g.* water, give rise to zeta potentials of as much as 0.1 V in contact with either polar (*e. g.* glass) or non-polar (*e. g.* graphite) surfaces [113].

For aqueous solutions at 25 °C, δ can be approximated by [107]

$$\delta = \frac{3 \cdot 10^{-10}}{z \, c^{0.5}} \, [m] \tag{5.5}$$

and depends on the ionic strength (or concentration) of the solution. It can assume values in the range of 10 - 100 nm for dilute electrolyte solutions. At higher concentrations of up to 0.1 M (high ionic strength) the thickness of the double layer is < 1 nm [114].
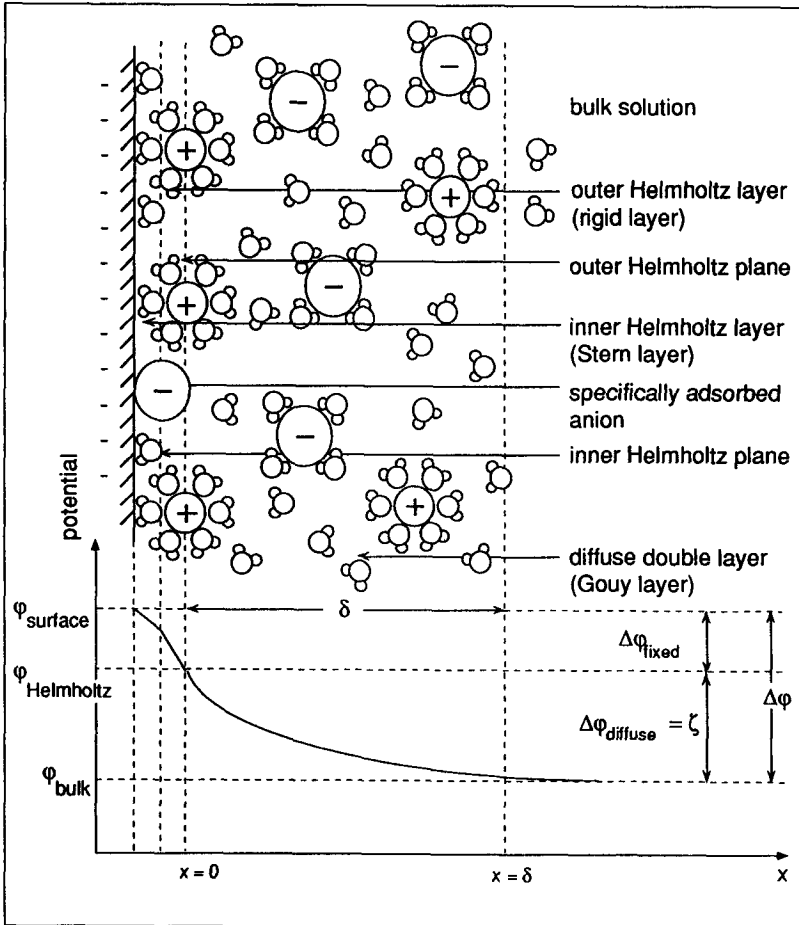
Fig. 5.1 - *Geometrical interpretation of the zeta potential* ζ.

5.2. Electroosmosis

Electroosmosis is the flow of liquid in contact with a solid surface which occurs under the influence of a tangentially applied electric field [115]. The electroosmotic force produced by this field is transmitted by the movement of ions acting in a thin sheath of fluid adjacent to the surface. Owing to frictional forces among the solvent molecules, this movement immediately spreads over the whole liquid phase. It can be assumed that the movement of the liquid never begins immediately next to the surface, but that a stationary layer with a thickness of one to several molecules is always present. The outside boundary of this layer is called slipping plane [107]. According to Poiseuille's law, the electric force is exactly balanced by the viscosity forces of the bulk fluid. The velocity of the fluid increases from the wall to the inner boundary of the sheath, and the bulk solution moves with the velocity of this boundary. The resulting flow profile is virtually rectangular (Figure 5.2).

According to the Helmholtz-Smoluchowski equation [116 - 118], the resulting electroosmotic flow velocity of the bulk solution is directly proportional to the zeta potential and the applied electric field E:

$$v_{osm} = \left(\frac{\varepsilon_0 \varepsilon_r}{\eta}\right) E \zeta \qquad (5.5)$$

Equation 5.5 shows that the electroosmotic flow velocity is independent of the geometry of the separation compartment, but it is only valid if surface conduction due to ions in the double layer (Section 3.6) is negligible. This, however, is not the case in extremely narrow channels ($< 1 \mu m$) at low ionic strength [117, 119]. Further limitation is caused by the fact that under the influence of high electric field strength, the dielectric constant and the viscosity change considerably [120].

5.3. Electroosmotic Flow in Capillaries

The electric charge in fused silica capillaries is generated through the dissociation of the acidic silanol groups of the surface when it comes into
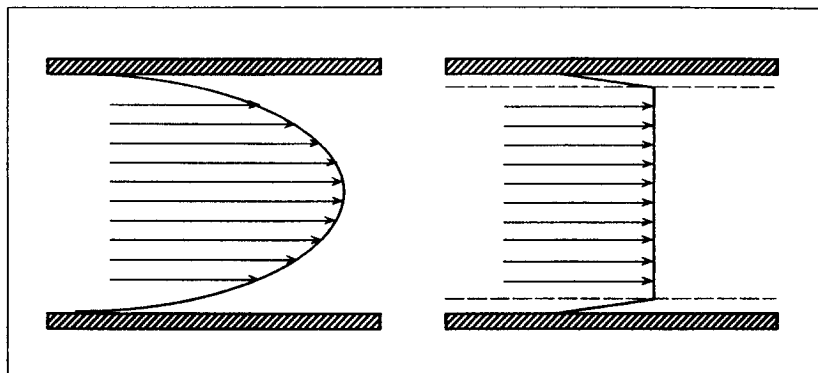
Fig. 5.2 - *Hydrodynamic (left) and electroosmotic flow profile (right).*

contact with an electrolyte solution. By assuming a concentration of 0.21 surface silanol groups / nm² on a fused-silica surface (Section 4.4) and a diffuse double layer of 10 nm, a zeta potential of 6 V should result according to Equation 5.4. However, according to Formula 5.5 values between 0.09 - 0.13 V were calculated from the velocity of the electroosmotic flow in fused silica capillaries filled with Na_2HPO_4 buffer (pH 8 - 9). This leads to the conclusion that most of the surface charge is balanced by counter ions from the solution that are adsorbed in the Stern layer, thus lowering the zeta potential.

The electroosmotic flow velocity usually is in the order of 0.3 - 2.2 mm s⁻¹ [24]. In a fresh fused silica capillary, the migration time steadily decreases for consecutive measurements, corresponding to an increase in the electroosmotic flow velocity [121]. This phenomenon is caused by rehydration processes and adsorption of ions on the surface of the capillary, which constantly change the zeta potential. This effect is the major problem for reproducing the electroosmotic flow velocity in untreated fused silica capillaries.

The dissociation of the surface silanol groups is a pH-dependent equilibrium (Section 3.5) and determines the electroosmotic flow rate in fused silica capillaries. Usually, at constant ionic strength of the buffer solution, the electroosmotic flow rate steadily increases up to a pH of 7 - 8 [24, 122 -125]. At pH values > 6, the electroosmotic flow is sufficiently high to ensure a net migration towards the cathode for most analytes, irrespective of their charge [126]. Cationic and anionic species can be separated in a single run. In some

cases, by using buffers of constant concentration, lower electroosmotic flow rates are also obtained at higher pH values. This effect is attributed to the ionic strength and is observed with buffers prepared by titrating a weak acid with a strong base [127].

5.4. Chemical Modification of Zeta Potential and Electroosmotic Flow

According to Equation 5.5, magnitude and direction of the electroosmotic flow are determined only by the amount and sign of the surface charge on the inner wall of the capillary column, which depend on the column material itself. Beside the effect of pH and ionic strength, there are two different possibilities to influence the zeta potential and the electroosmotic flow in capillaries:

(i) Additives to the mobile phase

(ii) Chemical modification of the surface with polymers (a) or silanes (b)

(i) It is possible to modify or completely reverse the direction of the electroosmotic flow by the use of organic solvents [121] or mobile phase additives [123, 128 - 130]. The modifying agent should bear a charge of opposite sign to that of the original surface and also have the property of being tightly adsorbed onto or equilibrated with the column surface. Modifiers like cetyltrimethylammonium bromide have been successfully used in CE [131].

(ii) (a) Stable polymeric coatings, immobilized on the fused silica surface by cross-linkage or strong adsorption, usually decrease the electroosmotic flow and the degree of solute adsorption on the surface, depending on the functional groups of the polymerized layer. With surface coatings having strong acidic or basic groups, the flow is independent of pH and buffer. Good flow reproducibilities can be achieved with polyacrylamide-coated capillaries [132]. The electroosmotic flow can be completely suppressed by a polyethylene glycol surface coating [133 - 136]. Other possible modifications are methylcellulose [137], glycol [138], poly(vinylpyrrolidone) [124] and glycerol-glycidoxypropyl [124] coatings. For poly(ethyleneimine)-coated tubes [139] the direction of the electroosmotic flow is completely reversed. The long-term stability of these coatings at higher pH still presents major problems.

(ii) (b) The surface of a fused-silica capillary can be chemically modified by bonding a silanization reagent to the surface silanol groups. Specifically functionalized organosilanes are attached to the capillary wall *via* Si-O-Si siloxane linkage:

$$\text{surface-Si-OH} + X_nSiR_{4-n} \rightarrow \text{surface-Si-O-SiX}_{n-1}R_{4-n} + HX$$
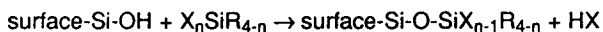
where n = 1 to 3, R is an alkyl or substituted alkyl group and X is an easily hydrolyzable group, such as halide, amine, alkoxy or acyloxy [74].
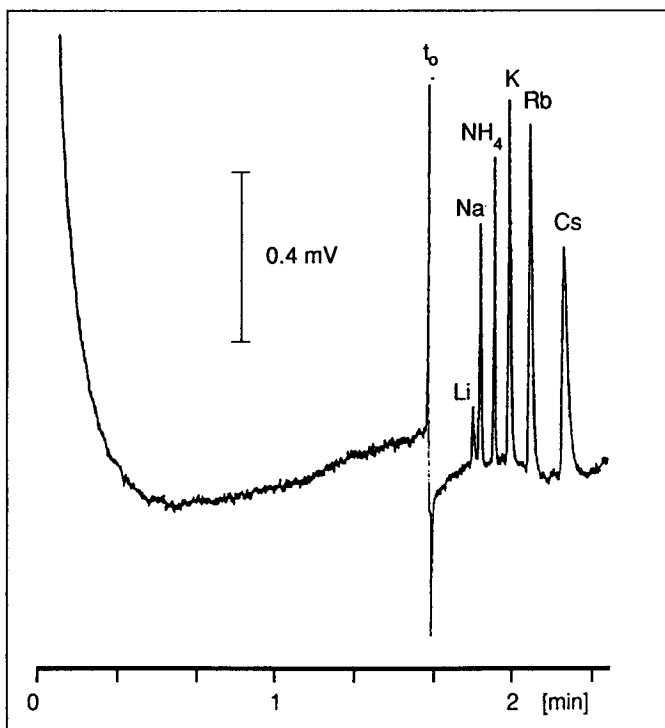
Fig. 5.3 - *Chromatographic separation of alkali and ammonium ions in a fused-silica capillary coated with 3-sulfopropylsilanetriol [140]. Sample 10^{-4} - 10^{-3} M alkali chlorides in water; mobile phase 10^{-2} M formic acid; pressure 202 atm; capillary length 114.4 cm, i.d. 4.6 μm; detector ion-selective microelectrode (liquid membrane composition 1, Table 9.1), on-column. The chromatographic retention decreases for subsequent runs due to the chemical instability of the bonded phase.*

When a monofunctional silane (n = 1) is used, only a single surface-silane linkage is possible so that an intrinsically reproducible monolayer is formed. Di- or trifunctional silanes (n = 2, 3) react with the silica surface in the presence of a small amount of water to give an organic layer. Although this dynamic coating procedure is a very elegant and rapid method, it presents severe disadvantages. With multifunctional silanes, the dynamic coating method does not allow to control the polymerization process, resulting in irreproducible phase thicknesses. In addition, its application is limited by the long-term instability of the siloxane layer [140]. The use of silanes, such as trimethylchlorosilane [141], glycidoxypropyl-trimethoxysilane and trimethoxy-aminopropylsilane [142], organosilane-bonded acrylamide [137] and poly(ethylene) glycol phases [135] as coating agents in CE has been described. Due to the unsatisfactory hydrolytic stability of the Si-O-Si-C linkage, this type of bonded phase does not meet all the requirements regarding long-term column stability and performance [143 -147]. Better results are achieved with bonded phases bearing direct Si-C linkages with the capillary surface [148 - 150], thus obtaining a denser covering with organic functional groups and hydrolytically more stable bonded phase [151].

5.5. Migration Time and Separation Efficiency

Due to the electroosmotic flow, the equations for migration time t and separation efficiency (given as the number of theoretical plates, N) have to be modified:

$$t = \frac{L^2}{(\mu_{el} + \mu_{osm})\, V} \qquad (5.6)$$

$$N = \frac{(\mu_{el} + \mu_{osm})\, V}{2D} \qquad (5.7)$$

where μ_{osm} is the electroosmotic mobility, L the total length of the capillary, D the diffusion coefficient and V the applied voltage.

Equation 5.7 obviously indicates that a high electroosmotic flow rate will yield

good separation efficiencies in terms of theoretical plates. However, the flow itself does not accomplish any separation and is actually detrimental to the resolution [141], as it reduces the time for zones to separate. In the presence of electroosmotic flow the resulting zones will therefore appear sharper (due to the higher number of theoretical plates) but more poorly resolved.

It has to be pointed out that the width of a peak in an electropherogram does not reflect the actual length of the zone in the separation compartment. A zone migrating slowly will give a broader peak than a faster one, even if the two zones have the same length when they pass the detector [152].

5.6. Resolution

In CE, the resolution, R_S, of two zones is given by [49]

$$R_s = \frac{\sqrt{N}}{4} \frac{(\mu_{el,1} - \mu_{el,2})}{(\mu_{el,av} + \mu_{osm})} \tag{5.8}$$

or

$$R_s = 0.177 \, (\mu_{el,1} - \mu_{el,2}) \left(\frac{V}{(\mu_{el,av} + \mu_{osm}) D} \right)^{0.5} \tag{5.9}$$

where $\mu_{el,1}$ and $\mu_{el,2}$ are the electrophoretic mobilities of the two solutes to be separated, $\mu_{el,av}$ is their average mobility and V the applied voltage.

At constant length of the capillary, the resolution of two separated zones can be affected by the electroosmotic flow velocity. To optimize the resolution, the procedure employed for controlling μ_{osm} must not significantly reduce the separation efficiency. Due to the flat flow profile provided by the electroosmotic flow, the separation efficiency according to Equation 5.7 can only be expressed in the absence of Joule heat and extra-column band broadening. In the presence of Joule heat however, a radial viscosity gradient establishes inside the capillary and as a result, the separation efficiency may decrease considerably [50, 141, 153 - 155]

6. Detection Systems in Capillary Electrophoresis

6.1. General Requirements for a Detection System

In every electrophoretic separation a compromise between the dispersive influences of longitudinal diffusion and Joule heat has to be found. As shown in Figure 3.7, these two parameters have a complementary effect. Fast separations carried out under high voltage reduce the deteriorating influence of the longitudinal diffusion, but may generate a pronounced temperature gradient due to Joule heat in the separation compartment. The latter can be minimized by employing separation compartments of small volume (short and narrow capillaries). As many CE separations are carried out in capillaries of 50 - 100 μm i.d., the effective detection volume is below the picoliter level when a sample zone of 0.5 mm length is assumed (Table 6.1). Zone concentrations in the milli- and micromolar range therefore require a suitable detection system with high molar sensitivity. Additional features like fast response times and a sufficient linear dynamic range are also required. The data given below can be compared with the detection limits of systems reported in the literature (Figure 6.1). Obviously, not all detection methods are suitable for miniaturized separation systems.

Capillary i.d.	Volume of a sample zone of 0.5 mm length	Moles per zone volume for a sample concentration of 10^{-5} M
500 μm	98 nl	98 pmol
200 "	16 "	16 "
100 "	4 "	40 fmol
50 "	982 pl	10 "
25 "	250 "	3 "
10 "	40 "	400 amol
5 "	10 "	100 "
1 "	400 fl	4 "

Table 6.1 - *Required molar sensitivity of a detection system as a function of the i.d. of the capillary.*
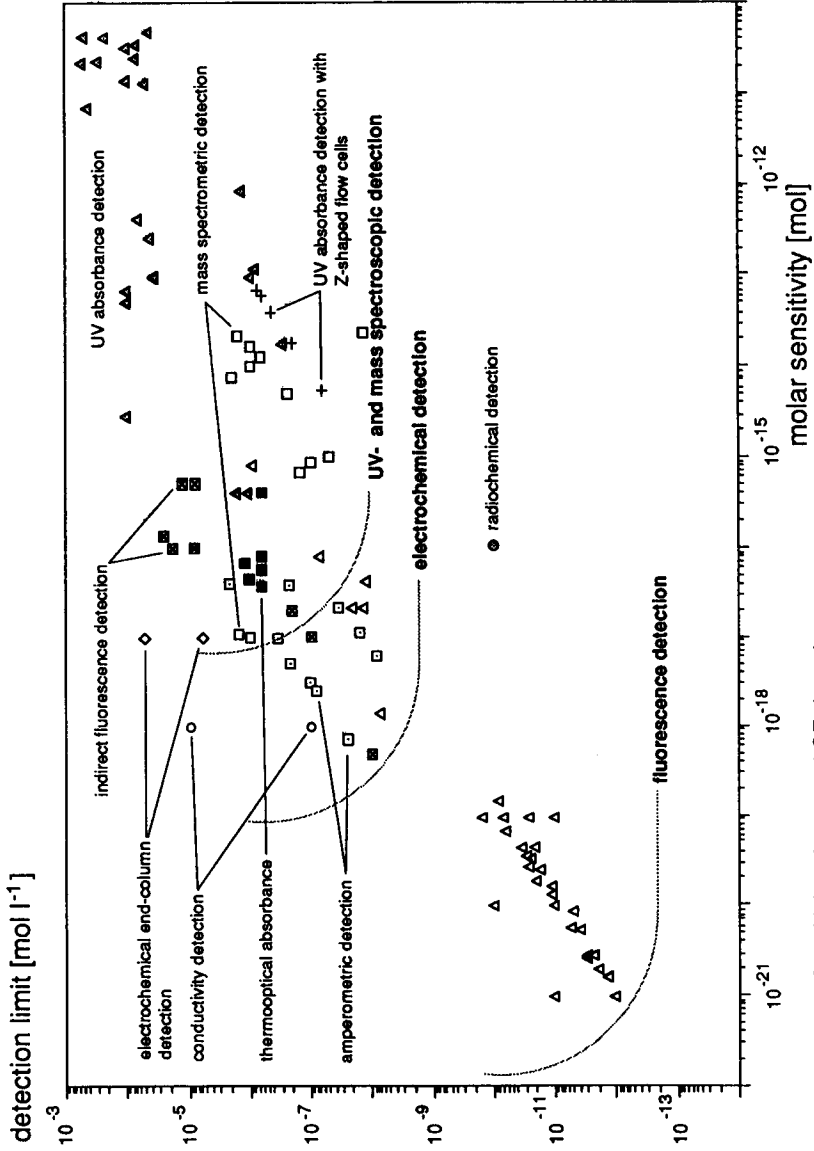
Fig. 6.1 - *Sensitivity of reported CE detection systems.*

6.2. Detection Methods in Capillary Electrophoresis

In general, the detection methods used in CE can be classified into four principal types:

- Optical and spectroscopic detection
- Fluorescence detection
- Radioactivity detection
- Electrochemical detection

6.2.1. Optical and Spectroscopic Detection

The most widespread detection method in CE is UV spectroscopy [156]. It is almost universally applied for different kinds of solutes, including the important domain of biopolymers (proteins, nucleic acids and their constituents, polysaccharides, *etc.*). The UV detection follows Lambert-Beer's Law and depends on the pathlength of the absorbing material. Even for strongly absorbing species, the detection limit for on-column UV detection increases drastically with decreasing i.d. of the capillary. Although this disadvantage can partly be overcome by focusing the light beam in a Z-shaped flow-cell along the migration path [157], this optical method generally suffers from bad molar sensitivity.

By combining CE with mass spectrometry (CE-MS), high sensitivities and detailed structural information about the individual sample constituents can be obtained [158]. The end of the capillary is placed into an electrospray interface combined with a quadrupole mass filter to permit on-line detection. A metal needle or a thin conductive film deposited on the capillary end ensures electric contact between anode and cathode. Sensitivities achieved by MS detection usually range between those of optical and electrochemical detection methods.

6.2.2. Fluorescence Detection

Detection by fluorescence [141] is a much more sensitive method than UV absorption. As the intensity of the fluorescence is directly proportional to that of the excitation radiation, it is possible to achieve remarkable results by using

lasers. Detection limits in the range of a few thousand molecules have been attained [159]. A certain drawback of this technique is the need for marking the sample with fluorescence tags prior to detection, since only few molecules emit adequate fluorescence light. An interesting alternative is the detection by indirect fluorescence, i.e. 'looking at what is not there' [160]. The fluorophore is simply added to the buffer, and each individual sample zone then leads to a drop in the fluorescence intensity at the detector. The method requires no preparation of derivatives, but detection limits are considerably higher than those obtained with direct detection.

6.2.3. Radioactivity Detection

Radioactivity detection can be achieved by passing radioactively labeled sample zones through a solid block of scintillator material or a cadmium telluride probe [161]. The sensitivity of the detector can be increased by increasing the residence time of the sample zones within the detection zone, thus prolonging the scintillation counting. A stopped flow mode obtained by sophisticated voltage programming leads to detection limits that are comparable with those of fluorescence detection.

6.2.4. Electrochemical Detection

6.2.4.1. Potential Gradient Detection

In the literature, potential gradient detection is often incorrectly referred to as potentiometric detection. This terminology is misleading since the potentiometric response of an electrochemical sensor corresponds to the electromotive force due to changes in the ionic activity according to the Nernst equation. The potential gradient response, on the other hand, is based on Ohm's law and is generated by a difference in the electric field strength between the migrating zones depending on the individual ionic conductivities. Potential gradient detection was employed by Virtanen [60], who inserted a glass pipette, containing a Pt wire coated with Ag / AgCl in contact with a chloride solution, into a separation tubing of 215 μm i.d. He obtained electropherograms for some inorganic cations (K^+ , Na^+ , Li^+) injected in the millimolar range.

Potential gradient detection can also be carried out by measuring the difference in the electric field strength between two axially shifted sensing electrodes in the separation compartment which are in direct contact with the electrolyte solution. Usually, the resulting signal is very low, since according to commonly employed separation conditions, the concentration of the detected sample ions is by two orders of magnitude lower than that of the background electrolyte. The drift and noise due to electrochemical reactions at the sensing electrodes prevent sensitive detection and reliable quantitative interpretation of the recorded signal [37].

6.2.4.2. Conductivity Detection

Conductivity detection is a two-electrode potential gradient detection. The sensing electrodes are arranged opposite to each other in the separation compartment and are in direct contact with the electrolyte solution. The signals arise from changes in the conductivity between the different eluting zones. It can be positive or negative in respect to the baseline, thus indicating whether a zone has a lower or higher conductivity than the background electrolyte. From the electronic point of view it is important that the detection cell is kept at ground potential. The sensing electrodes must be separated from the electrometer by resistors and should be placed near the grounded end of the separation capillary, so that the current leakage *via* the electronic system is minimized [37].

Zare and coworkers [162, 163] introduced an on-column conductivity detector consisting of two Pt wires (25 μm o.d.) fixed in diametrically opposite holes of the fused-silica capillary tubing (50 or 75 μm i.d.). Detection limits of about 10^{-7} mol l^{-1} for Li^+ were obtained.

6.2.4.3. Amperometric Detection

Amperometric detection in CE is employed for easily oxidizable compounds. The working electrode consists of a carbon fiber [164] of 5 μm o.d. which is inserted into the end of the capillary. A fiber electrode potential of + 0.8 V (vs. Ag / AgCl) is maintained during the detection process. With this method, Wallingford and Ewing obtained remarkable detection limits for some catecholamines separated in capillaries of 9 μm [165] and 12.7 μm [166] i.d.

(see Table 6.2). A major drawback lies in the fact that the detected signal can be as low as 0.1 pA, whereas the electric current in the separation capillary usually is higher by six orders of magnitude when a potential of 10 - 30 kV is applied. This incompatibility can be overcome by grounding the current-conducting effluent, prior to the detection point, with an electrically conducting joint [21, 167, 168] (see also Chapter 9).

Solute	Detection limit		Capillary i.d.
	[amol]	[mol l^{-1}]	[μm]
dopamine	2.4	8.3 · 10^{-8}	9
serotonin	6.0	8.5 · 10^{-9}	12.7
norepinephrine	11	1.6 · 10^{-8}	12.7
epinephrine	4.5	2.5 · 10^{-7}	9
isoproterenol	22	3.4 · 10^{-8}	12.7
L-DOPA	39	2.2 · 10^{-6}	9

Table 6.2 -*Detection limits for some catecholamines obtained with amperometric detection [165, 166].*

7. Potentiometric Detection in Capillary Electrophoresis

7.1. Characterization of the Ion-Selective Microelectrode

An ion-selective electrode is a potentiometric sensor with which the activity of an ion in solution can be determined in the presence of other ions. It consists of an ion-selective membrane which is electrically connected with an internal reference electrode *via* an electrolyte solution [169] (Figure 7.1). Under ideal conditions, the potentiometric signal only depends on the activity of the sample ion.

Ion-selective electrodes are generally classified according to the type and composition of their membrane:

- Solid state membranes [170, 171]
- Glass membranes [172, 173]
- Liquid membranes, which according to their ion-selective composition can be further classified into ion-exchanger [174], neutral carrier [175] and charged carrier [175] membranes.

Ion-selective microelectrodes usually have a tip diameter between 0.1 - 1 µm [176]. The tip is filled with a lipophilic liquid membrane solution up to a height of 200 - 300 µm. For better stabilization of the membrane and to ensure additional insulation between the microelectrode and the sample, the walls of the glass pipette are previously made hydrophobic by silanization [177] (see Chapter 10). The membrane is then covered by the inner filling solution which establishes the electric contact with the internal reference electrode.

In recent years, the use of ion-selective microelectrodes as on-column detectors in open-tubular liquid chromatography has been described in all its theoretical and practical aspects [178, 182, 184, 190, 191]. In this work, the fundamentals of the microelectrode as a potentiometric detector in CE will be presented.
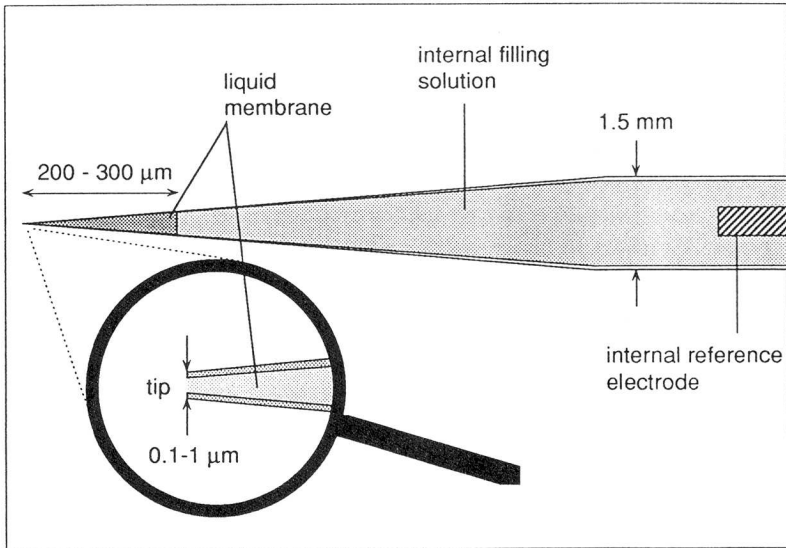
Fig. 7.1 - *Ion-selective microelectrode.*

7.2. Electromotive Response of the ISE

The activity of an ion in solution is measured by combining the ion-selective sensor with a reference half-cell whose potential ideally is sample-independent. In order to improve the stability of the measured signal, the circuit is extended with a low-impedance or common electrode (differential registration method) [179].

The electromotive force (emf) of a complete potentiometric cell assembly, *e. g.*

$$Hg \Big| Hg_2Cl_2 \Big| KCl\ (sat.) \Big| KCl\ (3M) \Big| \begin{matrix} sample \\ solution \end{matrix} \Big\| membrane \Big\| MgCl_2\ (0.02\ M) \Big| AgCl \Big| Ag$$

$$\underbrace{\hspace{5cm}}_{reference\ electrode} \qquad \underbrace{\hspace{5cm}}_{ion\text{-}selective\ microelectrode}$$
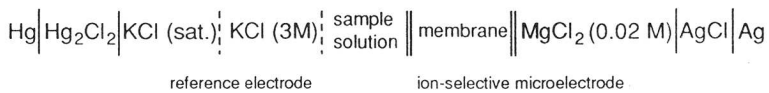
can be approximated by the Nicolsky-Eisenman equation [180]:

$$E = E_0 + 2.303 \frac{RT}{z_iF} \log \left(a_i + \sum_{i \neq j} K_{ij}^{pot} a_j^{z_i/z_j} \right) \qquad (7.1)$$

where E is the value of the emf, E_0 is a potential difference comprising a constant potential plus the electrolyte-dependent liquid junction potential at the reference electrolyte / sample solution interface, R_0 the gas constant, T the absolute temperature and F the Faraday constant; z_i, z_j and a_i, a_j are the charges and activities, respectively, of the ions, i and j, in the sample solution. For a singly charged cation ($z = 1$) at 25 °C, the factor $2.303 \frac{RT}{F}$ has a value of 59.16 mV.

Fig. 7.2 - *Illustration of the functional characteristics of an ion-selective electrode. I and J are the electrode response functions for singly charged cations ($z_i = z_j = +1$), K for a doubly charged cation ($z_k = +2$) at 25 °C.*

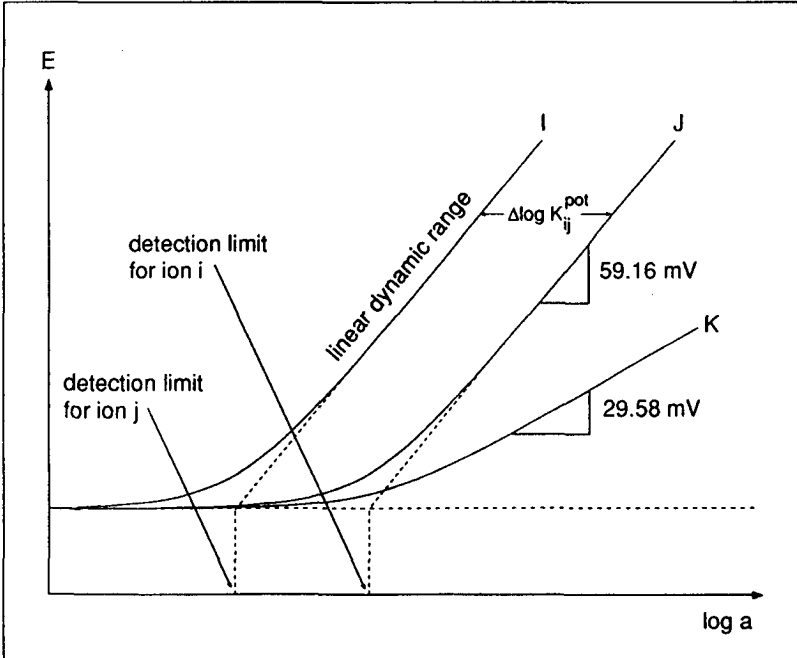The dimensionless so-called potentiometric selectivity coefficient, K_{ij}^{pot}, describes the degree of interaction between the ions, i and j, in solution and the ion-complexing component of the membrane (ionophore). For an ideal ion-selective electrode with Nernstian response, $K_{ij}^{pot} = 1$ for the analyte ion, i, and $K_{ij}^{pot} < 1$ for all other (interfering) ions, j. When displayed on a logarithmic scale, a selectivity difference of one logarithmic unit (at 25 °C) is equivalent to a difference of 59.16 mV for a singly charged and 29.58 mV for a doubly charged ion.

Theoretically, the difference in the selectivity coefficients for two ions, i and j, of equal charge is constant over the whole linear activity range (Figure 7.2). In practice, however, this is not the case since the slopes of the corresponding electrode response functions usually differ from each other, so that the selectivity coefficient is not a constant value but depends on the activity of the measured ions [181]. For ions of different charge, the empirical Nicolsky-Eisenman equation is not exactly defined since the selectivity ratio in this case is not constant either.

7.3. Selectivity and Sensitivity of a Potentiometric Detector in a Flow-Through System

In a zone electrophoretic experiment, as shown in Figure 7.3, the total activity and ionic strength of the electrolyte solutions are time-dependent. The value of the electromotive force therefore varies with time according to the activity changes of the eluting sample zones. Equation 7.1 becomes

$$E(t) = E_0 + 2.303 \frac{RT}{z_i F} \log \left(a_i(t_k) + \sum_{i \neq j} K_{ij}^{pot} a_j(t_m)^{z_i/z_j} \right) \qquad (7.2)$$

At $t = t_k$, the electromotive force is only a function of the activity a_i. At $t = t_m$ and with only one ion j being present, the emf changes to a value determined by the activity of this ion j and its selectivity coefficient in respect to the background ion i (in presence of a reduced activity, a_i').
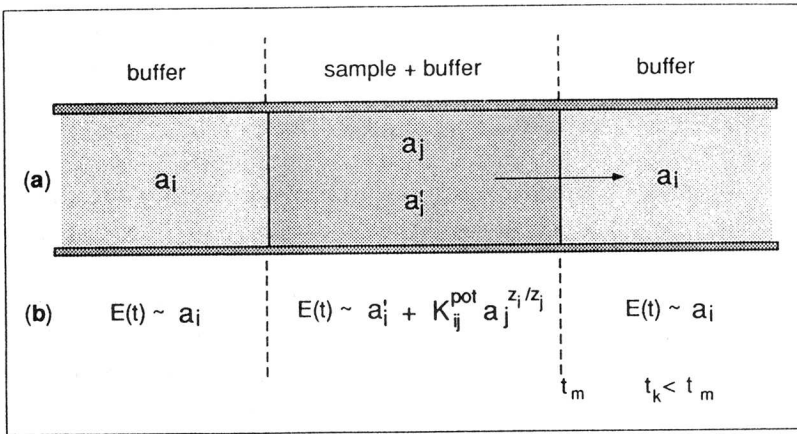
Fig. 7.3 - *Changes in the ionic activity (a) and in the corresponding electromotive force, E(t), (b) due to the migration of a sample zone.*

In CE, the selectivity requirements for sample and background ions differ from those in analytical applications of ion-selective electrodes. An ideal potentiometric detector should have identical selectivities for all ions which have already been (selectively) separated by CE according to their individual migration times. The selectivity coefficients for these ions relative to the background ion determine the sensitivity of the system.

When a sample zone containing the ion j (activity a_j) migrates in a background electrolyte containing the ion i (activity a_i), the meaning of the potentiometric selectivity factor, K_{ij}^{pot}, is defined as follows:

- $K_{ij}^{pot} < 1$:   the background ion i is preferred over the sample ion j
- $K_{ij}^{pot} = 1$:   equal selectivity for ions i and j
- $K_{ij}^{pot} > 1$:   higher preference of the sample ion j against the background ion i (with $K_{ij}^{pot} = 1/K_{ji}^{pot}$).
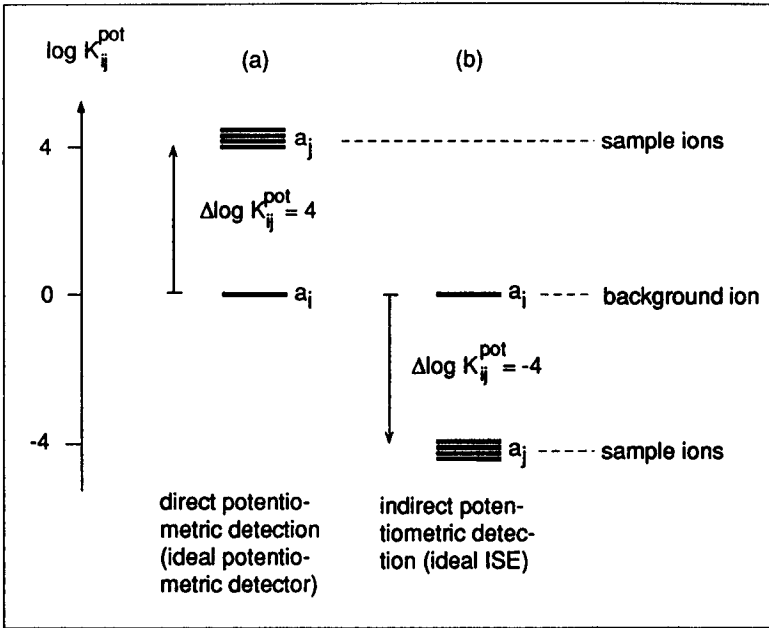
Fig. 7.4 - *Required selectivities for the ideal potentiometric detector (a) and the ideal ion-selective electrode (ISE) (b). Direct or indirect potentiometric detection is determined by the selectivity of the background ion relative to the sample ions.*

The difference, ΔE, between the electromotive forces corresponding to the sample ions and the background ion, j and i, is given by

$$\Delta E = 2.303 \frac{RT}{z_i F} \log \left(\frac{(a_i - a_j) + K_{ij}^{pot} a_j^{z_i/z_j}}{a_i} \right) \qquad (7.3)$$

As a consequence of Equation 7.3, the electromotive response of the potentiometric detector is not linear in the activity of the eluted ions. The recorded signals therefore are broader and show more overlap than conventional profiles, which are linear functions of the concentration of the eluted species [182].

The difference in the electromotive forces is strongly dependent upon the

activities of the components i and j and their selectivity ratio. The selectivity coefficient and activity of the background ion thus determine the sensitivity of the entire system. This fact is illustrated in Figure 7.4. The so-called ideal ion-selective electrode prefers one single ion, i, and discriminates the interfering ions, j. In contrast, the ideal potentiometric detector prefers all ions except that which is used as the background ion. Two different detection modes are therefore possible and are distinguished according to the value of the potentiometric selectivity coefficient:

1) The direct potentiometric detection (for log $K_{ij}^{pot} > 0$). The emf signals of the sample are measured directly against a background electrolyte containing an ion i with low selectivity relative to the sample ions j (Figure 7.4 - (a)).

2) The indirect potentiometric detection (for log $K_{ij}^{pot} < 0$). A background ion is chosen which has a high selectivity with respect to the sample ions. The migrating sample zones then give rise to negative emf signals whose magnitude reflects the displacement of the ionic background by these ions (Figure 7.4 - (b)).

Figure 7.5 is a plot of Equation 7.3, comparing the theoretical detection limits that can be obtained with the direct and the indirect method for a set of selectivity coefficients, log K_{ij}^{pot}, ranging from 4 to -4. The detection limit of an ion-selective electrode is defined as the point of intersection between linear response and constant emf [183] (see Figure 7.2). The higher the selectivity difference between sample and background ions, the lower the detection limit in the direct mode. The situation is reversed for the indirect mode, the detection limit of the ion-selective electrode being almost four orders of magnitude higher. The theoretical curves also indicate that negative signals are to be expected.
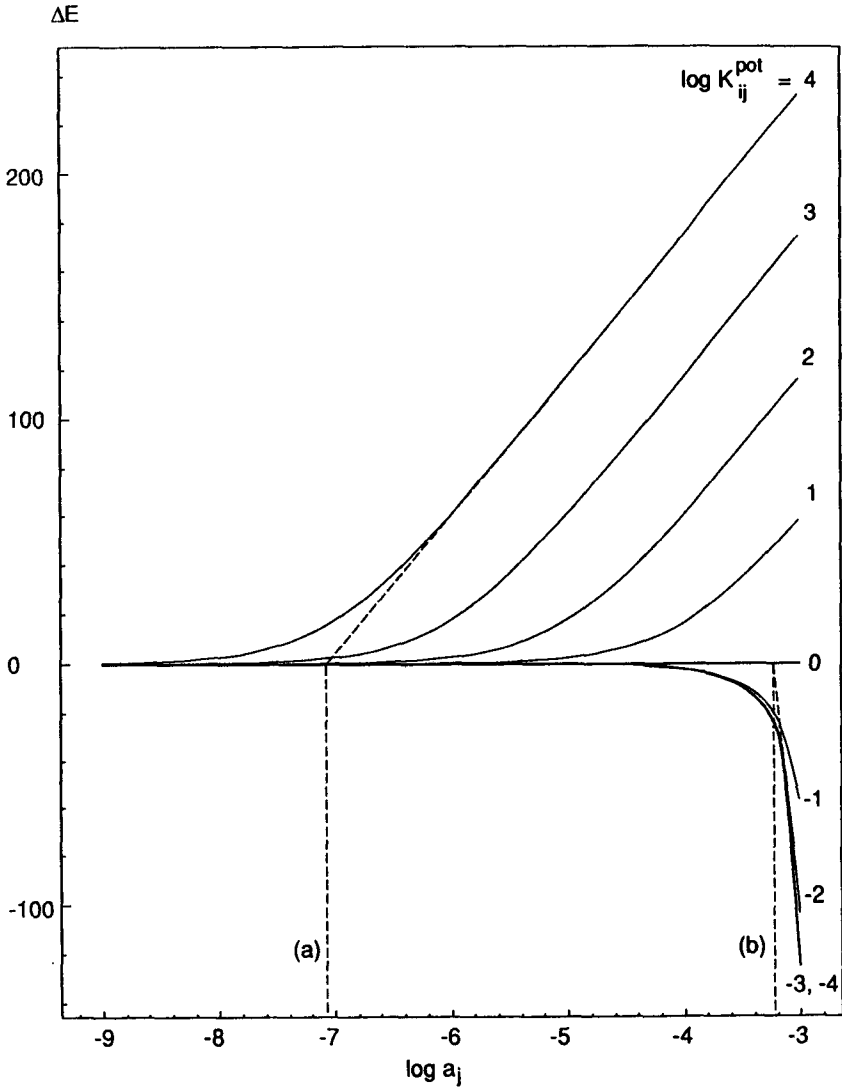
Fig. 7.5 - *Theoretical detection limits obtained with direct (a) and indirect (b) potentiometric detection, assuming a selectivity difference of four orders of magnitude between sample and background ion.*

7.4. Response Time

The total response time (t_{total}) of a potentiometric detection system is dictated by the slowest step of the response process. From the moment an activity change occurs at the detector tip until the signal is recorded on the strip chart, the following steps are involved:

$$t_{total} = t_{diff} + t_{inter} + t_{memb} + t_{electronics} \qquad (7.4)$$

In this equation, t_{diff}, t_{inter}, and t_{membr} denote the time required for the sample ions to diffuse through the stationary layer around the electrode tip, to penetrate through the interface between aqueous and lipophilic phase, and to be transported through the ion-selective membrane, respectively. The term $t_{electronics}$ is characteristic of the electronic setup used [184]. For ion-selective electrodes containing neutral ionophores, the time-limiting step usually is the ion transport through the membrane [185], whereas with liquid ion-exchanger membranes the rate-determining step is the diffusion of the sample ion through the stationary aqueous layer around the electrode tip [186].
Owing to the high internal impedance of microelectrodes (10^{10} - 10^{11} Ω) [187] which is mainly due to a relatively low concentration of charge-carrying species and a small membrane area (10^{-12} m^2), the response characteristics are expressed rather in terms of a resistance-capacitance behaviour [188]. With R = 10^{10} Ω and a capacitance, C, of 10 pF, the time constant, τ, given as [189]

$$\tau = RC \qquad (7.5)$$

typically is 100 ms. This time constant depends on the geometry of the microelectrode and the composition of its membrane phase. A low electrode impedance therefore is an important design feature.

7.5. Detection Volume

The detection volume of the potentiometric detector is primarily determined by the surface area of the electrode tip and the stationary diffusion layer extending from the membrane into the sample solution [178]. As tip diameters of easily pulled micropipettes range between 0.06 and 1 μm, the volume in which the sample ions are sensed is estimated to be approximately 10^{-19} - 10^{-15} l [176]. The effective volume of the hemisphere over an electrode tip with a surface of $8 \cdot 10^{-13}$ m^2 corresponds to 0.5 fl. When the tip of the potentiometric microsensor is introduced into the end of an open tubular column of 3.5 μm i.d., a detection volume of 6 pl is obtained [190]. Detection limits were found to be $5 \cdot 10^{-7}$ M for I$^-$ [191], $< 10^{-9}$ M for Ca^{2+} [192] and 10^{-12} for H$^+$ [193]. The corresponding molar sensitivity for I$^-$ is 3 amol in the case of an open-tubular column of 3.5 μm i.d., or even 0.25 zmol (150 ions) when considering an effective volume of 0.5 fl. Such measurements, however, can only be performed when the ions in the detection volume are in equilibrium with an adequate buffering system [176]. Due to the fast exchange equilibria between the free and the complexed ions, the actual amount of ions leading to a measurable response may be considerably larger [184].

8. The Electrophoretic Instrument

8.1. General Description

The general setup of an electrophoretic system is relatively simple in comparison with an HPLC apparatus. Instead of sophisticated pressure pumps and injection valves, only a high-voltage power supply is required and electrokinetic injections are easily performed by switching between sample and buffer vials.

In Figure 8.1 the electrophoretic system is shown schematically. The anodic site of a high-voltage power supply, adjustable from 0 to 50 kV, is connected with a Pt wire (fixed at the end of the cable extension) which is immersed in a vial containing the electrolyte solution. The injection end of the fused-silica capillary is arranged in parallel to the Pt electrode at a distance of approximately 2 mm. Buffer and sample vials are carried by an autosampler (with a remote control unit) which allows rapid switching between different electrolyte solutions. Some metallic pieces of the sampler were replaced by plastic ones, to avoid the presence of metal near the high-voltage electrode. The anodic end of the power supply and the autosampler are housed in a plexiglass box to protect the operator. The detection end of the fused-silica capillary is kept in a small plexiglass vessel filled with background electrolyte. The microelectrode is placed at a distance from the column end which approximately corresponds to the i.d. of the capillary. The common wire, cathode (grounded Pt wire) and a saturated calomel reference electrode (SCE) of the free-flowing free-diffusion type [194] are immersed in the background electrolyte of the detection compartment. The geometrical arrangement of the microelectrode relative to common electrode and cathode at the detection end of the capillary was found to have a considerable influence on the signal to noise ratio and will be discussed later (Section 9.3). Mechanical micromanipulators allow to accurately locate the microelectrode at the desired distance from the capillary end. In the horizontal plane, the relative position is controlled through a microscope and a TV camera with monitor, in the vertical plane by comparing the sharpness of focus of the electrode tip and the capillary end under the microscope. The eluting zones are detected by measuring the potential of the liquid membrane microelectrode with respect to an appropriate reference signal (differential potentiometry) [179]. To monitor the current during the electrophoretic experiments, a resistor of 10 kΩ is placed between detection compartment
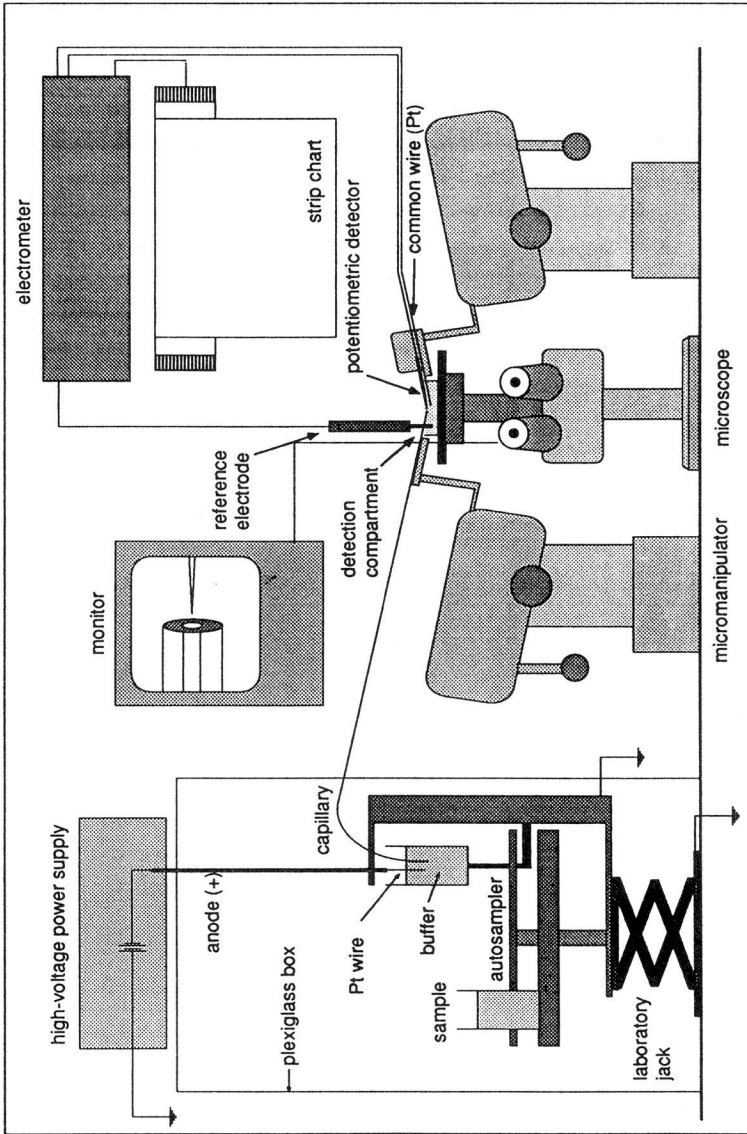
Fig. 8.1 - *Electrophoretic system.*

and ground (Figure 8.2). The current, which is proportional to the voltage drop across the resistor, is measured with a digital multimeter and continually displayed on the strip chart recorder.

8.2. Electric Amplification of the Potentiometric Signal

The electromotive force (emf) of an electrochemical cell must be measured under zero or almost zero current conditions. For this purpose, the electrometer used should have a high input resistance and a sufficiently low input leakage current. The internal resistance of the potentiometric detector is mainly governed by the resistance of the membrane components and reaches values of approximately 10^{10} Ω. For measurements in the range of ± 100 mV with a precision of 0.1 mV a minimum input resistance of 10^{13} Ω and a leakage current ≤ 10 fA are calculated [169].

Fig. 8.2 - *Schematic for the measurement of current and electromotive force (emf) in a capillary electrophoretic system.*

The emf signals are measured in the differential mode [179], *i. e.* the potential of the microelectrode is determined differentially against the reference electrode in the presence of a third electrode of low resistance (Pt wire) which is connected with the differential amplifier ground terminal. This method ensures a high stabili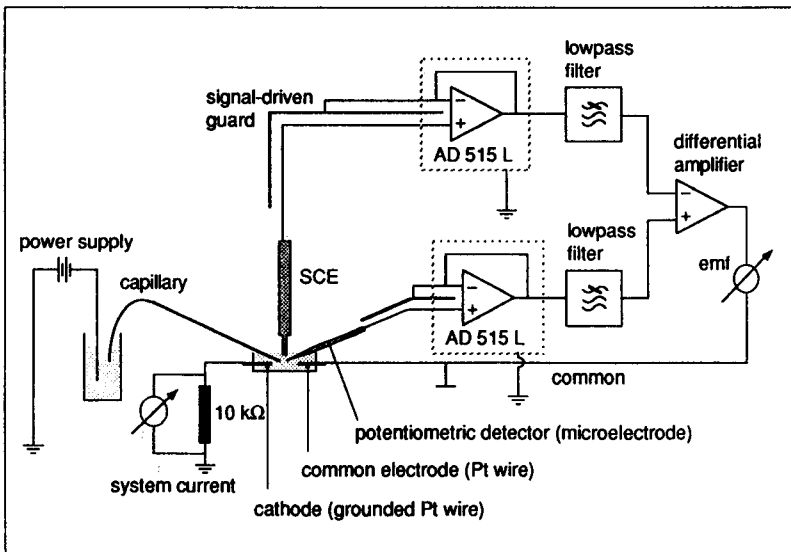ty of the measured signal, since junction or galvanic potentials of the circuitry are separated from the chemical activity measurement. To minimize the influence of external noise, the high-impedance signal is converted to a low-impedance one as close as possible to the source of the emf potential. For that purpose, an impedance converter (FET operation amplifier AD 515 L) is connected directly with the internal reference of the microelectrode and the SCE. Signal-driven guarding at the source input is used to reduce stray capacity. In addition, all high-resistive components are shielded in an aluminum Faraday cage. The signals are graphically displayed on a two-channel strip chart recorder.

8.3. Porous Glass Joint

The required zero current conditions for potentiometrically detecting cations (activity changes in the mV range) at the end of the capillary may not be fulfilled when a potential of 15 - 25 kV is applied at the injection end. In order to avoid any interference from the high-voltage source, the detection unit is insulated from the electrophoretic system by introducing an electrically conductive joint just before the detection end of the capillary [167]. The capillary is therefore cut in two at the desired position (2 - 3 cm from one end). The two pieces are then coupled again by placing a section of porous (electrically conductive) glass tubing over the ends (see Section 10.3). The joint is kept immersed in a buffer reservoir together with a grounded Pt wire (cathode). The high voltage is applied across the longer segment of the capillary and drops to almost zero at the glass joint, while the resulting electroosmotic flow 'pumps' the solute zones through the detection segment towards the microelectrode. In this way, interferences from the electric field gradient are largely kept off the detection end of the capillary. On the other hand, the method entails a significant loss in resolution due to back pressure and because the absence of an electric gradient in the detection segment causes the plug-shaped profile of the electroosmotic flow to be transformed into a parabolic one.

As will be shown later, potentiometric detection is also feasible in the presence of an electric field gradient without a porous glass joint.
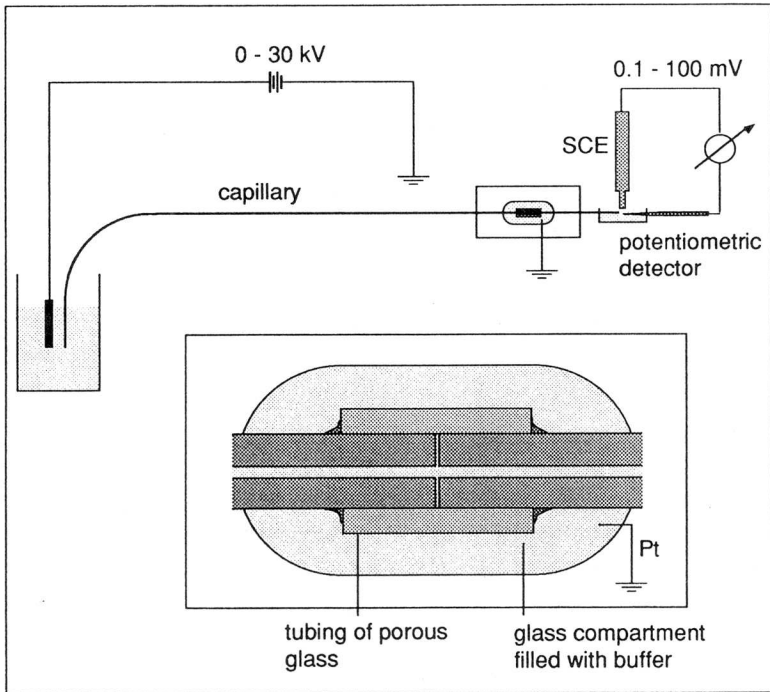
Fig. 8.3 - *Porous glass joint.*

8.4. Preparation of Microelectrodes

The basic design features of the potentiometric detector have already been described in Section 7.2.1. Throughout this work, only microelectrodes with a liquid membrane of appropriate composition have been used.

Pyrex glass tubings with an outer diameter of 1.5 mm are treated with nitric acid, rinsed with doubly distilled water and dried, according to a procedure commonly employed in this laboratory [193]. The glass tubings are then cut to a length of 3 - 5 cm and pulled with an electromechanical glass puller to give

pipettes which usually have tip diameters of approximately 0.3 µm [187]. If necessary, they can be broken under the microscope to tip diameters between 1 - 3 µm.

For better adhesion of the lipophilic liquid membrane phase to the glass surface, all pipettes are silanized with gaseous N,N-dimethyltrimethylsilyl-amine at 200 °C prior to the filling procedure [187]. The pipette is then filled with electrolyte, a slight pressure being applied from the back until the solution reaches the tip. The liquid membrane is then introduced by dipping the pipette into a droplet of the membrane cocktail and keeping the back end under vacuum for a few seconds (so-called front-filling technique). A chlorinated silver wire is then inserted into the pipette and fixed by sealing with candle wax. A final check under the microscope for air bubbles in the microelectrode is strongly recommended.

9. Results and Discussion

9.1. Composition and Selectivities of the Liquid Membranes Used

According to the theoretical considerations in Section 7.2.3, the ideal detector membrane should provide an adequate electromotive response to all analytically relevant cations and reject one which is used as the background ion. For practical purposes, however, a membrane with almost the same selectivities and response times for singly and doubly charged cations would be adequate. In addition, it should exhibit low selectivity for H^+, since for capillary electrophoretic separations high detection sensitivies at low pH values may also be required.

Membrane no.	1	2	3	4
Potassium tetrakis (4-chlorophenyl) borate	3.00 %	2.61%	2.21%	0.51%(*)
ETH 1571		2.69%	2.51%	
ETH 1001			2.28 %	
V 212				1.00%
Solvent	DMNB	DMNB	DMNB	o-NPOE

(*) corresponding to 68.5 mol % relative to the ionophore

Table 9.1 - *Composition of the liquid membrane phases (in wt. % relative to the membrane solvent). For full chemical names and constitutions see Section 10.7.*

The subject of the present work primarily was the separation and potentiometric detection of cations. For this purpose, an important part consisted in investigating membrane components (neutral carrier, borate additive and solvent) and studying their influence on the selectivities. The best results were obtained with the liquid membrane cocktails 1 to 4 shown in Table 9.1. Their selectivities (Figure 9.1) were determined by the separate solution method (SSM) [195] with 0.1 M chloride solutions of the respective cations.
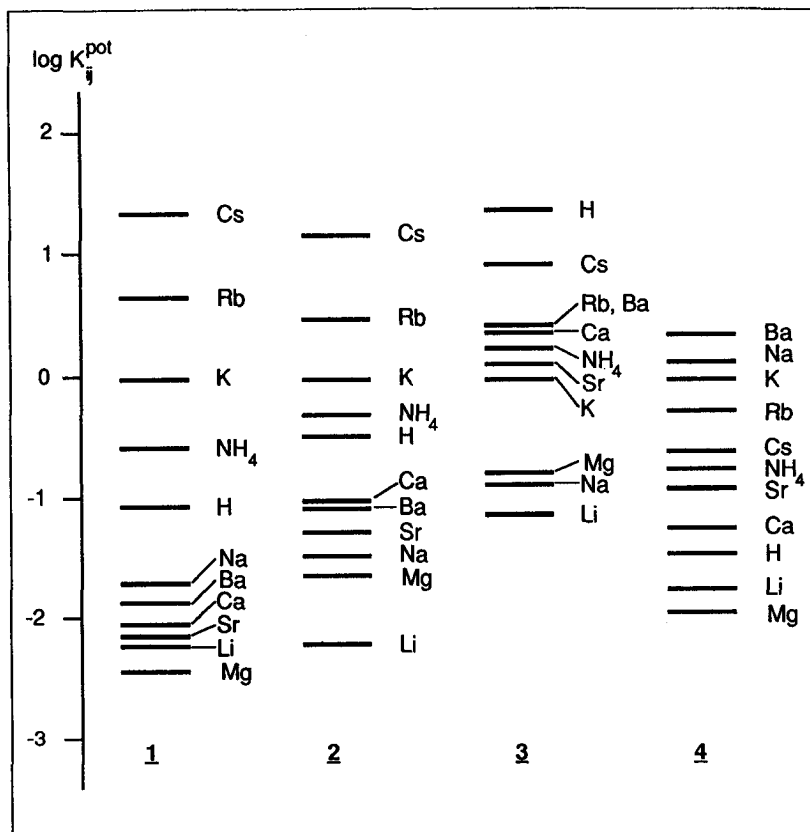
Fig. 9.1 - *Selectivities of liquid membranes (for compositions see Table 9.1).*

The internal electrolyte of the microelectrodes consisted of 3 M KCl. For the electrophoretic experiments it was substituted by a chloride solution of the pertinent background cation with the corresponding concentration. The selectivities were found to be reproducible within 0.5 log K_{ij}^{pot} units for microelectrodes with unbroken tips (0.3 - 0.5 µm i.d.). Surprisingly, by subsequently breaking the tips, drastically different selectivity patterns resulted [196]. This could be due to a lower internal resistance of the microsensor because of a larger tip area. Other experiments revealed that the *microelectrodes under electrophoretic conditions sometimes showed* increased noise and spontaneous potential drifts after accidentally having

broken their tip during manipulation. These results indicate that a high internal resistance of the microsensor is generally advantageous when employed in CE, since it provides additional insulation and reduces interference from the electrophoretic current. All the experiments presented hereafter were therefore carried out with microelectrodes having unbroken tips.

9.2. Electrophoretic Separation of Cations in Segmented Capillaries of 50 µm I. D.

9.2.1. Experimental Setup

The first electrophoretic experiments with microelectrodes as potentiometric detector were carried out with the experimental setup shown in Figure 9.2 in fused-silica capillaries of 50 µm i.d. The separation segment of the capillary had a length of 70 cm followed by a detection segment of 2.1 cm, which was electrically insulated with a porous glass joint (cf. Section 8.3). The polyimide coating at the end of the capillary was completely removed by carefully burning it off to ensure better optical control when positioning the sensor tip. The capillary and buffer reservoirs were filled with 50 mM NaH_2PO_4 buffer solution of pH 6 (adjusted with NaOH).
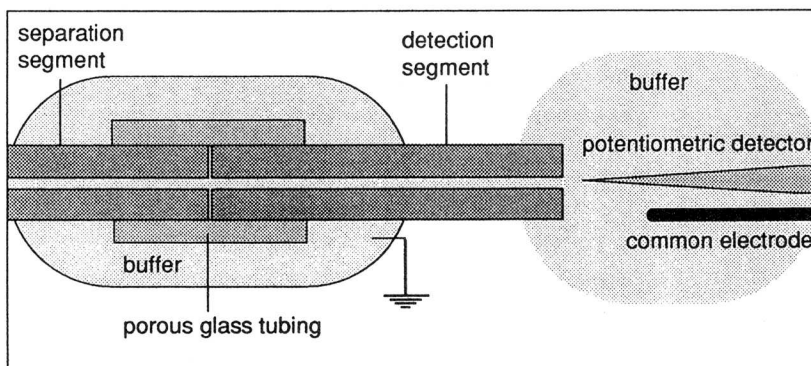
Fig. 9.2 - *Position of the potentiometric detector at the end of a segmented fused-silica capillary.*

The liquid membrane of the potentiometric detector corresponded to composition 2 (Table 9.1). Injections were performed electrokinetically by applying a short voltage pulse across the capillary while keeping the injection end immersed in the sample solution.

9.2.2. Sensor Signal and Detector Position in the Presence of an Electric Field

According to the Nicolsky-Eisenman equation (7.1), the electromotive force of a microelectrode is determined by the ion activity of the electrolyte solution. Initial electrophoretic experiments indicated that the potentiometric detector also responded to the electric field gradient, which caused a certain shift in the
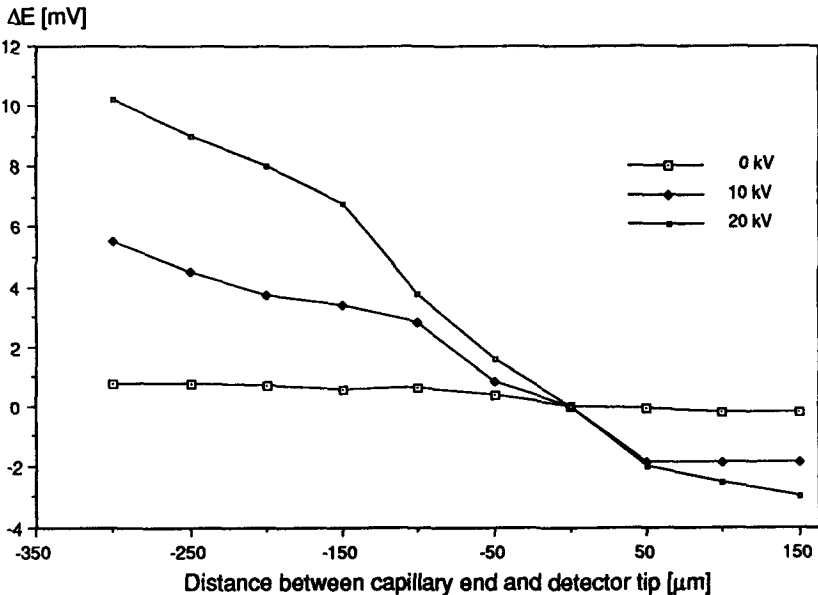
Fig. 9.3 - *Potential gradient response of a potentiometric detector in different positions relative to the end of a segmented fused-silica capillary (50 μm i.d.) for externally applied voltages of 0, 10 and 20 kV (negative distance values indicate that the sensor tip is inserted into the capillary end, see Figure 9.6). Liquid membrane composition 2 (see Table 9.1); total length of the capillary 72.1 cm (detection segment 2.1 cm) [196].*
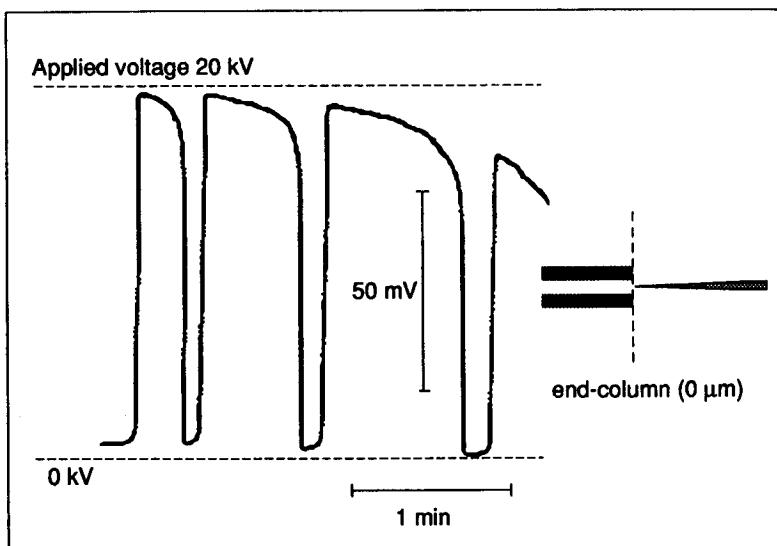
Fig. 9.4 - *Potential gradient response of a microelectrode placed in end-column position (see Figure 9.6) of a segmented fused-silica capillary (50 μm i.d.). Voltage applied at the injection end 0 or 20 kV. Liquid membrane composition 2 (see Table 9.1); total length of the capillary 72.1 cm (detection segment 2.1 cm) [196].*

baseline. This potential gradient response can be studied by altering the position of the electrode tip relative to the end of the capillary in the presence of an electric field and subsequently monitoring the electromotive force [196]. The results obtained without any sample injection are shown in Figure 9.3, negative distance values denoting that the tip of the microelectrode is inserted into the lumen of the capillary.

Similar experiments in open tubular liquid chromatography indicated that the membrane electrode potential also changes with the flow rate of the liquid [190]. In order to determine this unknown (electroosmotic) flow potential, the two datasets at 10 and 20 kV are compared with the data obtained under zero current conditions (0 kV) with a hydrostatic flow of liquid, generated by a level difference between injection and detection end of the capillary, which approximately corresponded to the electroosmotic flow rate at 20 kV. The results showed that in this case, roughly 10 - 20 % of the total non-Nernstian response of the microelectrode are due to the electroosmotic flow potential

and around 80 - 90 % generated by the potential gradient response.

The reproducibility of the data points is limited by the fact that the mechanical micromanipulators may give rise to slight deviations in the positioning of the microelectrode.

A typical potential gradient response is displayed in Figure 9.4. With the detector tip placed at the end of the capillary (end-column position), the potential difference reached 90 mV for an externally applied voltage of 20 kV. These observations indicate that considerable field effects are still present at the electrically insulated detection end of the capillary [196].

An electrophoretic run from experiments presented later, is shown in Figure 9.5. At t = 0, the separation potential is applied across the capillary. The electrophoretic current and the potential gradient response of the sensor steadily increase until a constant level is reached after 5 - 10 min. The Nernst response of the sensor due to activity changes in the eluting zones is superimposed to the stationary potential gradient response.
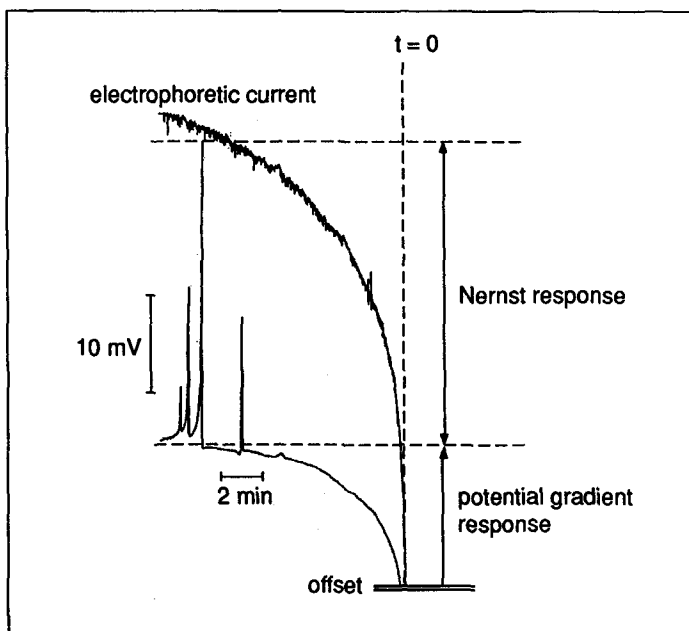

Fig. 9.5 - *Potential gradient and Nernst response of a potentiometric detector. Measurement of the electrophoretic current gives only qualitative information about the system (no scale).*

9.2.3. Noise and Potential Drift of the Sensor Signal

During an electrophoretic experiment, the baseline noise strongly varies with the position of the potentiometric detector relative to the capillary end. In Figure 9.6, the noise is shown for three relevant positions of the microelectrode relative to the column end. When the tip is inserted into the capillary end (on-column position a), the noise can be as high as 1 mV, but decreases to a value of approximately 0.5 mV for end-column position (b). The lowest noise level (< 0.1 mV) was obtained when the detector tip was placed at a distance of 50 μm (corresponding to the i.d. of the column) from the capillary end (post-column position c) [196].

Another major problem of the potentiometric detection method consists in signal instabilities of the sensor which result in drifting baselines. These time-dependent instabilities can be due to the electrophoretic system or the sensor itself. Although these effects have not been studied systematically, some observations are listed in Table 9.2.

Causes for baseline drifts in:	
CE system	Potentiometric detection system
- Electric instabilities of the power supply (indicated by changes in the system current) - Changes in the potential gradient due to zones of different conductivity - Change in the electroosmotic flow rate (indicated by change in the system current) - Leaking detection compartment	- Air bubbles in the microelectrode - Loss of internal filling electrolyte - Internal filling electrolyte of the sensor different from CE electrolyte - Deterioration of membrane phase and chlorinated Ag wire - Saturated calomel reference electrode (SCE) - Unstable position of the sensor (thermal effects, vibrations, unstable mechanical micromanipulators) - Critical distance between reference electrode and detector - Broken detector tip

Tab. 9.2 - *Possible reasons for a drifting baseline.*
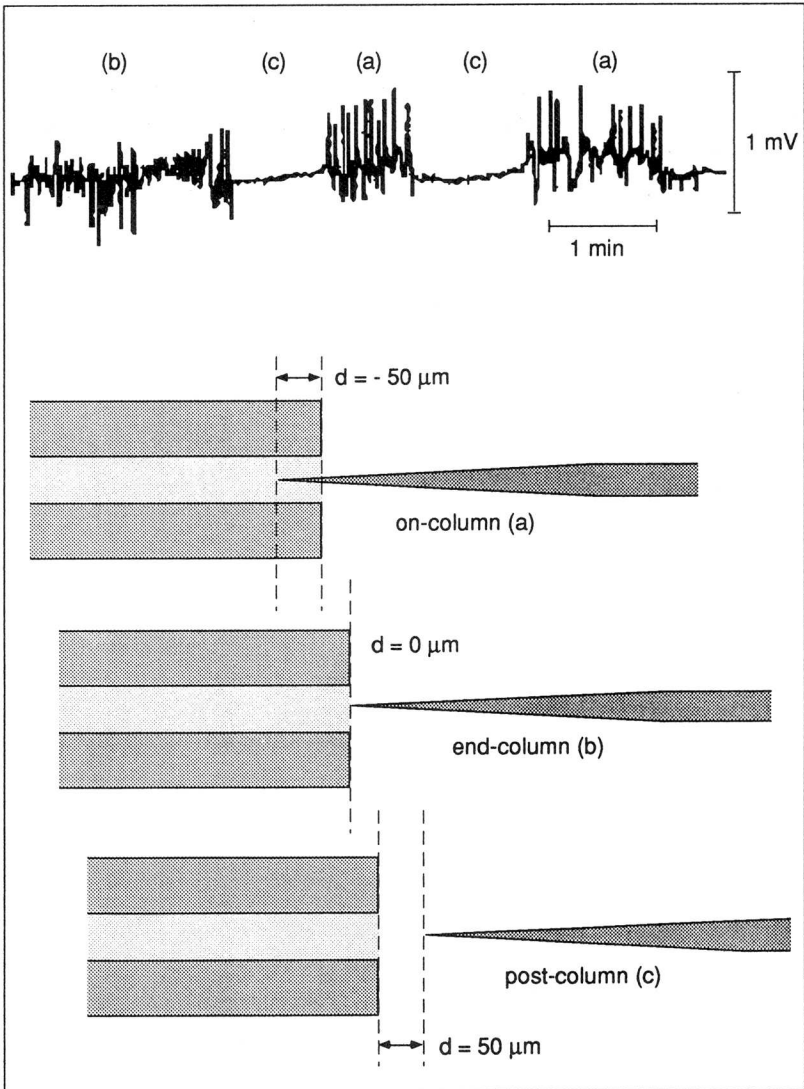
Fig. 9.6 - *Noise levels recorded for different positions of a potentiometric detector relative to the capillary end in the presence of an external voltage of 20 kV; (a) on-column, with d = - 50 µm; (b) end-column; (c) post-column, with d = 50 µm. Liquid membrane composition 2 (see Table 9.1); total length of the capillary 72.1 cm (detection segment 2.1 cm), i.d. 50 µm [196].*

9.2.4. Electrophoretic Separation of Alkali Metal Ions

Electrophoretic separations were carried out with a 10^{-2} M solution of alkali metal and ammonium chlorides. Injections were performed electrokinetically by applying a potential of 20 kV for 1 - 2 s, while the injection end of the capillary was kept immersed in the sample solution. The injected amount Q [mol] can be calculated according to the formula [197]

$$Q = \frac{\pi\, r^2\, L\, c_s\, t_{inj}}{t_{system}} \tag{9.1}$$

With c_s (concentration of the sample) = 10^{-2} M, L (capillary length) = 0.7 m, r (capillary radius) = $25 \cdot 10^{-6}$ m, t_{inj} (injection time) = 2 s and t_{system} (retention time for the system peak or a neutral component) = 260 s, a value of approxi-
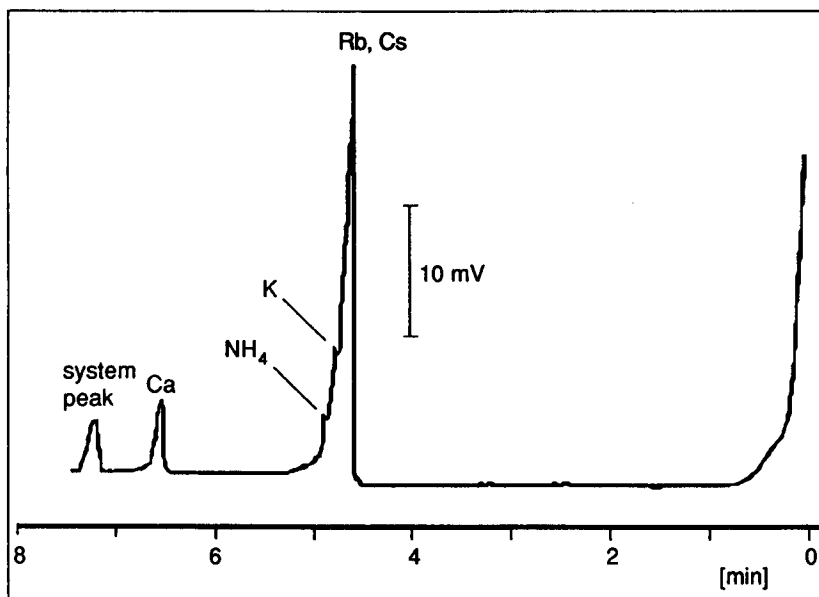
Fig. 9.7 - *Electrophoretic separation of 10^{-2} M alkali and alkaline-earth metal cations in a segmented fused-silica capillary detected with the potentiometric detector in on-column position (d = - 30 µm). Background electrolyte $5 \cdot 10^{-2}$ M NaH_2PO_4, pH 6; electrokinetic injection, 20 kV for 1 - 2 s; separation potential 20 kV; liquid membrane composition 2 (see Table 9.1); total length of the capillary 72.1 cm (detection segment 2.1 cm), i.d. 50 µm [196].*

mately 10^{-10} mol is obtained for an injection volume of 10 nl. The resulting electropherogram is shown in Figure 9.7. The insufficient resolution of the signal at t = 4.7 min corresponding to Rb^+, Cs^+, K^+ and NH_4^+ is mainly due to back pressure effects and hydrodynamic flow conditions in the detection segment. Furthermore, the selectivity properties of the liquid membrane 2 (see Table 9.1) is not suitable for the detection of Li^+ and Na^+.

9.2.5. Extra-Column Band Broadening

With increasing distance between detector tip and capillary end, the eluting zones get broader due to spherical diffusion. Similar experiments with the microelectrode employed in open tubular ion chromatography indicate a loss of about 15 % in column performance (number of theoretical plates) when the detector is placed at a distance d of approximately one capillary i.d. from the end of the separation compartment (post-column detection). It has been shown that with increasing distance (d > 0) between column end and detector tip the signal amplitude, which first is more or less constant, begins to drop at a certain distance, depending on the flow rate. At this point, a transition from laminar to spherical flow probably occurs [190]. The following experimental data were obtained from the electrophoretic separation of a mixture of inorganic cations (10^{-2} M alkali metal and ammonium chlorides, $5 \cdot 10^{-2}$ M $CaCl_2$ and $BaCl_2$). The apparent plate height, H^* (see Section 9.4.2), was determined from the half-width of the unresolved Rb^+ and Cs^+ signal (Equation 9.2) when varying the distance between detector tip and capillary end. Figure 9.8 shows that the extra-column band broadening increases by a factor of two when the tip of the microelectrode is moved from end-column position (d = 0 µm) to a distance of 50 µm ($\equiv$ one column i.d.) from the capillary end. It is probably enhanced by the presence of the porous glass joint, as band broadening already occurs due to the hydrodynamic flow conditions in the short detection segment of the capillary. Post-column detection (d = capillary i.d.) offers the best compromise between current-induced detector noise (see Figure 9.6) and extra-column band broadening.

H* [μm]
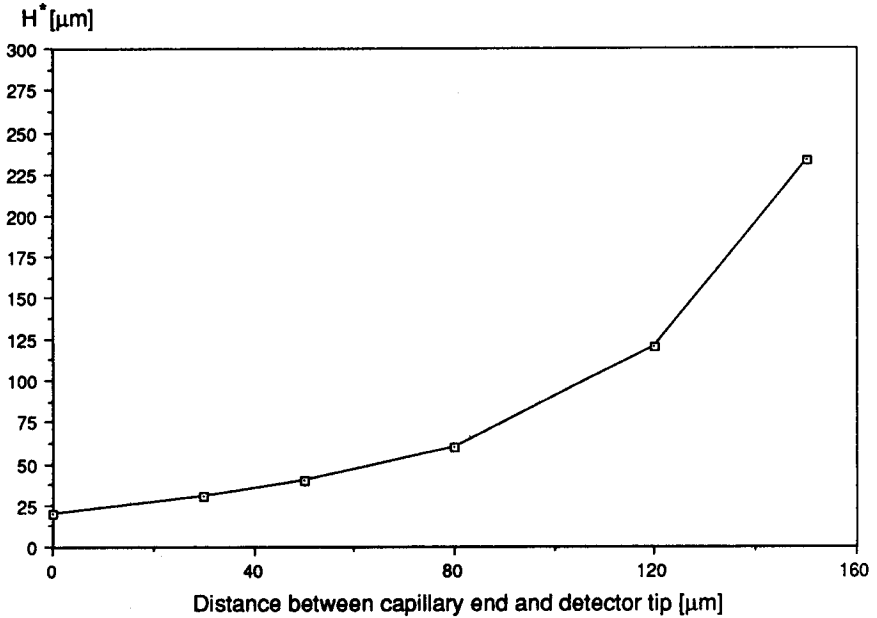
Fig. 9.8 - *Apparent plate height, H*, as a function of the distance between the end of a segmented capillary (50 μm i.d.) and the tip of the microelectrode [196].*

9.3. Electrophoretic Separation of Cations in Unsegmented Capillaries of 50 μm I.D.

The general observations made in the previous chapter indicate that electric field effects are still present at the detection end of a segmented capillary. Obviously, it is not possible to completely eliminate interferences from the electrophoretic current by means of a porous glass joint. On the other hand, it would be desirable to avoid additional band broadening in the detection segment and the difficult fabrication and handling of segmented capillaries. All subsequent experiments were therefore carried out with unsegmented fused-silica capillaries.

9.3.1. Cathode - Detector Arrangement A

Initially, the cathode - detector arrangement A, as shown in Figure 9.9, was chosen. The microelectrode (liquid membrane composition 3, Table 9.1) was placed directly at the end of an unsegmented fused-silica capillary of 50 µm i.d. In addition, the detection compartment, filled with the buffer solution (10^{-2} M NaH_2PO_4 of pH 8.3), was provided with a grounded Pt wire (cathode), so that the electric field is applied across the entire length of the capillary.
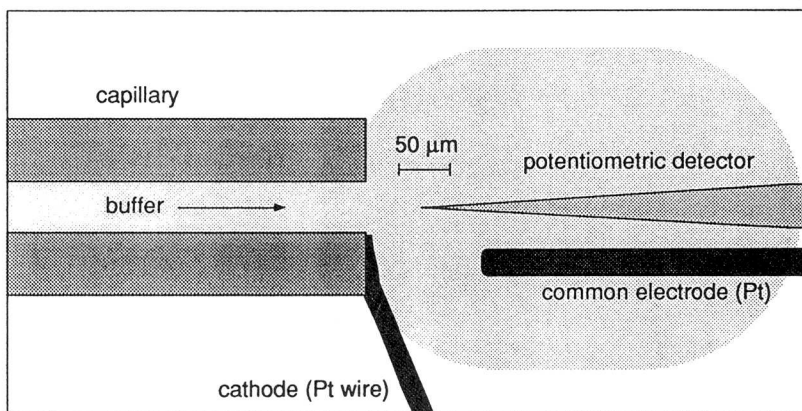
Fig. 9.9 - *Cathode - detector arrangement A.*

9.3.1.1. Position of the Cathode

The position of the cathode was found to be critical in terms of noise and potential drift of the sensor signal. When the Pt cathode was moved into or close to the lumen of the capillary, spontaneous formation of gas bubbles (H_2) was observed, generated by a cathodic decomposition reaction in the presence of an electric field. The effect caused the sensor signal to drift irreproducibly and disappeared again when the Pt cathode was moved away from the capillary end or, as shown in Figure 9.9, towards the side of the opening. The bubble formation probably occurs at a critical current density, which reaches a maximum value with the cathode in or close behind the capillary lumen, and decays spherically into the buffer reservoir. The

undesirable faradaic reaction can also be suppressed by decreasing the external potential (< 17 kV), or, as will be shown later, by reducing the capillary i.d. and / or the buffer concentration.

9.3.1.2. Reference Signal

The electrophoretic experiments carried out with cathode - detector arrangement <u>A</u> described above showed that major instabilities in the baseline were caused by spontaneous changes in the reference signal of the saturated calomel electrode (SCE). These instabilities persisted when the SCE was placed in a remote reservoir connected with the detection compartment through an electrolyte bridge.

Fig. 9.10 - *Potentiometric detection of* Ca^{2+}, Rb^+ *and* Cs^+. *Both electropherograms were obtained simultaneously. The upper trace was recorded 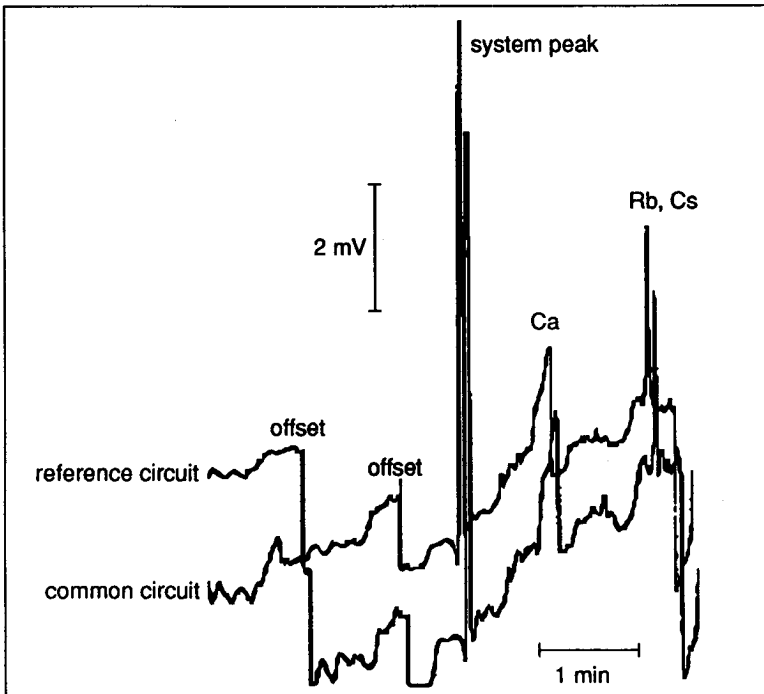vs. a saturated calomel reference electrode (SCE), whereas the lower one was obtained with the microelectrode - common electrode circuit without the SCE [196].*

Surprisingly the circuit with microelectrode - SCE gave almost the same electropherogram as that with microelectrode - common electrode alone (see Figure 9.10). Under electrophoretic conditions, the microelectrode - common-electrode circuit obviously yielded the same trace but with better stability. This could be due to a reaction at the common electrode, leading to a quasi-stationary potential at the Pt surface. The extent of the reaction is expected to depend on the current density and on the composition of the electrolyte in the detection compartment. In the following experiments, the SCE was removed and the potential of the microelectrode was measured with respect to the stable signal of the common electrode. As a consequence, junction and galvanic potentials are no longer compensated and might lead to a variable shift in the baseline. However, these potentials are time-independent (or quasi-stationary), whereas an eluting zone will give rise to a time-dependent change in ionic activity and thus to a potentiometric signal which is superimposed to the baseline. Accurate integration of the corresponding peak will furnish the quantitative information about the eluted zone. The offset potential (or baseline) should therefore be free from noise and drift rather than electrochemically defined.

9.3.1.3. Sensor Signal and Detector Position in the Presence of an Electric Field

The potential gradient response of the potentiometric detector (in arrangement A) was measured at a constant potential of 3 kV, varying the distance between the tip and the capillary end (Figure 9.11). Similar measurements at potentials > 3 kV gave no constant emf values for the on-column positions due to heavy drifts. For an externally applied voltage of 30 kV the noise was found to be as high as 5 mV when the microelectrode was placed in end-column position and increased to about 20 mV after inserting the tip into the capillary. In Figure 9.11, these measurements are compared with those obtained from similar experiments with a segmented capillary (see Figure 9.3). They clearly show that the potential gradient response of the microelectrode is considerably higher without a porous glass joint.

In Figure 9.12, the potential gradient response of the sensor is displayed for three different externally applied potentials and a sensor-tip distance of 80 μm from the capillary. The sensor signal varied between 50 mV (for 10 kV) and 180 mV (for 30 kV). Interestingly, the time necessary until the sensor reached

ΔE [mV]

Distance between capillary end and detector tip [μm]
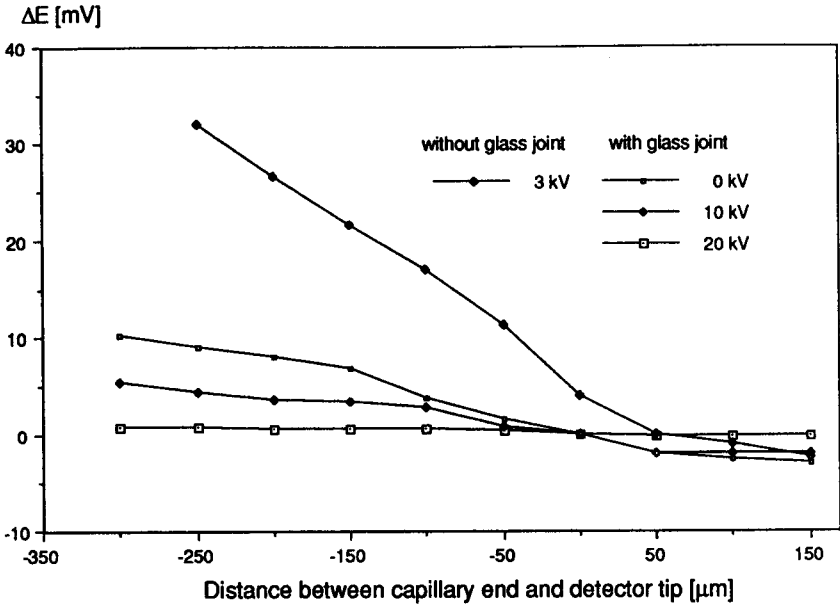
Fig. 9.11 - *Potential gradient response of a microelectrode placed in different positions relative to the end of a segmented capillary (50 μm i.d.; externally applied voltage of 0, 10 and 20 kV, cf. Fig. 9.3) and an unsegmented capillary of identical i.d. (external voltage 3 kV). Negative distance values indicate that the sensor tip is inserted into the capillary [196].*
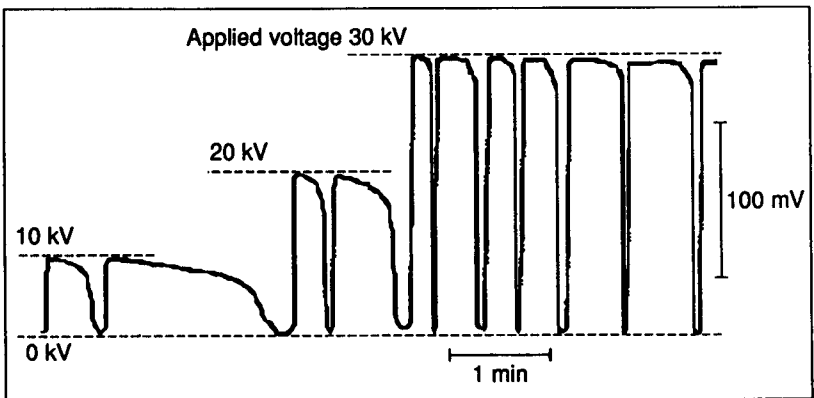
Fig. 9.12 - *Potential gradient response of a potentiometric detector placed at a distance of 80 μm from the end of an unsegmented capillary (50 μm i.d.) [196].*

a constant value was reduced from 3 min (at 10 kV) to 30 s (at 30 kV). This phenomenon can be related to capacitive charging and electric polarization of the membrane.

9.3.1.4. Noise and Potential Drift of the Sensor Signal

The distance between the common electrode and the detector tip (Figure 9.9) was found to have an influence on the potential drift behaviour of the sensor signal. Distances < 300 μm gave rise to an increasing (positive) drift in the baseline, whereas for distances > 300 μm the baseline drifted in the opposite direction (negative drift). A tolerable baseline drift of about 1 mV / min was obtained for a distance of 280 μm.

For an externally applied potential of 25 kV, the noise reached 5 mV when placing the detector tip 50 μm (one column i.d.) behind the capillary end. This level is too high and small signals would completely disappear.

9.3.2. Cathode - Detector Arrangement B

Better results were obtained when the detector was placed nearer the Pt cathode at a distance of 10 to 50 μm from the border of the capillary lumen (Figure 9.13)
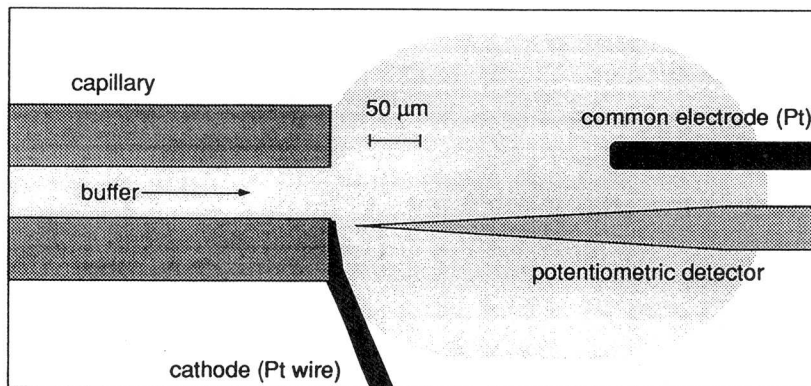
Fig. 9.13 - *Cathode - detector arrangement B*.

For an externally applied potential of 25 kV, the potential drift was found to be approximately 5 mV / min and the noise was below 1 mV. The lowest noise level (0.1 - 0.2 mV) and drift rate were obtained by placing the tip of the microelectrode at a distance of 10 - 20 µm behind the capillary end (post-column position) and the common electrode, in turn, at 250 µm behind the detector tip [196].

9.3.2.1. Electrophoretic Separation of Alkali Metal Ions
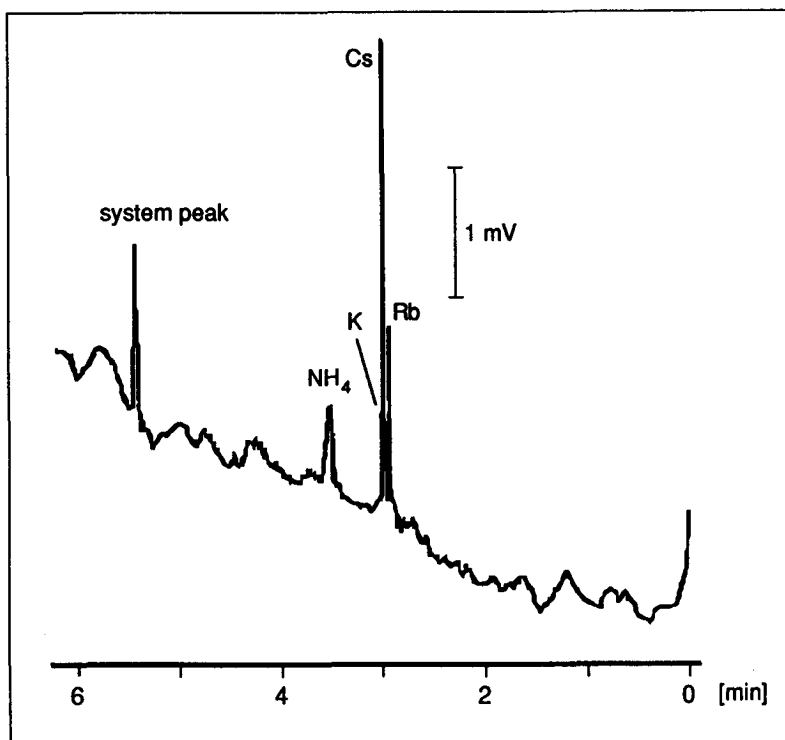
Fig. 9.14 - *Electrophoretic separation of 10^{-4} M alkali and alkaline-earth metal cations detected with the potentiometric detector in post-column position (d = 20 µm) and at a distance of ≈ 10 µm from the Pt cathode (see Fig. 9.13). Buffer 10^{-2}M NaH_2PO_4, pH 8.3; electrokinetic injection, 10 kV for 0.5 s; separation potential 25 kV; liquid membrane composition 3 (see Table 9.1); capillary i.d. 50 µm [196].*

Figure 9.14 shows the electrophoretic separation of a 10^{-4} M solution of ammonium and alkali metal chlorides obtained with the cathode - detector arrangement B. The signals in the electropherogram appear sharper and are better resolved as compared to the electrophoretic separation in a segmented capillary (Figure 9.7) having the same i.d. (50 μm). On the other hand, due to interferences from the electrophoretic current the baseline now suffers more from noise and potential drift [196].

9.3.2.2. Extra-Column Band Broadening

The influence of the distance between column end and detector tip on the apparent plate height (as determined according to Equation 9.2 from the half-width of the Cs^+ signal) is represented in Figure 9.15. It shows that when increasing this distance from 15 to 50 μm, the extra-column band broadening almost doubles.
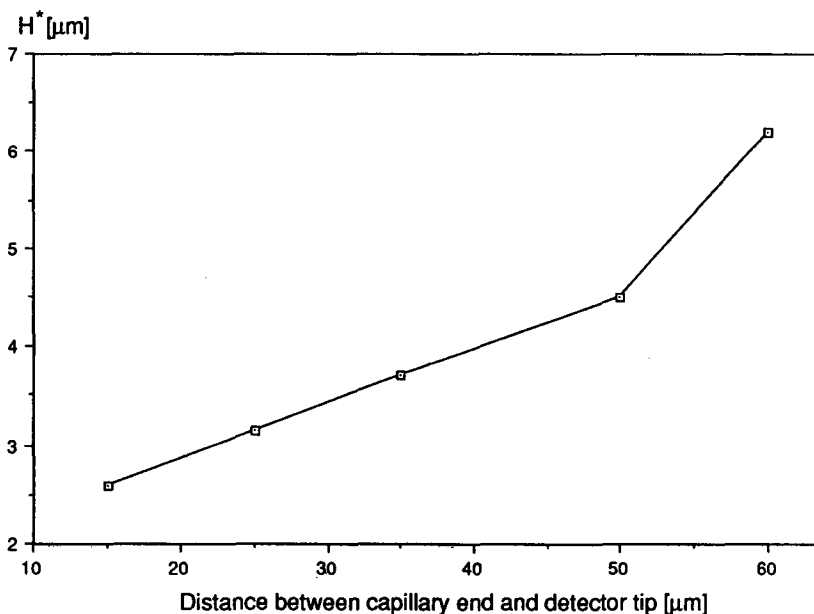
Fig. 9.15 - *Apparent plate height (determined from the Cs^+ signal) as a function of the distance between the end of an unsegmented capillary (50 μm i.d.) and the tip of the microelectrode [196].*

9.3.3. Cathode - Detector Arrangement C

The results obtained so far indicate that the geometrical arrangement of the ground wire and electrode tip with respect to the capillary end is critical for the noise level of the baseline. Arrangement B allows current-induced interferences to be rejected quite acceptably, but suffers from the disadvantage that the potentiometric detector cannot be placed in the center of the capillary lumen. In addition, the geometrical arrangement of detector and ground wire is not exactly reproducible from run to run owing to the relatively coarse micromanipulation procedure. Obviously, good protection of the sensor from the influence of the electrophoretic current is assured when the ground wire is placed close to the sensor tip.

In the following arrangement C (Figure 9.16), the cathode is deposited as an electrically conductive metal layer on the glass surface of the microelectrode tip. The layer consisted of gold or platinum (thickness $\approx 0.5\ \mu m$) and was connected with a grounded Pt wire by means of conductive carbon paste.
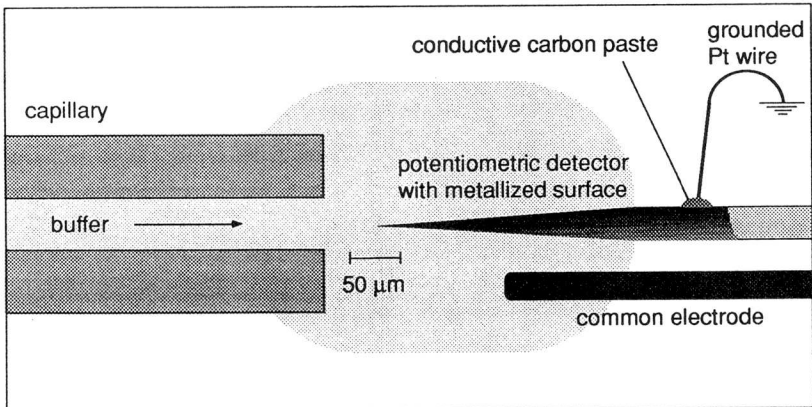
Fig. 9.16 - *Cathode - detector arrangement C*.

9.3.3.1. Baseline Noise

In Figure 9.17, two electropherograms for electrokinetic injections of 10^{-6} M KCl are given. Trace (a) was obtained with a non-metallized microelectrode

(cathode - detector arrangement A), whereas for trace (b) a metallized microelectrode was used (cathode - detector arrangement C). Comparison of two baseline noise levels ($\approx$ 1 mV for setup A and $\approx$ 0.4 mV for setup C), showed that with metallized microelectrodes slightly better results are achieved. However, it is difficult to quantitatively determine the baseline noise, since it depends on a considerable number of system parameters (conductivity of the buffer, capillary dimensions, internal resistance and position of the microelectrode). With capillaries of 50 μm i.d. it is not possible to completely eliminate the influence by the electrophoretic current. The baseline noise still increases drastically when the (metallized) detector tip is moved closer to the capillary lumen. This effect is shown in Figure 9.18. For an externally applied potential of 15 kV, the noise amounts to 1 - 2 mV for post-column (d = 20 μm), 2 - 3 mV for end-column (d = 0 μm) and 3 - 4 mV for on-column position (d = - 30 μm) of the tip. In the last case, the K^+ signal completely disappears within the noise. Potentials above 17 kV could not be applied due to bubble formation (H_2) on the surface of the metallized tip and consequent baseline drift.
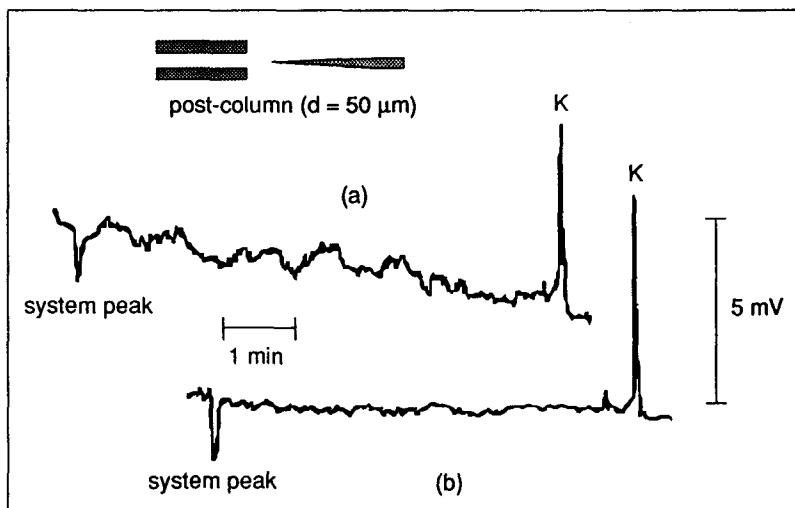
Fig. 9.17 - *Comparison of the baseline noise for two electrophoretic runs with cathode - detector arrangement A (a) and C (b). Sample 10^{-6} M KCl; buffer 10^{-2} M Na_2HPO_4, pH 9.1; electrokinetic injection, 5 kV for 3 s; separation potential 15 kV; liquid membrane composition 1 (Table 9.1); detector in post-column position (d = 50 μm); capillary length 88.6 cm, i.d. 50 μm.*
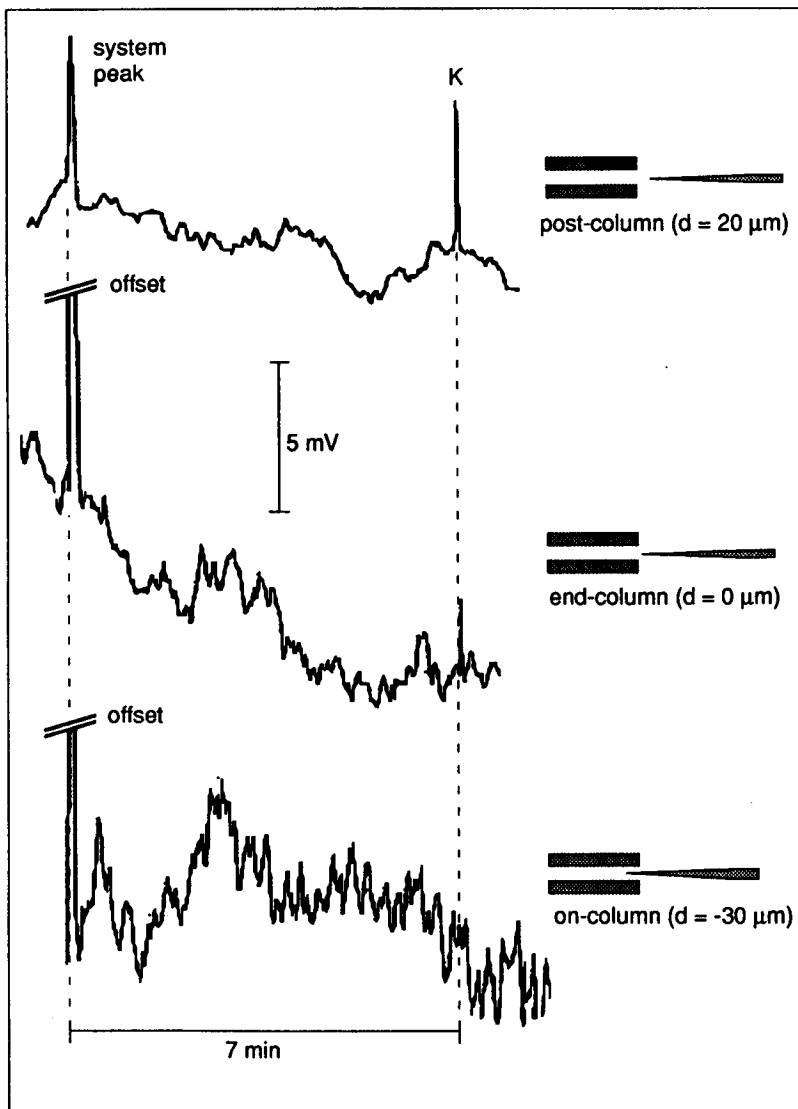
Fig. 9.18 - *Influence of the position of the potentiometric detector (metallized microelectrode) on the baseline noise. Sample 10^{-6} M KCl; buffer 10^{-2} M Na_2HPO_4, pH 9.1; electrokinetic injection, 5 kV for 4 s; separation potential 15 kV; liquid membrane composition 1 (see Table 9.1); capillary length 88.6 cm, i.d. 50 µm.*

9.3.3.2. System Peak

Interestingly, the height of the system peak in Figure 9.18 increases when moving the detector tip from post-column to on-column position, while the K^+ signal gradually disappears in the baseline noise.

The system peak corresponds to a zone having a lower concentration than the background electrolyte and this concentration is maintained between two stationary boundaries for the duration of an electrophoretic run. According to the theory of electrophoresis (Chapter 2) it can be explained as a consequence of the values of the regulating function in the sample zone and the ionic background being different. Usually, the sample is injected at a lower activity than that of the background electrolyte, so that the value of the regula-
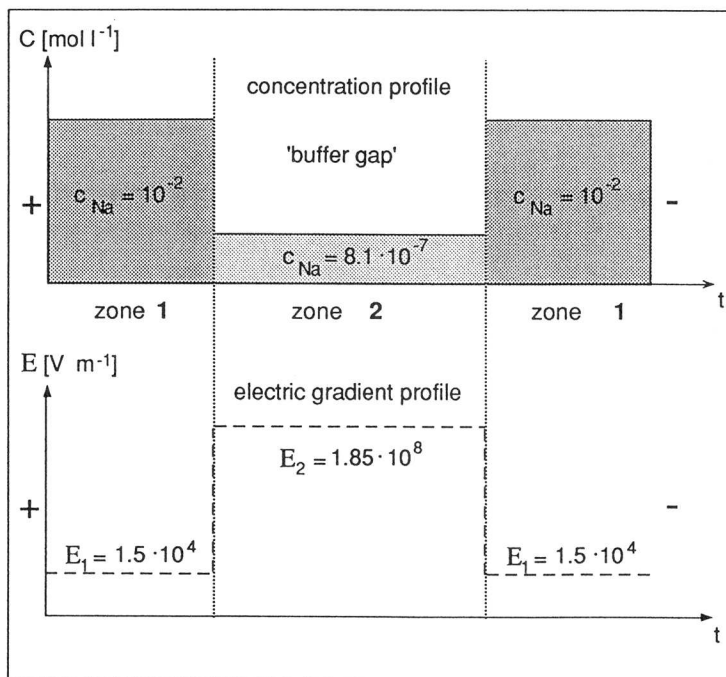
Fig. 9.19 - *Concentration profile (top) and electric gradient profile (bottom) of the 'buffer gap'.*
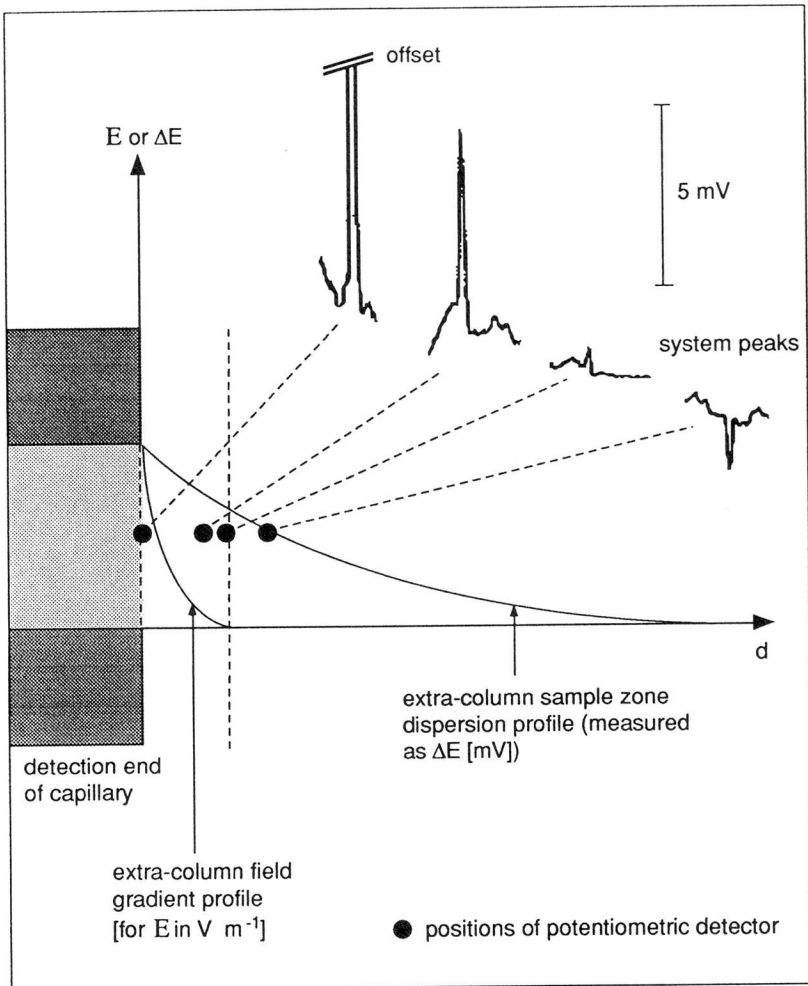
Fig. 9.20 - *Influence of the detector position on the system peak.*

ting function in this zone is lower. The profile of the regulating function is time-independent and remains unaltered even when the sample ions in the course of electrophoretic migration are replaced by the ionic background. As a consequence of the lower background concentration in this stationary zone ('buffer gap'), the field strength is higher, thus accelerating the background

ions across this zone in order to maintain a constant ionic transfer rate.

For example, an inital sample zone of 10^{-6} M KCl is placed in a 10^{-2} M NaCl background electrolyte, and a field gradient of 15 kV m^{-1} is applied across the separation compartment. Due to the constant profile of the regulating function, a lower concentration of $8.1 \cdot 10^{-7}$ M NaCl (calculated with Equation 2.19) will persist at the original site of the sample zone. According to Equation 2.14, for the given background concentration the local field gradient in this stationary zone has a value of $1.85 \cdot 10^8$ V m^{-1} (Figure 9.19). The field gradient therefore changes by four orders of magnitude when the stationary zone boundary of the 'buffer gap' reaches the detector tip. The system peak therefore represents the response of the potentiometric detector to the local electric field gradient of the 'buffer gap'. The phenomenon can only be detected in end-column and on-column positions, where the profile of the regulating function is maintained, and allows to determine the electroosmotic flow rate. When the detector tip is moved further away from the capillary end, the direction of the system peak is often reversed (see Figure 9.20), thus indicating that the eluting 'buffer gap' indeed has a lower concentration than the background electrolyte.

9.4. Electrophoretic Separation of Cations in Unsegmented Capillaries of 25 μm I.D.

The results obtained in Sections 9.2 and 9.3 illustrate that it is necessary to reduce interferences from the electrophoretic current in order to obtain a stable and noise-free baseline. This can be achieved by optimizing the detection setup and increasing the resistance of the separation compartment, e. g. by employing capillaries with smaller i.d.

9.4.1. Experimental Setup

For the following experiments, cathode - detector arrangement $\underline{C}$ was used, together with the liquid membrane composition $\underline{4}$ (Table 9.1). The major advantage of this membrane is a better response to doubly charged cations and a relatively good rejection of the hydrogen ion (see Figure 9.1). As background electrolyte magnesium acetate was chosen since, according to the SSM measurements (Figure 9.1), Mg^{2+} is the most rejected cation. Thus,

the eluting ionic constituents can be detected with a peak sensitivity which is determined by the electromotive force according to their activity and selectivity ratios relative to Mg^{2+} (Equation 7.3). To eliminate diffusion processes across the liquid membrane of the microelectrode, $MgCl_2$ of the same activity as the background electrolyte was used as internal filling solution.

9.4.2. Detector Position and Baseline Noise

Typical baseline noise levels for capillaries of 25 µm i.d. operated with $MgAc_2$ at separation potentials between 15 and 25 kV are shown in Figure 9.21. For on-column position of the detector, the current-induced interferences amounted to 1 - 2 mV, while for post-column position the baseline noise was as low as 0.05 - 0.10 mV.
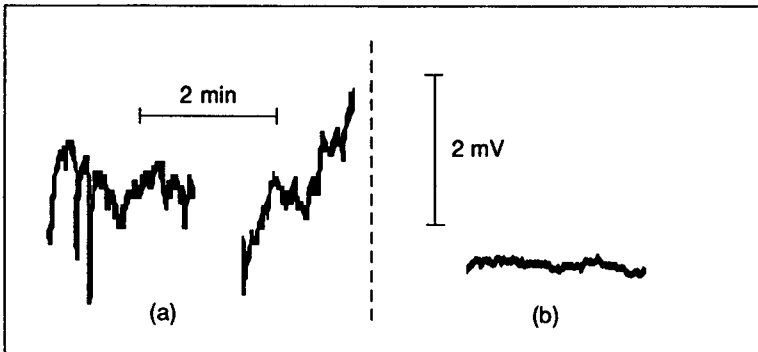
Fig. 9.21 - *Baseline noise for on-column (a) and post-column position of the potentiometric detector.*

Figure 9.22 shows two electropherograms recorded with the potentiometric detector in on-column (a) and post-column position (b). Electropherogram (a) illustrates that on-column detection is possible with capillaries 25 µm i.d. or less. However, the noise can be as high as 2 mV and spontaneous drifts of the baseline may occur. Both electropherograms again demonstrate that a compromise has to be made between interferences from the electrophoretic current and extra-column band broadening. This effect can be studied by

calculating the separation efficiencies for the K^+ and Li^+ signals (detected in on-column and post-column positions) in terms of the number of theoretical plates, (or their plate height, H) N, using the expression:

$$H = \frac{L}{N} = \frac{w_{0.5}^2}{5.54 \, L} \qquad (9.2)$$

where L is the distance between the point of injection and the detector and $w_{0.5}$ the peak width at half height. According to the Nicolsky-Eisenman equation (7.1), the potentiometric detector signals are proportional to the logarithm of the measured activity and are therefore broader than the corresponding linear profiles. The determination of the geometrical half-width of a potentiometric signal therefore yields an apparent separation efficiency. The real separation efficiency for a logarithmic profile is only obtained when the signal is displayed on a linear scale. On the other hand, the half-width of a potentiometrically recorded profile can be read off at the corresponding height, $\Delta E_{0.5}$, of the peak in logarithmic units calculated according to the formula [184]

$$\Delta E_{0.5} = \frac{RT}{zF} \ln \left(0.5 \left[\exp \left(\frac{\Delta E_{max} \, zF}{RT} \right) + 1 \right] \right) \qquad (9.3)$$

where ΔE_{max} is the value of the electromotive force at the point of maximum activity in an elution profile relative to the baseline.

For small signals (< 10 mV), apparent and real system efficiencies are the same. For larger signals, the values can differ significantly but show the same trend. The apparent system efficiency represents an overall value which can be compared with the efficiencies obtained from other systems. For quantitative determinations, however, the real system efficiency according to Equations 9.3 and 9.2 must be determined.

The real number of theoretical plates for the K^+ and Li^+ signals of Figure 9.22 are listed in Table 9.3. The results show that the extra-column band broadening amounts to ~ 10 % for the profile of K^+ and and to ~ 36 % for the

more slowly eluting Li⁺ profile, when the detector is moved from on-column to post-column position (Figure 9.22). For capillaries of 25 μm i.d., the best compromise between the disturbing influences of noise and extra-column band broadening of the zone profiles is found by placing the sensor at a distance of one column i.d. from the capillary end.

Ion	N (for on-column detection)	N (for post-column detection)	Extra-column band broadening due to post-column detection
K⁺	304'776 ± 13'107	273'538 ± 26'670	10.3 %
Li⁺	156'841 ± 25'050	104'130 ± 16'901	35.6 %

Table 9.3 - *Extra-column band broadening as determined by the number of theoretical plates, N, for the K⁺ and Li⁺ profiles in Fig. 9.22.*

9.4.3. Electrophoretic Separation of Inorganic Cations

Figure 9.23 shows an electropherogram of a 10^{-5} M sample solution of alkali and alkaline-earth metal cations. The different peak heights roughly reflect the selectivity pattern determined by the SSM (Figure 9.1). In addition to the identification based on the respective migration times the relative peak intensities therefore provide supplementary information about the ionic constituent.

The liquid membrane 4 (Table 9.1) of the potentiometric detector is barium-selective [198], hence Ba^{2+} gives the most intense signal (60 mV in Figure 9.1). As regards Rb^+ and Cs^+, the difference in their ionic mobilities (see Table 1.1) is so small that they are not separated by the present system. K^+ and NH_4^+ also have nearly the same ionic mobilities and are only partly resolved. For this and all the subsequent electrophoretic separations, no system peak appeared so that the electroosmotic flow rate could not be determined. The apparent and real plate heights of the resolved ionic constituents, determined according to Equations 9.3 and 9.2, are listed in Table 9.4.
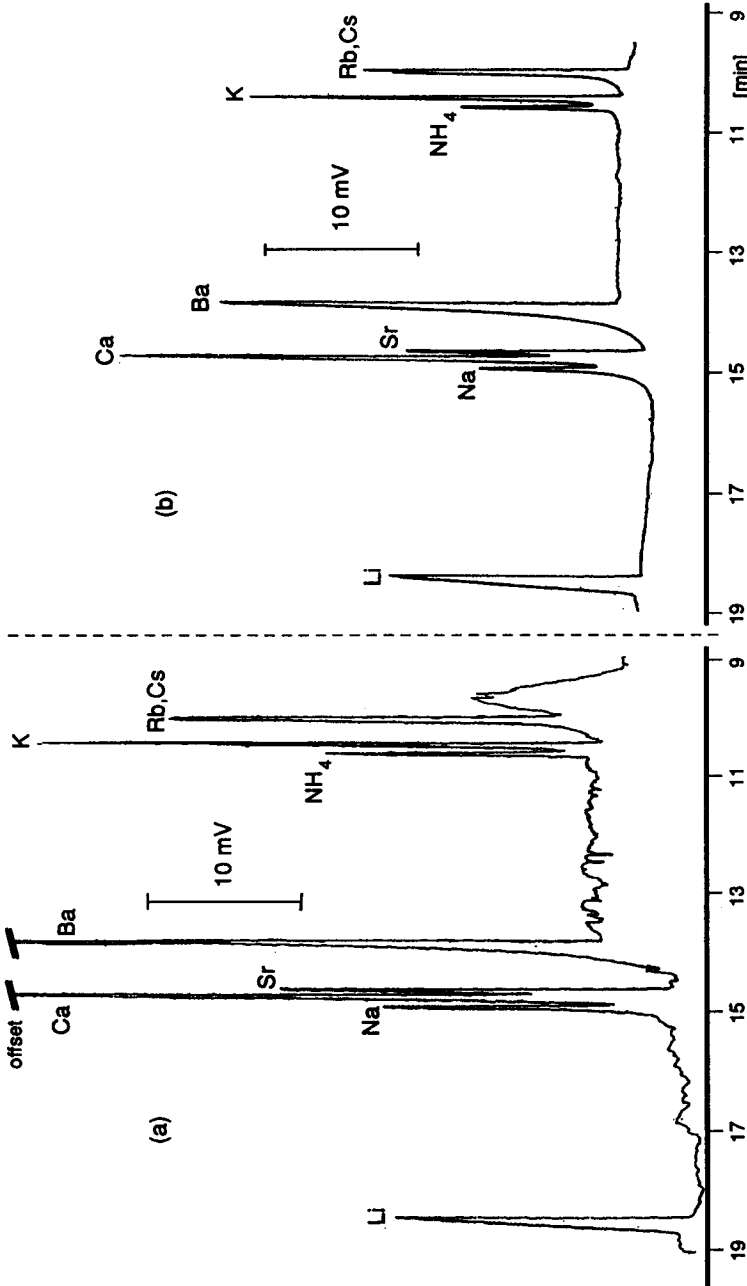
Fig. 9.22 - Electrophoretic separations of 10^{-5} M alkali and alkaline-earth metal cations detected with the potentiometric detector in on-column ($d \approx -30 \mu m$) position (a) and post-column ($d \approx 30 \mu m$) position (b). Background electrolyte $2 \cdot 10^{-2}$ M $MgAo_2$, pH 7.8; electrokinetic injection, 5 kV for 4 s; separation potential 20 kV; liquid membrane composition 4 (see Table 9.1); capillary length 97.5 cm, i.d. 25 μm.
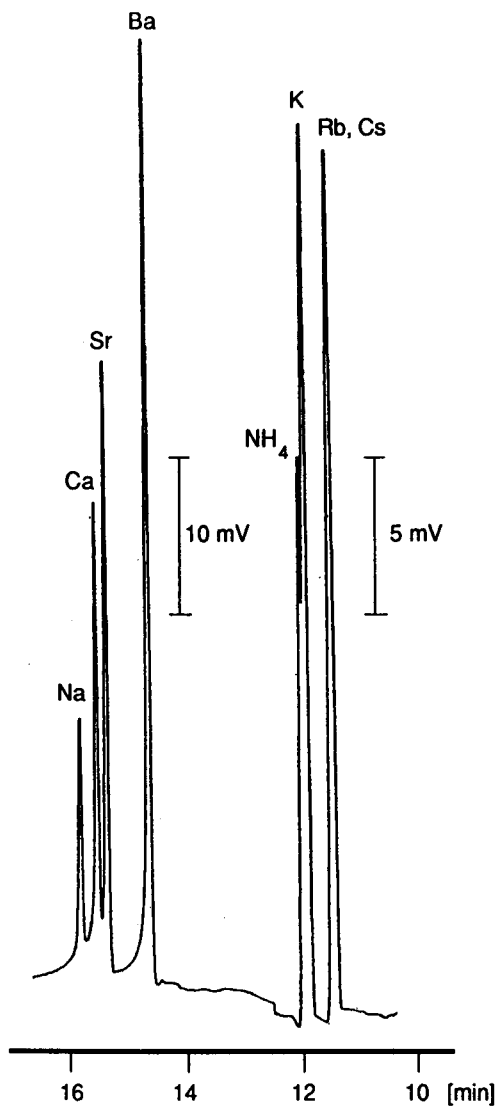
Fig. 9.23 - *Electrophoretic separation of 10^{-5} M alkali and alkaline-earth metal cations detected with the potentiometric detector in post-clumn position (d ≈ 25 - 30 µm from the end of the capillary (post-column). Background electrolyte 2 · 10^{-2} M MgAc$_2$, pH 7.8; electrokinetic injection, 5 kV for 2 s; separation potential 15 kV; liquid membrane composition 4 (see Table 9.1); capillary length 99.0 cm, i.d. 25 µm.*

Ion	Apparent plate height [μm]	Real plate height [μm]
K^+	8.57 ± 0.84	6.23 ± 0.38
Ba^{2+}	2.95 ± 0.09	1.10 ± 0.10
Sr^{2+}	2.95 ± 0.17	0.78 ± 0.07
Ca^{2+}	3.44 ± 0.09	1.42 ± 0.11
Na^+	3.31 ± 0.17	2.43 ± 0.08

Table 9.4 - *Apparent and real plate heights for the cations obtained from the electropherogram in Figure 9.23.*

The electropherograms shown in Figure 9.24 were obtained by electrokinetic injection of deionized water (a) and of additionally doubly quartz distilled water (b) from our laboratory. All sample solutions were injected from small polypropylene vials to exclude any leaching effects of the wall material. The plate heights, calculated as mentioned above, are listed in Table 9.5. The signals obviously reflect a remarkable sensitivity of the potentiometric detection system, since signals as intense as 13 mV (for K^+ in (a)) result from the electrophoretic separation of deionized water (total activity $\approx 10^{-7}$ M). As the sample concentration adapts to the value of the regulating function of the ionic background, the actual zone concentration of the resulting signals may be higher (by approximately 2 - 3 orders of magnitude) than the initial concentration of the ions in the sample. This adaptation process already happens during electrokinetic injection (Section 4.2.4), so that the sample plug actually reaches a higher concentration level than the sample solution. If the sensitivity of the system is to be determined quantitatively, the sample solution must be injected hydrostatically. Finally, in order to determine the sensitivity of the potentiometric detector, the sample solution must be dissolved in background electrolyte (see also Section 3.3). This assures equal ionic strength of sample and ionic background and therefore excludes concentration effects due to the regulating function.

Another problem concerning the quantification of a potentiometrically recorded profile is caused by changes in the potential gradient of a specific zone. As this effect is inversely proportional to the conductivity of the zone, in addition to the Nernst response it will actually give rise to a higher signal for ions with a lower mobility than the ionic background, and vice versa. As during
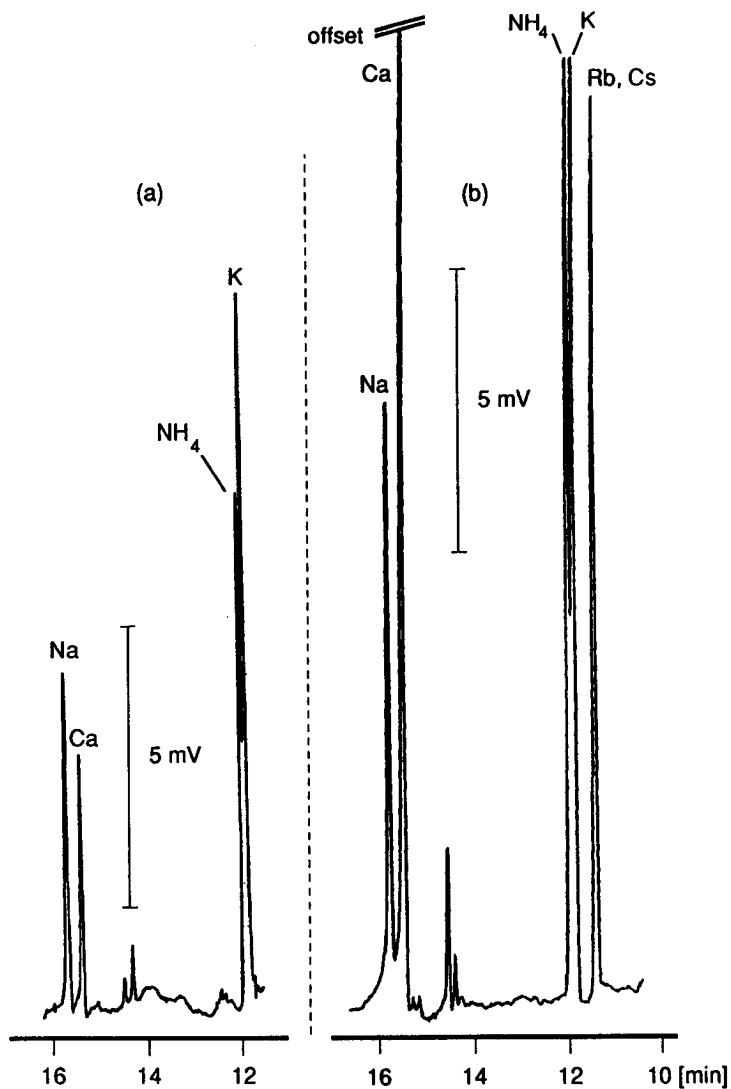
Fig. 9.24 - *Capillary electrophoretic separations of deionized water (a) and doubly quartz distilled (prepared from deionized) water from a wash bottle (b), detected with the potentiometric detector in post-column position (d ≈ 25 -30 μm). Background electrolyte 2 · 10⁻² M MgAc₂, pH 7.8; electrokinetic injection, 5 kV for 2 s; separation potential 15 kV; liquid membrane composition 4 (see Table 9.1); capillary length 99.0 cm, i.d. 25 μm.*

the electrophoretic process the individual zones are increasingly mixed with background elecytrolyte (due to electromigration dispersion), this sample-specific potential gradient response is expected to be insignificant compared with the Nernstian response of the sensor.

Ion	Apparent plate height [μm]	Real plate height [μm]
K^+ (a)	4.72 ± 0.33	2.90 ± 0.11
Ca^{2+} (a)	1.66 ± 0.15	1.38 ± 0.09
Na^+ (a)	2.76 ± 0.19	2.42 ± 0.24
K^+ (b)	6.25 ± 0.17	4.84 ± 0.34
NH_4^+ (b)	6.77 ± 0.32	4.68 ± 0.48
Na^+ (b)	4.07 ± 0.35	3.31 ± 0.09

Table 9.5 - *Apparent and real plate heights of the resolved ionic constituents for electropherograms (a) and (b) determined from Figure 9.24.*

The four electropherograms in Figures 9.25 and 9.26 again represent electrophoretic separations of water samples from our laboratory and provide interesting information. The background electrolyte was $MgAc_2$ of pH 5.1. As before, all samples were injected electrokinetically from small polypropylene vials. Although the sensitivity is expected to decrease with lower pH, the signals are still remarkably intense.

The electrophoretic separations in Figure 9.25 were obtained with doubly quartz distilled water (prepared from deionized water) kept in a PE storage container. When comparing the resulting signals with the electropherogram obtained from deionized water (Figure 9.26 (a)), the profiles of K^+ / NH_4^+, Ca^{2+} and Na^+ indicate, as expected, a lower activity in the doubly distilled water sample. However, an additional Li^+ signal appeared after the distillation process. Surprisingly, the electrophoretic separation of doubly distilled water stored in a wash bottle gave the electropherogram (b) presented in Figure 9.26, indicating a higher ionic activity than prior to distillation. The same can be seen in Figure 9.24. This contamination does not come from the plastic material of the wash bottle, but from aerosols present in the laboratory air and aspirated through the tip of the wash bottle.
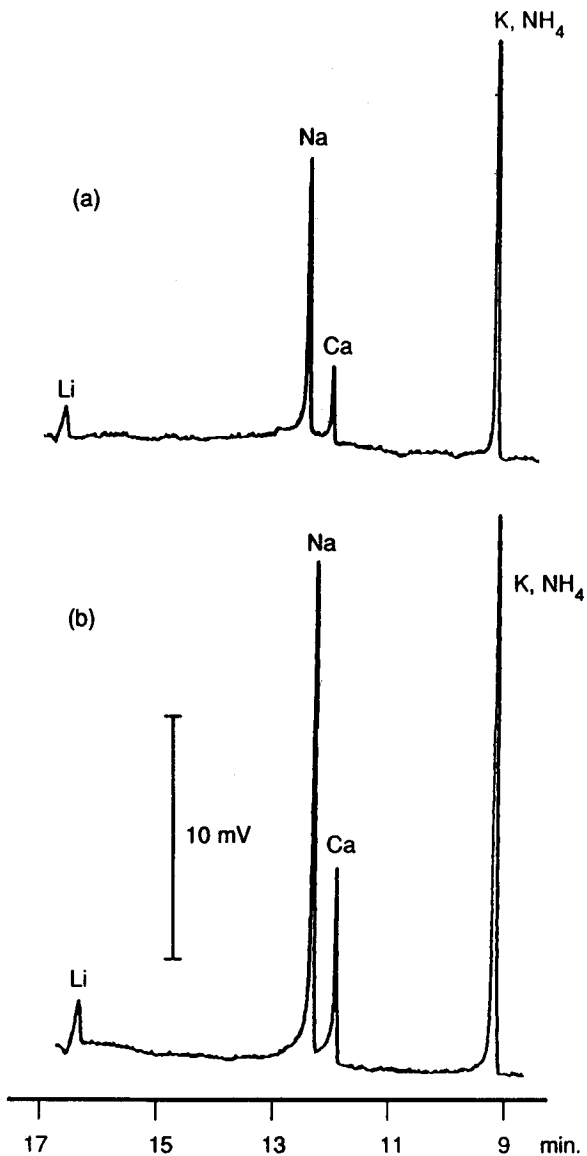
Fig. 9.25 - *Electrophoretic separation of doubly distilled water (obtained from two different distillation apparatuses, a and b) detected with the potentiometric detector in post-column position (d ≈ 25 μm). Background electrolyte $2 \cdot 10^{-2}$ M MgAc$_2$, pH 5.1; electrokinetic injection, 5 kV for 4 s (a); separation potential 20 kV; liquid membrane composition 4 (see Table 9.1); capillary length 99.0 cm, i.d. 25 μm.*
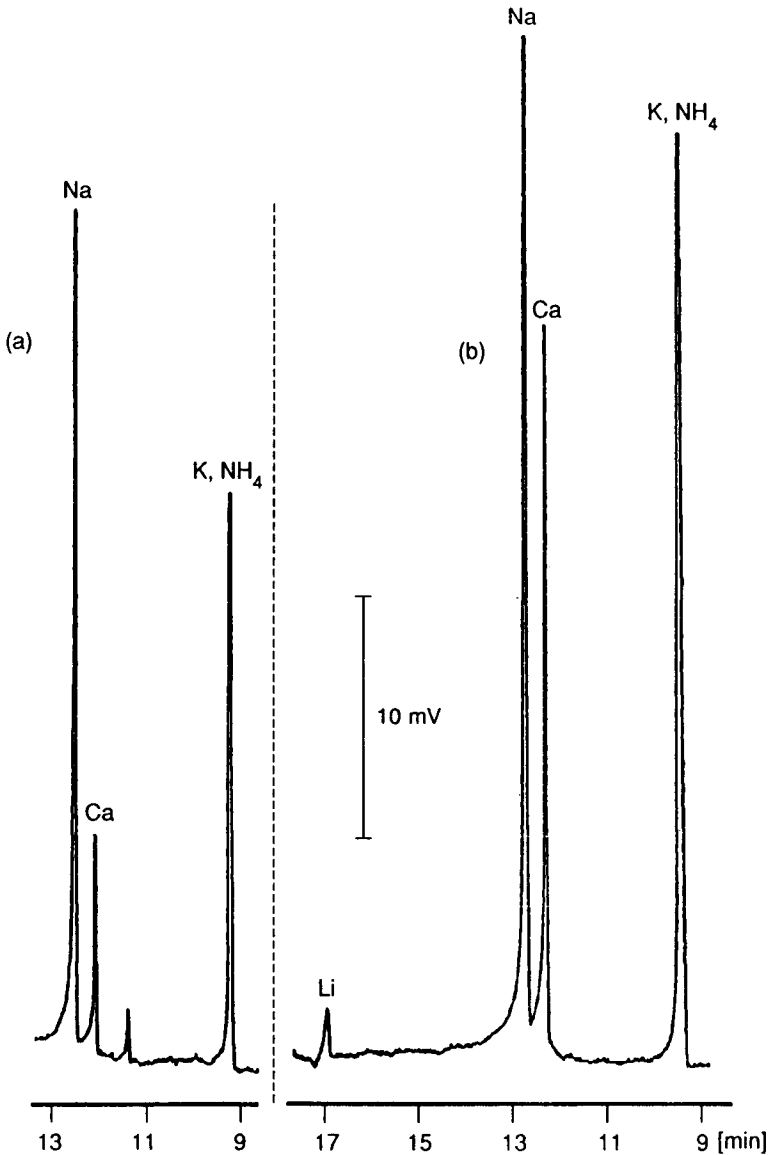
Fig. 9.26 - *Electrophoretic separation of deionized (a) and doubly distilled water (from a wash bottle (b)) detected with the potentiometric detector in post-column position (d ≈ 25 μm). Background electrolyte $2 \cdot 10^{-2}$ M MgAc$_2$, pH 5.1; electrokinetic injection, 5 kV for 4 s; separation potential 20 kV; liquid membrane composition __4__ (see Table 9.1); capillary length 99.0 cm, i.d. 25 μm.*

9.4.4. Electrophoretic Separation of Organic Cations

The results obtained in the last section indicate that ions for which the selectivity coefficient against the ionic background (Mg^{2+} in the case of the liquid membrane composition <u>4</u>) is high, give rise to a considerable electro-
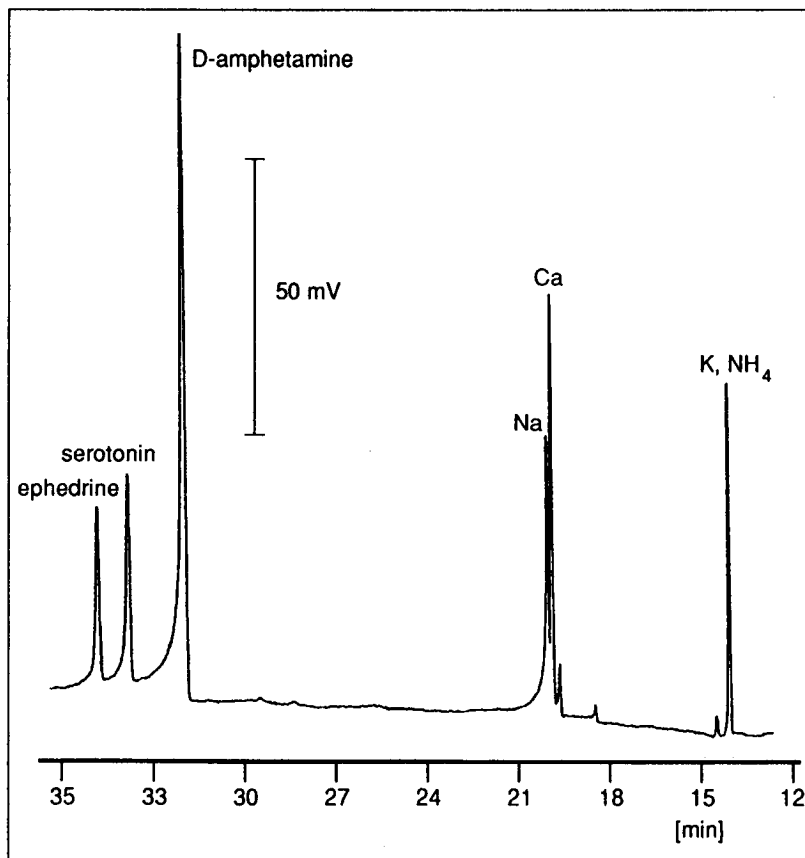
Fig. 9.27 - *Electrophoretic separation of a sample containing 10^{-6} M D-amphetamine, serotonin and (+)-ephedrine (dissolved in doubly quartz distilled water) detected with the potentiometric detector in post-column position (d ≈ 25 μm). Background electrolyte $2 \cdot 10^{-2}$ M MgAc$_2$, pH 7.8; electrokinetic injection, 5 kV for 5 s; separation potential 20 kV; liquid membrane composition <u>4</u> (see Table 9.1); capillary length 110 cm, i.d. 25 μm.*

Ion	Apparent plate height [μm]	Real plate height [μm]
Amphetamine · H⁺	2.19 ± 0.10	1.64 ± 0.11
Serotonin · H⁺	7.54 ± 0.45	3.52 ± 0.13
Ephedrine · H⁺	5.84 ± 0.38	3.21 ± 0.12

Table 9.6 - *Apparent and real plate heights for amphetamine, serotonin and ephedrine obtained from Figure 9.27.*

motive response. Since the selectivity coefficient for a cation increases with its lipophilicity [199], the analysis of organic cations could be potentially attractive.

Figure 9.27 shows an electrophetic separation of amphetamine, serotonin and ephedrine in the presence of alkali and alkaline-earth metal ions (from the doubly quartz distilled water used). The location of the organic ions was determined from electrophoretic runs of the individual compounds. Apparent and real plate heights are listed in Table 9.6.
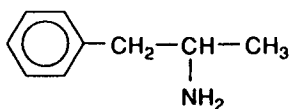
amphetamine [$C_9H_{13}N$]
M_r = 135.20
pK = 9.8 (T = 25 °C) [200]
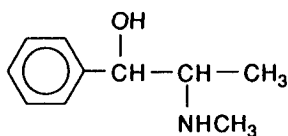
ephedrine [$C_{10}H_{15}NO$]
M_r = 165.23
pK = 9.6 (T = 25 °C) [200]
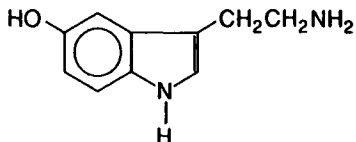
serotonin (5-hydroxytryptamine) [$C_{10}H_{12}N_2O$]
M_r = 176.21
pK_1 = 4.9, pK_2 = 10.0,
pK_3 = 11.1 [201]

The electromotive signal, ΔE_{max}, amounted to 100 mV for amphetamine (Figure 9.27). Further dilution of the sample to 10^{-8} M and subsequent electrophoretic separation still gave a signal of approximately 7 mV (see Figure 9.28). The detection limit for amphetamine was thus estimated to be below 10^{-8} M.
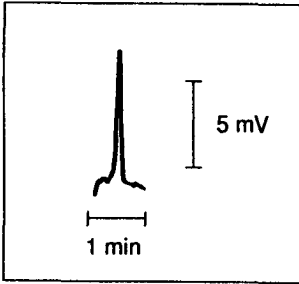
Fig. 9.28 - *Potentiometric signal resulting from electrokinetic injection of a 10^{-8} M solution of amphetamine in doubly quartz distilled water. Detector in post-column position (d $\approx$ 25 μm). Background electrolyte $2 \cdot 10^{-2}$ M MgAc$_2$, pH 7.8; electrokinetic injection, 15 kV for 3 s; separation potential 15 kV; liquid membrane composition 4 (see Table 9.1); capillary length 90.0 cm, i.d. 25 μm.*

10. Experimental

10.1. Determination of the Inner Diameter of Fused-Silica Capillaries (Figure 4.3)

The inner diameter of a fused-silica capillary was determined by a method described by Guthrie et al. [202]. The capillary was filled with mercury and the electric resistance across the length of the column was measured with a digital ohmmeter. The resistance, R, is related with the inner diameter, d_c, of the capillary by the following equation:

$$d_c = 2 \left(\frac{\rho L}{R \pi} \right)^{0.5} \qquad (10.1)$$

with ρ being the specific electric resistance of mercury (0.95783 $\mu\Omega$ m at 20 $^{\circ}$C) and L the length of the capillary. By this technique, an average value for the inner diameter is obtained.

10.2. Coating Procedure with 3-Sulfopropylsilanetriol (Figure 5.3)
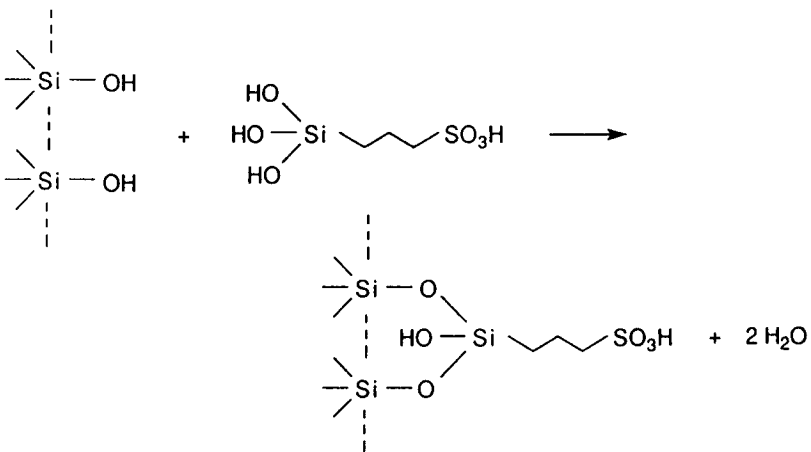
For immobilizing the silane in the column, a dynamic coating procedure [140, 203] was used. A fused-silica capillary of 4.6 µm i.d. (length 114.4 cm) was treated for 15 min with an aqueous solution consisting of 2.6 % (w/w) HF and 3.1 % (w/w) HNO_3, for another 15 min with 1 % (w/w) HCl and finally rinsed with water until neutrality. Then it was rinsed for 10 min with an aqueous solution 5 % (w/w) of 3-sulfopropylsilanetriol (the pH of which had been adjusted to 4.4 with concentrated ammonia solution) and allowed to stand for 1 h. Subsequently, the capillary was emptied by means of a gentle stream of nitrogen (50 bar) and mounted in a gas chromatograph. The silane was immobilized by heating the column with the following temperature program: 1/3 °C min^{-1} from 50 to 180 °C and for 19 h isothermally at 180 °C.

A detailed description of different coating procedures is given elsewhere [203].

10.3. Preparation of the Porous Glass Joint [167]

A fused-silica capillary is cut in two at the desired position. Under the microscope, the two ends are inserted in a porous glass tubing of 2 cm length (Figure 10.1; see also Section 8.3) to form a clean joint. In order to exactly put
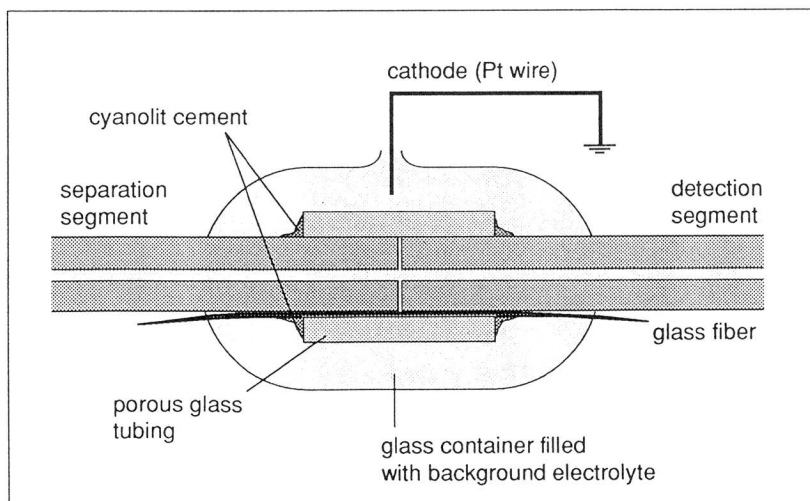
Fig. 10.1 - *Cross section of a porous glass joint.*

the two pieces of the capillary in place again, it is important that the o.d. of the capillary precisely matches the i.d. of the porous glass tubing. If this is not the case, additional insertion of a glass fiber of appropriate thickness (pulled from a glass rod) might be helpful (see Figure 10.1). The ends of the porous glass tubing are then sealed with cyanolit cement. The extremely fragile joint is kept immersed in a small glass vessel filled with background electrolyte, in which a Pt wire is placed as the cathode. For the electrophoretic experiments, the potential is applied across the longer segment of the capillary. The electric field is grounded at the small (conductive) gap, which remains between separation and detection segment of the column.

10.4. Preparation of Metallized Microelectrodes

Metallization of the microelectrodes is carried out after having silanized them (see Section 8.4). With a special device, the empty pipettes are fixed horizontally in the upper part of a glass compartment. Underneath, a small vessel of molybdenum is fixed between two electrodes and provided with the metal to be deposited on the lower side of the pipettes. The system is evacua-

silanized glass pipettes

metal vapor

vessel of molybdenum (heated)

electrodes

glass compartment (evacuated, $p \approx 10^{-5}$ torr)
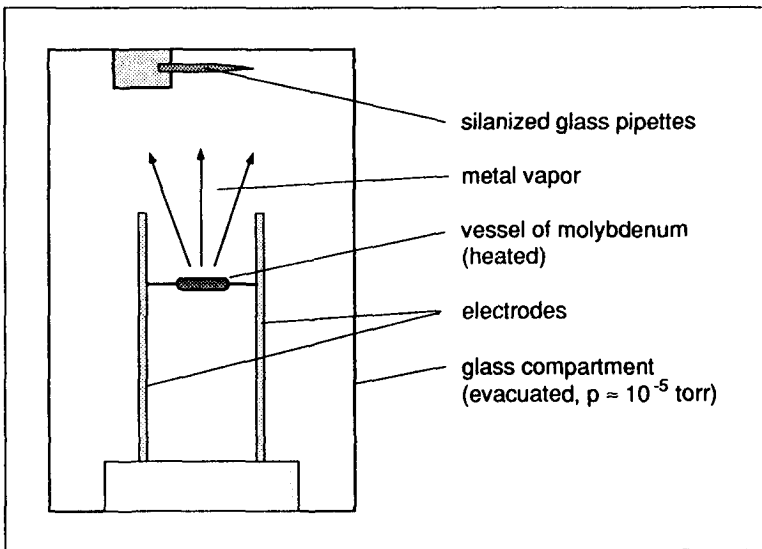
Fig. 10.2 - Surface metallization of glass pipettes.

ted to 10^{-5} torr and the Mo vessel heated by applying a current to the electrodes until the metal melts and slowly begins to evaporate. The thickness of the deposited layer is controlled by a quartz-crystal thin-film monitor. First, chromium, which serves for better adhesion of the subsequent metal layer, is deposited up to a thickness of 50 Å and afterwards platinum or gold up to a thickness of approximately 0.5 µm. As the pipettes remain transparent from one side, the filling procedure can be carried out as described in Section 8.4. Finally, a platinum wire is fixed with conductive carbon paste on the metallized surface of the microelectrode.

10.5. Preparation of the Internal Reference Electrode

The internal reference of the microelectrodes consisted of Ag / AgCl. Silver wires of 0.5 mm diameter were cut into pieces of 2 - 3 cm length. One end of the wire was fixed in a socket (outer diameter 0.8 and 1.5 mm). In order to smooth the front part, the Ag wires were held into the flame of a small gas-burner for a few seconds . The wires were then cleaned by immersing them (up to their socket) in concentrated nitric acid for about 30 s. After rinsing with doubly quartz distilled water, the Ag wires were chlorinated anodically in 0.1 M HCl at a current density of 150 µA overnight [187]. Finally, the Ag / AgCl electrodes were stored in doubly distilled water. In order to prevent damage of the AgCl layer, the sharp border of the glass pipettes should be smoothed over the flame before the wire is inserted.

10.6. Instrumentation

- Power supply: Bertan 205A - 50R (0 - 50 kV, 0 - 3 mA)

Bertan Associates, 121 New South Road, Hicksville, NY 11801 (USA) (Distributor: Altrag AG, Mühlehaldenstr. 6, CH-8953 Dietikon)

- Microscope: Zeiss Invertoskop D with camera and monitor

Carl Zeiss AG, Grubenstr. 54, CH-8021 Zürich

-Micro-   Wild & Leitz AG, CH-8021 Zürich
manipulators:

- Impedance   AD 515 L (input-impedance 10^{13} Ω / 1.6 pF differential,
  converter: 10^{15} Ω / 0.8 pF common mode, leak current at the input
       < 75 fA
       Analog Devices, One Technology Way, P.O. Box 9106,
       Norwood, MA 02062-9106 (USA)

- Electrometer: Model F-223A Dual Electrometer, Serial No. 120
       WP-Instruments Inc., 60 Fitch Street, P.O. Box 3110,
       New Haven, CT 06515 (USA)
       (Distributor: WPI-Germany, Wiesenbacher Weg 6, D-6901 Mauer)

- Digital multimeter: 179 TRMS Digital Multimeter
       Keithley Instruments, Taunton, MA (USA)
       (Distributor: Keithley Instruments, Kriesbachstr. 4,
       CH 8600 Dübendorf)

- Strip chart   W + W Recorder 314 and 1100
  recorder: Kontron Electronics, In der Luberzen 1, CH-8902 Urdorf

- Paper for strip   Diagrammrollen W + W 15-1076
  chart: Diagramma AG, Zürcherstr. 152, CH-8953 Dietikon

- Autosampler: Metrohm Model 624, Control Unit 643
       Metrohm AG, CH-9100 Herisau

- Fused-silica   50 µm i.d.: 10 VS 050 ID, P/N 062463, silica tubing JO5,
  capillaries: 25 µm i.d.: 10 VS 025 ID, P/N 062460, silica tubing LO2,
       Scientific Glass Engineering (SGE), Ringwood,
       Australia (Distributor: Infochroma AG, Baarerstr. 57,
       CH-6300 Zug).
       4.6 µm i.d. (batch 1984) and
       3.3 µm i.d. (batch 1988):
       Polymicro Technologies Inc., Phoenix, AZ (USA)
       2.3 µm i.d.: MicroQuartz GmbH, Kistlerhofstr. 243,
       D-8000 München 70

- Porous glass tubing :	BIORAN Capillaries (Charge # 2072, pore volume 0.47 ml/g, pore diameter 8.8 nm, specific surface (BET) : 172 m^2/g, i.d. of tubing 303 μm
	Schott Glaswerke, Hattenbergstr. 10, D-6500 Mainz 1
- Cement (for glass joint)	Cyanolit
	3M, CH-8803 Rüschlikon
- Pipette puller :	Vertical Pipette Puller 700 C
	David Kopf Instruments, 7324 Elmo St., P.O. Box 636, Tujunga, CA 91042-0636 (USA)
	(Distributor: Consultants GmbH, Fürstenwall 178, D-4000 Düsseldorf)
- Glass tubings for microelectrodes :	Pyrex glass tubing GC 150T-15
	Clark Electromedical Instruments, P.O. Box 8, Pangbourne (UK)
- Autoclave (for coating the capillaries)	HR 500
	Berghof GmbH Labortechnik, Harretstr. 1, D-7412 Eningen (Distributor: O. Kleiner AG, Schützenmattweg 26, CH-5610 Wohlen)
- Ferrules and fittings :	Vespel Graphit 0.4 mm (Art. No. 1000-1712 A)
	Brechbühler AG, Steinwiesenstr. 3, CH-8952 Schlieren

10.7 Chemicals

a) Ionophores:

- ETH 1001
[R-(R*,R*)]-13,17,18,22-Tetramethyl-14,21-dioxo-16,19-dioxa-13,22-
diazatetratriacontanedioic acid diethylester
$M_r = 685.01$
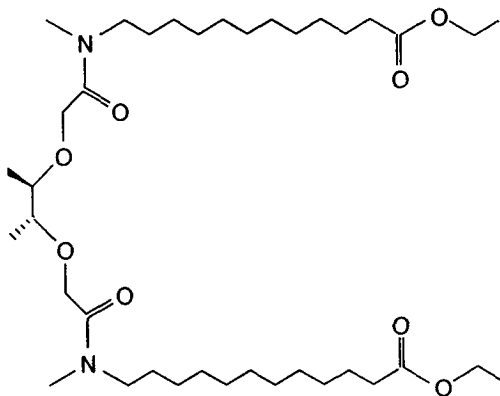
- ETH 1571
Pyridine 2,6-dicarbonic acid N,N'-diheptyl-N,N'-dimethyl diamide
$M_r = 389.58$
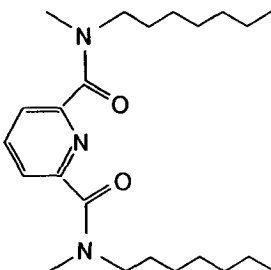
- V 212

2,2'-[1,2-Phenylenebis(oxy-2,1-ethanediyloxy)]bis(N,N-diphenylacetamide)

$M_r = 616.73$
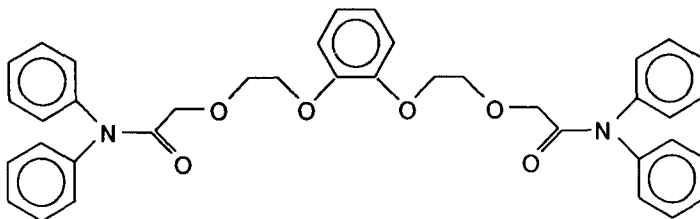
b) Solvents

1,2-Dimethyl-3-nitrobenzene (DMNB) $[M_r = 151.17]$	Selectophore®; > 99 % Fluka AG, P.O. Box 260, CH-9470 Buchs
2-Nitrophenyl octyl ether (o-NPOE) $[M_r = 251.33]$	Selectophore®; > 99 % (GC) Fluka AG, P.O. Box 260, CH-9470 Buchs

c) Additive

Potassium tetrakis-(4-chlorophenyl)borate $[M_r = 496.12]$	Selectophore®; > 98 % (Cl) Fluka AG, P.O. Box 260, CH-9470 Buchs

d) Silanes

3-Sulfopropylsilanetriol $[M_r = 202.26]$	~ 50 % in water as a solvent (Degussa-Silane Si 285; CAS-No. 70942-24-4) Degussa AG, D-6000 Frankfurt
N,N-Dimethyltrimethylsilylamine $[M_r = 117.27]$	Selectophore®; Fluka AG, P.O. Box 260, CH-9470 Buchs

e) Other

(+)-Ephedrine hydrochloride   purum; > 99% (Cl)

[M_r = 201.70]   Fluka AG, P.O. Box 260, CH-9470 Buchs

Serotonin hydrochloride   Biochemika > 99% (HPLC)

(5-hydroxytryptamine, 5-HT)   Fluka AG, P.O. Box 260, CH-9470 Buchs

[M_r = 212.68]

D-Amphetamine sulfate USP   Dr. Bender + Hobein, Riedtlistr. 15a,

    CH-8042 Zürich

All electrolyte solutions were prepared from alkali and alkaline-earth metal chlorides or acetates in analytical purity (puriss., p. a.; Fluka AG, P.O. Box 260, CH-9470 Buchs and E. Merck AG, Frankfurter Str. 250, D-6100 Darmstadt 1), dissolved in doubly quartz distilled water.

11. References

[1]   F. von Reuss, Comment. Soc. Phys. Univ. Mosquens., **1**, 141 (1808)

[2]   J. W. Hittorf, Pogg. Ann. **89**, 177 (1853); **98**, 1 (1856)

[3]   J. W. Hittorf, Pogg. Ann. **103**, 1 (1858); **106**, 337 (1859)

[4]   W. Nernst, Z. Elektrochem. **3**, 308 (1897)

[5]   Kohlrausch, Ann. Phys. Chem. **62**, 209 (1897)

[6]   A. Tiselius, Thesis, University of Uppsala, Uppsala, Sweden (1930)

[7]   A. Tiselius, Nova Acta Regiae Soc. Sci. Ups. Ser. IV, **7**, (4) (1930)

[8]   T. Wieland and E. Fischer, Naturwissenschaften **35**, 29 (1948)

[9]   F. Turba and H. J. Enenkel, Naturwissenschaften **37**, 93 (1950)

[10]   E. L. Durrum, J. Am. Chem. Soc. **72**, 2943 (1950)

[11]   H. D. Cremer and A. Tiselius, Biochem Z. **320**, 273 (1950)

[12]   L. Ornstein, Ann. N. Y. Acad. Sci. **121**, 321 (1964)

[13]   H. Svensson, Acta Chem. Scand. **15**, 325 (1961)

[14]   A. Martin and F. Everaerts, Anal. Chim. Acta **38**, 233 (1967)

[15]   F. M. Everaerts, J. L. Beckers and Th. P. E. M. Verheggen,
        Isotachophoresis - Theory, Instrumentation and Applications,
        Elsevier Scientific Publishing Company, Amsterdam-Oxford-New
        York (1976)

[16]   L. Arlinger and R. J. Routs, Sci. Tools **17**, 21 (1970)

[17]   Th. P. E. M. Verheggen, E. C. van Ballegooijen, C. H. Massen and F.
        M. Everaerts, J. Chromatogr. **64**, 185 (1972)

[18]   F. E. P. Mikkers, F. M. Everaerts, Th. P. E. M. Verheggen, J.
        Chromatogr. **169**, 11 (1979)

[19]   J. W. Jorgenson and K. D. Lukacs, J. Chromatogr. **218**, 209 (1981)

[20]   S. Hjérten, J. Chromatogr. **270**, 1 (1983)

[21]   R. A. Wallingford and A. G. Ewing, J. Chromatogr. **441**, 299 (1988)

[22]   A. S. Cohen and B. L. Karger, J. Chromatogr. **397**, 409 (1987)

[23]   S. Terabe, K. Otsuka and T. Ando, Anal. Chem. **57**, 834 (1985)

[24]   T. Tsuda, K. Nomura and G. Nakagawa, J. Chromatogr. **248**, 241
        (1982)

[25]   G. J. M. Bruin, P. P. Tock, J. C. Kraak and H. Poppe, J. Chromatogr.
        517, 557 (1990)

[26]   C. A. Monning and J. W. Jorgenson, Anal. Chem. **63**, 802 (1991)

[27]   A. Manz, N. Graber and H. M. Widmer, Sens. Actuators **B1**, 244
        (1990)

[28]   F. E. P. Mikkers, Isotachophoresis and Zone Electrophoresis in
       Narrow Bore Tubes, Dissertation, Eindhoven (1980)
[29]   M. Bier (ed.), Electrophoresis - Theory, Methods and Applications,
       Academic Press Inc., New York, USA (1959)
[30]   J. Sargent and S. George, Methods in Zone Electrophoresis, BDH
       Chemical Ltd., Poole, England (1975)
[31]   L. Vamos, Elektrophorese auf Papier und anderen Trägern,
       Akademie Verlag, Berlin (1972)
[32]   F. Everaerts, Chem. Listy **67**, 9 (1973)
[33]   G. Moore, J. Chromatogr. **106**, 1 (1975)
[34]   F. Kohlrausch, Ann. Phys. Chem. **62**, 209 (1897)
[35]   J. Beckers, Thesis, Eindhoven University of Technology, Eindhoven,
       The Netherlands (1973)
[36]   G. Kortüm, Lehrbuch der Elektrochemie (5th edn.), Verlag Chemie,
       Weinheim (1972)
[37]   F. Foret and P. Bocek, Advances in Electrophoresis, Vol. 3, Verlag
       Chemie, Weinheim, Germany (1989)
[38]   P. Bocek, M. Deml, P. Gebauer and V. Dolnik, Analytical
       Isotachophoresis, Electrophoresis Library, Weinheim, Germany
       (1988)
[39]   L. G. Longsworth, Electrophoresis, Theory, Methods and
       Applications, Academic Press, New York (1959)
[40]   R. Wieme, in E. Heftman (ed.), Chromatography, 2nd edition,
       Reinhold Publ. Corp., New York (1967)
[41]   E. B. Dismukes and R. A. Alberty, J. Amer. Chem. Soc. **76**, 191
       (1954)
[42]   W. Thormann and R. A. Mosher, Advances in Electrophoresis Vol. 2,
       Verlag Chemie, Weinheim (1988)
[43]   W. Thormann, R. A. Mosher and M. Bier, Electrophoresis **6**, 78
       (1985)
[44]   R. A. Alberty and J. C. Nichol, J. Amer. Chem. Soc. **70**, 2297 (1948)
[45]   P. Bocek, P. Gebauer and M. Deml, J. Chromatogr. **219**, 21 (1981)
[46]   D. L. Massart, B. G. M. Vandeginste, S. N. Deming, Y. Michotte and
       L. Kaufman, Chemometrics: A Textbook, Elsevier, Amsterdam (1988)
[47]   X. Huang, W. F. Coleman and R. N. Zare, J. Chromatogr. **480**, 95
       (1989)
[48]   A. S. Said, Theory and Mathematics of Chromatography, Verlag
       Hüthig, Heidelberg (1981)

[49]   J. C. Giddings, Sep. Sci. **4**, 181 (1969)

[50]   F. Foret, M. Deml and P. Bocek, J. Chromatogr. **452**, 601 (1988)

[51]   J. C. Sternberg, Adv. Chromatogr. **2**, 205 (1966)

[52]   H. K. Jones, N. T. Nguyen and R. D. Smith, J. Chromatogr. **504**, 1 (1990)

[53]   P. W Atkins, Physical Chemistry, 2nd edition, Oxford University Press, London (1983)

[54]   F. E. P. Mikkers, F. M. Everaerts, Th. P. E. M. Verheggen, J. Chromatogr. **169**, 1 (1979)

[55]   F. E. P. Mikkers, F. M. Everaerts and J. A. F. Peek, J. Chromatogr. **168**, 293, (1979)

[56]   S. Hjérten, Electrophoresis **11**, 665 (1990)

[57]   J. F. Brown and J. O. N. Hinckley, J. Chromatogr. **109**, 218 (1975)

[58]   S. Hjérten, Chromatogr. Rev. **9**, 122 (1967)

[59]   P. Bocek, Top. Curr. Chem. **95**, 131 (1981)

[60]   R. Virtanen, Acta Polytech. Scand. **123**, 1 (1974)

[61]   J. L. Anderson and W. K. Idol, Chem. Eng. Commun. **38**, 93 (1985)

[62]   D. G. Sharp, M. H. Hebb, A. R. Taylor and J. W. Beard, J. Biol. Chem. **142**, 217 (1942)

[63]   R. A. Alberty, J. Am. Chem. Soc. **70**, 1675 (1948)

[64]   A. G. Ogston, Nature **157**, 193 (1946)

[65]   K. J. Mysels, J. Chem. Phys. **24**, 371 (1956)

[66]   K. J. Mysels and P. C. Scholten, Science **136**, 693 (1962)

[67]   R. Datta and V. R. Kotamarthi, AIChE J. **5**, 916 (1990)

[68]   W. Thormann, R. A. Mosher and D. A. Saville, in: B. J. Radola (ed.), Electrophoresis Library, The Dynamics of Electrophoresis, Verlag Chemie, Weinheim, Germany (1992)

[69]   R. A. Mosher, D. Dewey, W. Thormann, D. A. Saville and M. Bier, Anal. Chem. **61**, 362 (1989)

[70]   P. Gebauer, W. Thormann and P. Bocek, J. Chromatogr., submitted for publication

[71]   M. Bier, O. A. Palusinski, O. A. Mosher and D. A. Saville, Science **219**, 1281 (1983)

[72]   contributed by W. Thormann, Department of Clinical Pharmacology, University of Bern, Bern, Switzerland

[73]   W. Jennings, J. High Resolut. Chromatogr. & Chromatogr. Commun. **3**, 601 (1980)

[74]   K. K. Unger, Porous Silica, J. Chromatogr. Libr. (Vol. 16), Elsevier
       Scientific Publishing Company, Amsterdam - Oxford - New York
       (1979)

[75]   S. R. Lipsky, W. J. McMurray, M. Hernandez, J. E. Purcell and K. A.
       Billeb, J. Chromatogr. Sci. **18**, 1 (1980)

[76]   R. Dandeneau and E. Zerenner, J. High Resolut. Chromatogr. &
       Chromatogr. Commun. **2**, 351 (1979)

[77]   W. G. Jennings, Comparisons of Fused Silica and Other Glass
       Columns in Gas Chromatography, Hüthig Verlag, Heidelberg,
       Germany (1981)

[78]   R. K. Iler, The Chemistry of Silica, Wiley, New York, (1979)

[79]   V. Ya Davidov, L. T. Zhuravlev and A. V. Kiselev, Russ. J. Phys.
       Chem. **38**, 1108 (1964)

[80]   C. A. Coulson, Valence, Oxford University Press, London (1963)

[81]   L. R. Snyder and J. W. Ward, J. Phys. Chem. **70**, 3941 (1966)

[82]   J. B. Peri and A. L. Hensley, Jr., J. Phys. Chem. **72**, 2926 (1968)

[83]   Personal communication by Prof. Dr. Erwin sz. Kováts, Swiss
       Federal Institute of Lausanne, Lausanne, Switzerland (1989)

[84]   L. Boksanyi, O. Liardon and E. Kováts, Adv. Colloid Interface Sci. **6**,
       95 (1976)

[85]   M. L. Hair and W. Hertl, J. Phys. Chem. **73**, 4269 (1969)

[86]   A. A. Agzamkhodzhaev, L. T. Zhuravlev, A. V. Kiselev and K. Y.
       Shengeliya, Kolloid. Zh. **36**, 1145 (1974)

[87]   G. J. Young, J. Colloid Sci. **13**, 67 (1958)

[88]   G. J. Young and T. P. Bursh, J. Colloid Sci. **15**, 361 (1960)

[89]   P. C. Carman, Trans. Faraday Soc. **36**, 964 (1940)

[90]   H. P. Boehm, Angew. Chemie **5**, 551 (1959)

[91]   H. P. Boehm, Adv. Catal. **16**, 226 (1966)

[92]   M. L. Hair, Infrared Spectroscopy in Surface Chemistry, Marcel
       Dekker, New York (1967)

[93]   L. R. Snyder, Principles of Adsorption Chromatography, Marcel
       Dekker, New York (1968)

[94]   B. W. Wright, P. A. Peaden, M. L. Lee and G. M. Booth,
       Chromatographia **15**, 584 (1982)

[95]   C. Haber, D. Scheidegger, S. Müller and W. Simon, J. High Resolut.
       Chromatogr. & Chromatogr. Commun. **14**, 174 (1991)

[96]   G. A. Mills and S. G. Hinden, J. Am. Chem. Soc. **72**, 5594 (1950)

[97]   L. R. Snyder, Sep. Sci. **1**, 191 (1966)

[98] J. Gobet and E. Kovàts, Ads. Sci. & Techn. **1**, 77 (1984)

[99] D. N. Strazhesko, V. B. Strelko, V. N. Belyakov and S. C. Rubank, J. Chromatogr. **102**, 191 (1974)

[100] S. Kittaka, J. Colloid Interface Sci. **55**, 431 (1976)

[101] J. J. Bikerman, Trans. Faraday Soc. **32**, 1648 (1936)

[102] M. Muroya and S. Kondo, Bull. Chem. Soc. (Japan) **6**, 1533 (1974)

[103] J. C. Rejenga, G. V. A. Aben, Th. P. E. M. Verheggen and F. M. Everaerts, J. Chromatogr. **260**, 241 (1983)

[104] K. Schwabe and H. Kelm, Physikalische Chemie, Vol. 2 (Elektrochemie), Akademie Verlag, Berlin (1986)

[105] D. R. Crow, Principles and Applications of Electrochemistry, Chapman and Hall, London (1988)

[106] D. C. Graham, Chem. Rev. **41**, 441 (1947)

[107] A. Kitahara and A. Watanabe, Electrical Phenomena at Interfaces, Marcel Dekker, New York (1984)

[108] J. Koryta and J. Dvorak, Principles of Electrochemistry, John Wiley (1987)

[109] G. J. Gouy, J. Phys. Radium **9**, 457 (1910); Ann. Phys. **9**, 129 (1917)

[110] D. L. Chapman, Phil. Mag. **25**, 475 (1913)

[111] O. Stern, Z. Electrochem. **30**, 508 (1924)

[112] J. O'M. Bockris and A. K. N. Reddy, Modern Electrochemistry, Vol. 2, Plenum Press, New York (1970)

[113] J. T. Davies and E. K. Rideal, Interfacial Phenomena, Academic Press, New York, London (1961)

[114] C. H. Hamann and W. Vielstich, Elektrochemie I, 2nd edition, Verlag Chemie, Weinheim, Germany (1985)

[115] A. W. Adamson, Physical Chemistry of Surfaces, 3rd ed., Wiley-Interscience, New York (1976)

[116] M. von Smoluchowski, Bull. Int. Acad. Sci. Cracovie 1903, 184

[117] V. Pretorius, B. J. Hopkins and J. D. Schieke, J. Chromatogr. **99**, 23 (1974)

[118] P. Delahay, Double Layer and Electrode Kinetics, Interscience, New York (1965)

[119] C. L. Rice and R. Whitehead, J. Phys. Chem. **69**, 4017 (1965)

[120] J. Lyklema and J. Th. G. Overbeek, J. Colloid Sci. **16**, 501 (1961)

[121] Ch. Schwer and E. Kenndler, Anal. Chem. **63**, 1801 (1991)

[122] K. D. Lukacs and J. W. Jorgenson, J. High Resolut. Chromatogr. & Chromatogr. Commun. **8**, 407 (1985)

[123] K. D. Altria and C. F. Simpson, Chromatographia **24**, 527 (1987)

[124] R. M. McCormick, Anal. Chem. **60**, 2322 (1988)

[125] K. Otsuka and S. Terabe, J. Microcolumn Sep. **1**, 150 (1989)

[126] D. M. Goodall, D. K. Lloyd and S. J. Williams, LC-GC **7**, 28 (1990)

[127] J. Vindevogel and P. Sandra, J. Chromatogr. **541**, 483 (1991)

[128] S. Fujiwara and S. Honda, Anal. Chem. **59**, 487 (1987)

[129] A. Emmer, M. Jansson and J. Roeraade, in: Proc. of the 13th International Symposium on Capillary Chromatography, Hüthig Verlag, Heidelberg (1991) p. 1222

[130] M. Zhu, D. L. Hansen, S. Burd and F. Gannon, J. Chromatogr. **480**, 311 (1989)

[131] T. Tsuda, J. High Resolut. Chromatogr. & Chromatogr. Commun. **10**, 622 (1987)

[132] J. Kohr and H. Engelhardt, in: Proc. of the 13th International Symposium on Capillary Chromatography, Hüthig Verlag, Heidelberg, Germany (1991) p. 1172

[133] G. Schomburg, Chromatographia **30**, 500 (1990)

[134] S. H. Chang, K. M. Gooding and F. E. Regnier, J. Chromatogr. **120**, 321 (1976)

[135] G. J. M. Bruin, J. P. Chang, R. H. Kuhlman, K. Zegers, J. C. Kraak and H. Poppe, J. Chromatogr. **471**, 429 (1989)

[136] J. A. Lux, H. F. Yin and G. Schomburg, J. High Resolut. Chromatogr. & Chromatogr. Commun. **13**, 145 (1990)

[137] S. Hjérten, J. Chromatogr. **347**, 191 (1985)

[138] J. W. Jorgenson, Trends Anal. Chem. **3**, 51 (1984)

[139] J. K. Towns and F. Regnier, J. Chromatogr. **516**, 69 (1990)

[140] R. Ranz, Diplomarbeit, ETH Zurich, Switzerland (1990)

[141] J. W Jorgenson and K. D. Lukacs, Anal. Chem. **53**, 1298 (1981)

[142] G. J. M. Bruin, R. Huisden, J. C. Kraak and H. Poppe, J. Chromatogr. **480**, 339 (1989)

[143] J. L. Glajch, J. J. Kirkland and J. Köhler, J. Chromatogr. **384**, 81 (1987)

[144] J. L. Glajch, J. C. Gluckman, J. G. Charikofsky, J. M. Minor and J. J. Kirkland, J. Chromatogr. **318**, 23 (1985)

[145] N. Sagliano, T. R. Floyd, R. A. Hartwick, J. M. Dibussolo and N. T. Miller, J. Chromatogr. **443**, 155 (1988)

[146] M. J. J. Hetem, J. W. de Haan, H. A. Claessens, L. J. M. van de Ven, C. A. Cramers and J. N. Kinkel, Anal. Chem. **62**, 2288 (1990)

[147] M. J. J. Hetem, J. W. de Haan, H. A. Claessens, L. J. M. van de Ven, C. A. Cramers, P. W. J. G. Wijnem and J. N. Kinkel, Anal. Chem. **62**, 2296 (1990)

[148] J. J. Pesek and S. A. Swedberg, J. Chromatogr. **361**, 83 (1986)

[149] K. A. Cobb, V. Dolnik and M. Novotny, Anal. Chem. **62**, 2478 (1990)

[150] M. Novotny, K. A. Cobb and J. Lui, Electrophoresis **11**, 735 (1990)

[151] J. E. Sandoval and J. J. Pesek, Anal. Chem. **63**, 2634 (1991)

[152] S. Hjérten, J. Liao and K. Yao, J. Chromatogr. **387**, 127 (1987)

[153] E. Grushka, R. M. McCormick and J. J. Kirkland, Anal. Chem. **61**, 241 (1989)

[154] J. H. Knox, Chromatographia **26**, 329 (1988)

[155] H. Lauer and D. McManigill, Trends Anal. Chem. **5**, 11 (1986)

[156] Y. Walbroehl and J. W. Jorgenson, J. Chromatogr. **315**, 135 (1984)

[157] J. P. Chervet, M. Ursem, J. P. Salzmann and R. W. Vannort, J. High Resolut. Chromatogr. & Chromatogr. Commun. **5**, 278 (1989)

[158] R. D. Smith and H. R. Udseth, Nature **331**, 638 (1988)

[159] Y. F. Cheng and N. J. Dovichi, Science **242**, 562 (1988)

[160] W. Kuhr and E. S Yeung, Anal. Chem. **60**, 1832 (1988)

[161] S. L. Pentoney and R. N. Zare, Anal. Chem. **61**, 1642 (1989)

[162] X. Huang, T. K. Pang, M. J. Gordon and R. N. Zare, Anal. Chem. **62**, 443 (1990)

[163] X. Huang, T. K. Pang, M. J. Gordon and R. N. Zare, Anal. Chem. **59**, 2747 (1987)

[164] L. A. Knecht, E. J. Guthrie and J. W. Jorgenson, Anal. Chem. **56**, 479 (1984)

[165] R. A. Wallingford, and A. G. Ewing, Anal Chem. **61**, 98 (1989)

[166] R. A. Wallingford, and A. G. Ewing, Anal. Chem. **60**, 1972 (1988)

[167] R. A. Wallingford and A. G. Ewing, Anal. Chem. **59**, 1762 (1987)

[168] R. A. Wallingford and A. G. Ewing, Anal. Chem. **60**, 258 (1988)

[169] K. Camman, Das Arbeiten mit ionenselektiven Elektroden, 2nd edn. Springer Verlag, Berlin (1977)

[170] M. S. Frant and J. W. Ross, Jr., Science **154**, 1553 (1966)

[171] E. Pungor and K. Tóth, The Analyst **95**, 625 (1970)

[172] N. W. Carter, F. C. Rector, D. S. Campion, D. W. Seldin, C. A. Nunn and W. Howard, J. Clin. Invest. **46**, 920 (1967)

[173] R. C. Thomas, J. Physiol. (London) **238**, 159 (1974)

[174] C. M. Baumgarten, Am. J. Physiol. **241**, C258 (1981)

[175] D. Ammann, Ion-selective Microelectrodes - Principles, Design and Application, Springer Verlag, Berlin, Heidelberg, New York (1986)

[176] T. Bührer, P. Gehrig and W. Simon, Anal. Sciences **4**, 547 (1988)

[177] J. L. Walker, Jr., Anal. Chem. **43**, 89A (1971)

[178] A. Manz and W. Simon, J. Chromatogr. Sci., **21**, 326 (1983)

[179] M. J. G. Brand and G. A. Rechnitz, Anal. Chem. **42**, 616 (1970)

[180] G. Eisenman, Glass Electrodes for Hydrogen and Other Cations, Marcel Dekker, New York (1967)

[181] W. E. Morf, D. Ammann, E. Pretsch and W. Simon, Pure Appl. Chem. **36**, 421 (1973)

[182] A. Manz, Z. Fröbe and W. Simon, J. Chromatogr. Libr. **30**, 297 (1985)

[183] G. G. Guilbault, R. A. Durst, M. S. Frant, H. Freiser, E. H. Hansen, T. S. Light, E. Pungor, G. Rechnitz, N. M. Rice, T. J. Rohm, W. Simon and J. D. R. Thomas, Pure Appl. Chem. **48**, 127 (1976)

[184] A. Manz, Dissertation No. 8135, ETH Zurich, Switzerland (1986)

[185] W. E. Morf, E. Lindner and E. Simon, Anal. Chem. **47**, 1596 (1975)

[186] P. L. Markovic and J. O. Osborn, Am. Inst. Chem. Eng. J. **19**, 504 (1973)

[187] T. Bührer, Dissertation 8984, ETH Zurich, Switzerland (1989)

[188] W. E. Morf, M. Oehme and W. Simon, in: E. Betz (ed.) Ionic Actions on Vascular Smooth Muscle, Springer, Berlin (1976)

[189] U. Tietze, C. Schenk, Halbleiter-Schaltungstechnik, 5th edn., Springer Verlag, Berlin (1980)

[190] A. Manz and W. Simon, Mikrochim. Acta **1986 I**, 147

[191] A. Manz and W. Simon, Anal. Chem. **59**, 74 (1987)

[192] D. Ammann, T. Bührer, U. Schefer, M. Müller and W. Simon, Pflügers Arch. **409**, 223 (1987)

[193] F. Lanter, No. Dissertation No. 7076, ETH Zurich, Switzerland (1982)

[194] R. Dohner, D. Wegmann, W. Morf and W. Simon, Anal. Chem. **58**, 2585 (1986)

[195] W. E. Morf and W. Simon, in: H. Freiser (ed.), Ion-Selective Electrodes in Analytical Chemistry, Ion-Selective Electrodes Based on Neutral Carriers, Plenum Press, New York (1978)

[196] S. Röösli, Diplomarbeit, ETH Zurich, Switzerland (1990)

[197] J. W. Jorgenson and K. D. Lukacs, Science **222**, 266 (1983)

[198] M. W. Läubli, Dissertation No. 7748, ETH Zurich, Switzerland (1985)

[199] A. Viviani-Nauer, Dissertation No. 6573, ETH Zurich, Switzerland (1980)

[200] E. B. Leffler, H. M. Spencer and A. Burger, J. Am. Chem. Soc. 73, 2611 (1951)

[201] J. R. Vane, Brit. J. Pharmacol. 14, 87 (1959)

[202] E. J. Guthrie, J. W. Jorgenson, L. A. Knecht and S. G. Bush, J. High Resolut. Chromatogr. & Chromatogr. Commun. 6, 566 (1983)

[203] S. Müller, Dissertation No. 8898, ETH Zurich, Switzerland (1989)

[204] private communication with Prof. Dr. W. Haber and B. Haber, Untergartelshauser Weg 10, 8050 Freising-Tüntenhausen (Germany)

12. Appendix

Symbols

$a(x)$	function characterizing the concentration profile of the regulating function $\omega(x)$ in a mixed zone
a_i	activity of ion i $[\text{mol } l^{-1}]$
a_s	factor for correcting the zone length due to concentration adaptation $[l \text{ mol}^{-1}]$
$b(t)$	time-dependent variation of the electrophoretic current flow in a mixed zone
C	capacitance $[F]$
$\bar{c}_A$	total (analytical) concentration of species A $[\text{mol } l^{-1}]$
c_b	concentration of the background electrolyte (buffer)
$\bar{c}_{i.1}$	total (analytical) concentration of species i in zone 1
c_k	concentration of species k $[\text{mol } l^{-1}]$
c_s	concentration of the sample
d	distance between the tip of the microelectrode and the end of the capillary $[m]$
d_c	inner diameter of the capillary
d_{o-o}	distance between the oxygen atoms of two neighbouring silanol groups
D	diffusion coefficient $[m^2 \text{ s}^{-1}]$
D_i	dispersion coefficient $[m^2 \text{ s}^{-1}]$
D_T	dispersion coefficient due to temperature effects (Joule heat) $[m^2 \text{ s}^{-1}]$
δ	thickness of the diffuse double layer $[m]$
δ_{mig}	total width of the sample band $[m]$
δ_T	temperature coefficient of the mobility μ $[K^{-1}]$
e	electric charge of an ion $[\pm 1.602 \cdot 10^{-19} \text{ C}]$
emf	electromotive force
e_s	surface charge per unit area $[\text{C m}^{-2}]$
E	value of the electromotive force $[V]$
E_0	constant potential of the electrochemical cell plus liquid junction potential
E	electric field strength $[\text{V m}^{-1}]$
ε_0	permittivity of vacuum $[8.854 \cdot 10^{-12} \text{ C}^2 \text{ J}^{-1} \text{ m}^{-1}]$
ε_r	relative dielectric constant

η	viscosity [Pa s]
F	Faraday constant [96484.6 C mol^{-1}]
φ	value of the Helmholtz potential ($\varphi_{Helmholtz}$) at a distance x > 0
φ_0	value of the Helmholtz potential at the outer Helmholtz plane (x = 0) [V]
$\varphi_{surface}$	value of the surface potential
$\Delta\varphi_{diffuse}$	potential difference between the outer Helmholtz plane and the bulk solution ($\equiv$ zeta potential) [V]
$\Delta\varphi_{fixed}$	potential difference between the surface and the outer Helmholtz plane [V]
H	plate height [m]
H*	apparent plate height [m]
I	electric current [A]
J	electric current density [A m^{-2}]
k_b	Boltzmann constant [1.38 · 10^{-23} J K^{-1}]
K_{ij}^{pot}	potentiometric selectivity coefficient
κ	electric conductivity [S m^{-1}]
κ_δ	conductivity in the diffuse double layer of thickness δ [S]
l_{det}	path length of the detector cell [m]
l_{inj}	initial width of the sample plug [m]
L	length of the separation compartment [m]
λ_T	thermal conductivity of the background electrolyte [W m^{-1} K^{-1}]
μ_{el}	electrophoretic mobility [m^2 s^{-1} V^{-1}]
$\mu_{el,1}$	electrophoretic mobility of compound 1
$\mu_{el,avg}$	average electrophoretic mobility
$\bar{\mu}_{i,1}$	effective mobility of species i in zone 1 [m^2 s^{-1} V^{-1}]
$\bar{\mu}_k$	effective mobility of species k
μ_k	ionic mobility of species k
μ_{osm}	electroosmotic mobility [m^2 s^{-1} V^{-1}]
n	number of ions in the diffuse double layer
N	number of theoretical plates
P	dissipated electric power along the separation compartment [W m^{-3}]
Q	injected amount of sample [mol]
r	radius of the separation capillary [m]
r_c	mobility of the counter ion relative to the buffer ion
r_s	mobility of the sample ion relative to the buffer ion

R	electric resistance $[\Omega]$
R_c	fractional concentration of free particles
R_0	gas constant $[8.314 \text{ J K}^{-1} \text{ mol}^{-1}]$
R_s	resolution of two zones
s	number of different ionic species present in the solution
S	area of a perpendicular plane in the separation compartment at a given point $[\text{m}^2]$
σ	standard deviation
σ^2	variance
σ_{ads}^2	variance due to adsorption effects (time-dependent)
σ_{det}^2	variance due to detection (time-independent)
σ_{diff}^2	variance due to longitudinal diffusion (time-dependent)
σ_i^2	individual contribution to variance
σ_{inj}^2	variance due to injection (time-independent)
σ_{mig}^2	variance due to electromigration dispersion (time-dependent)
σ_{temp}^2	variance due to temperature (Joule heat) effects (time-dependent)
t	migration time $[\text{s}]$
t_{diff}	time required for the sample ions to diffuse through the stationary layer around the electrode tip
$t_{electronics}$	time, characteristic of the electronic setup
t_{inj}	(electrokinetic) injection time
t_{inter}	time required for the sample ions to penetrate through the interface between aqueous and lipophilic phase
t_{memb}	time required for the sample ions to be transported through the ion-selective membrane
t_0	column dead time
t_{system}	retention time of the system peak or a neutral component
t_{total}	total response time of a potentiometric detection system
T	absolute temperature $[\text{K}]$
τ	time constant $[\text{s}]$
$v_{2 \to 1}$	migration velocity of the boundary between zones 2 and 1 $[\text{m s}^{-1}]$
v_{el}	electrophoretic velocity
v_i	migration velocity of constituent i
v_m	zone velocity
v_{osm}	electroosmotic velocity
V	externally applied voltage $[\text{V}]$
$w_{0.5}$	peak width at half height (half-width)
$w_{0.607}$	peak width at 60.7 % height

$\omega(x)$	Kohlrausch regulating function
x_{max}	maximum distance migrated by the sample zone [m]
x_{min}	minimum distance migrated by the sample zone
z, (z_i)	charge number (of ion i)
$Z(x,t)$	factor combining the non-linear variation of the concentration profile of the regulating function $\omega(x)$ with the corresponding electrophoretic current flow $I(t)$ in a mixed zone
ζ	zeta potential [V]

Curriculum vitae

Born on the 27th of August 1961 in Münster, Westphalia (Germany) [204]

1966 - 1971	Primary School in Freising, Bavaria (Germany)
1971 - 1981	High-School in Freising, Bavaria; graduated in 1981 (Abitur)
1981 - 1982	German Air Force
1982 - 1986	Undergraduate Student at the Department of Chemistry of the Technical University of Munich (Germany)
1986 - 1988	Undergraduate Student at the European Higher Institute of Chemistry (E.H.I.C.S.) in Strasbourg (France); Diplôme d'Ingénieur E.H.I.C.S. in 1988
1988	Postgraduate studies in Analytical Chemistry for the Degree of Doctor of Natural Sciences, Swiss Federal Institute of Technology (Eidgenössische Technische Hochschule) in Zurich (Switzerland); Supervisor Prof. Dr. Dr. h. c. W. Simon
1989	Assistant in Analytical Chemistry at the Department of Organic Chemistry, Swiss Federal Institute of Technology (ETH), Zurich
1992	married Eva Szabolcsi on March 7th

Zurich, March 1992

Carsten Haber